Thermodynamics and Kinetics of Antisense Oligonucleotide Hybridization to a Structured mRNA Target

by

S. Patrick Walton

B.ChE., Chemical Engineering, Georgia Institute of Technology

M.S., Chemical Engineering Practice, Massachusetts Institute of Technology

Submitted to the Department of Chemical Engineering In Partial Fulfillment of the Requirements for the Degree of Doctor of Science in Chemical Engineering

at the

Massachusetts Institute of Technology

February, 2002

Signature of Author.....
Department of Chemical Engineering
October 11, 2001

Certified By.....
Martin L. Yarmush
Helen Andrus Benedict Professor of Surgery and Bioengineering, Harvard Medical School
Thesis Co-Supervisor

Certified By.....
Gregory N. Stephanopoulos
Professor of Chemical Engineering
Thesis Co-Supervisor

Accepted By.....
Professor Daniel Blankschtein
Graduate Officer, Department of Chemical Engineering

Prefatory Material

Thermodynamics and Kinetics of
Antisense Oligonucleotide Hybridization

by

S. Patrick Walton

Submitted to the Department of Chemical Engineering
on October 11, 2001 in partial fulfillment of the
Requirements for the Degree of Doctor of Science in
Chemical Engineering

Abstract

Antisense oligonucleotides have the potential to selectively inhibit the expression of any gene with a known sequence. Antisense-based therapies are under development for the treatment of infectious diseases as well as complex genetic disorders. Although there have been some remarkable successes, realizing this potential is proving difficult because of problems with oligonucleotide stability, specificity, affinity, and delivery. Each of these limitations has been addressed experimentally through the use of chemically-modified oligonucleotides and oligonucleotide conjugates, with much success in enhancing oligonucleotide efficacy. These early studies have shown that selection of target site, once considered a trivial problem, is critical to the success of antisense strategies.

It has become clear that the efficacy of antisense oligonucleotides is a strong function of the structure of the target mRNA. Though single-stranded, RNA molecules are typically folded into complex three-dimensional structures, formed primarily by intramolecular Watson-Crick base-pairing. If an oligonucleotide is complementary to a sequence embedded in the three dimensional structure, the oligonucleotide may not be able to bind to its target site and exert its therapeutic effect. Because the majority of the structure of RNA molecules is due to Watson-Crick base-pairing, relatively accurate predictions of these folding interactions can be made from algorithms that locate the structure with the most favorable free energy of folding.

Taking advantage of the predictability of RNA structures, this thesis addresses the problem of antisense target site selection, first from a theoretical and subsequently an experimental standpoint. A thermodynamic model to predict the binding affinity of oligonucleotides for their target mRNA is described and validated using multiple *in vitro* and cell-culture based experimental data sets. Subsequently, direct experimental comparisons with theoretical predictions are made on the well-characterized rabbit-β-globin (RBG) mRNA, using a novel, centrifugal, binding affinity assay. The importance of the hybridization kinetics is also explored, as is the role of association kinetics in defining the rate of cleavage by the enzyme ribonuclease H (RNase H). Finally, the applicability of the model in identifying biologically active oligonucleotides is demonstrated.

Thesis Co-Supervisor: Martin L. Yarmush
Title: Helen Andrus Benedict Professor of Surgery and Bioengineering, Harvard Medical School

Thesis Co-Supervisor: Gregory N. Stephanopoulos
Title: Professor of Chemical Engineering

Table of Contents

List of Figures and Tables

Acknowledgments

This thesis is just one product of the effort of these last years. I know that I have grown as a person and a scholar, and that there are so many people to thank that I will inevitably forget some of them. Individuals have come into and out of my life, sometimes with obvious impact, and other times with impact so subtle and yet still so powerful. For each of these major and minor experiences, I am truly thankful.

I would like to thank my advisors, Maish Yarmush and Greg Stephanopoulos, for their support and instruction. They have proven themselves to be both skilled scientists and communicators and have helped me grow through both adversity and success. In providing big picture perspectives on work and life, they have been a tremendous help. In particular, I would like to thank Maish for always demanding more of me than I did of myself, making me rise to the challenge and emerge stronger. I would like to express my gratitude to Charlie Roth for his advice and assistance both early in my graduate career and throughout. To my thesis committee members, Rick Mitchell and Clark Colton, I appreciate your input and time in supporting my work outside of your many other time-consuming activities.

This research was funded by the NIH Interdepartmental Biotechnolgy Training Program, the Whitaker Foundation for Biomedical Engineering, the Center for Engineering in Medicine, the Shriners Hospitals for Children, and the Shell Foundation. Thanks to them for keeping clothes on my back, food in my stomach, and supplies in my hands.

Personally, I have benefited from so many different interactions with my lab mates, the other Chemical Engineering students at MIT, my housemates in Ashdown House, my teammates on the MIT Ultimate team, folks from the Shriners Hospital, Park Street Church and my Bible study group, and, of course, my family. Though a list of people is terse and lacking, the number of thanks I need to offer precludes my giving these people the credit they deserve. My hope is that they will recognize their impact on me and know that I will be forever grateful for their friendship and support.

To my lab mates:

Kyongbum Lee, with whom I have shared a life for the last 6 years and with whom I hope to remain forever connected; absolutely the ideal baymate;

Howard Davis, who has been through it all with Kyong and myself and remains one of smartest, most thoughtful people around;

Joe Le Doux, who as the 16th best scientist on Earth is a role model in science and in life;

Arul Jayaraman, without whom I never would have gotten this far, my favorite sounding board and as fine a lab scientist as there is;

Yoon Kang, with whom I shared too many meals to count and in whom I have a trusted friend;

Kris Chan, my working-too-hard/running-to-catch-the-last-train comrade;

Jeanne Classen and Jenny Cusick, two people that I hold in the highest regard;

Annette MacDonald, a surrogate mom for all of us;

Ken Steffan, the guy without whom the lab wouldn't function;

Danny Amaral, for taking care of us for so long at Kendall and at the Shrine;
Steve Reiken, Sangeeta Bhatia, Rob Schoen, Rick Snow, Kealy Ham, Greg Russo, Maura Collins Pavao, Jordana Zeltser, the original crowd, there at the beginning;
Stelios Andreadis, George Pins, Will Holmes, NamHeui Kim, Molly Williams, Ned Jastromb, Elliot DeHaan, the heart of the order, including some of the greatest basketball players on Earth.
Jen Mercury, Kristina Roberts, Kevin Phillips, Jane Tjia, Deanna Thompson, the new-school crowd who made the last year survivable;
Lynne Stubblefield, Ilana Reis, Anne Leeds, what would I/we have ever done without you guys, absolutely some of the greatest people I know;
Avi Robinson, Rochelle Kohen, and all the other summer students along the way, for reminding me that teaching can be just as difficult as learning;
and finally, the PIs, Mehmet Toner, Jeff Morgan, Livingston Van de Water, François Berthiaume, for their investment in my project and willingness to open their doors when I knocked.

To my ChemE comrades:
Daniel "DTMJ" Kamei, as brilliant a person as I have ever known, and a better person, without whom I never would have gotten this far, a man destined to change the world for the better;
Josh Taylor, for teaching me about being a human being as well as an engineer;
Jenny Fujii, Eric Fallon, and the rest of the gang, for enduring the first semester;
Chase Orsello, for taking me to that Natalie Merchant concert, and everything else;
David Quiram, Seif Fateen, Peter Moore, Anthony Nole, Norman Yeh, and Fallon, the P-School survivors;
Casim Sarkar, David Dewitt, Anne Dewitt, Tim Padera, Chris Dowd, Glen Bolton, Randy Myers, and all the other athletes, for making ChemE sports the envy of all;
Suzanne Easterly, Anne Fowler, for all their help in the end game;
Elaine Aufiero, who always had a good story to tell;
Janet Fischer, a person that makes wherever she is a special place to be, one of those people you hope you get a chance to meet in your life.

To my Ultimate teammates and friends:
Matty Secor, who convinced me to play and then taught me how, a friend I will always value, Instructor G;
Leon Hsu, the consummate captain, despite being Canadian;
Jeremy Lueck, mad skills and brain, literally;
Win Chevapravatdumrong, doesn't being able to spell it without looking say enough?;
Alex Lian, Thad Matuszeski, Ajit Sarnaik, Aaron Julin, Jim Fleming, Keith Randall, Charles Isbell, Henry Wong, Andy Wong, "Little" Aaron Moronez, Eddie Lee, my old-school teammates;
Hunter Fraser, Bart Hendriks, Benjie Chen, Dean Bolton, Gil Hung, Jay Bacow, Chris Wilmer, Ico San Martini, Geoff Cooney, my new-school teammates;
Tim Tuttle, Mike Jones, Lee Zamir, James Sarvis, the old-old-school boys, great teachers;

Olivera Kesler, Aimee Smith, Karen Plaut, Susan Dacy, James Sarvis (only with the dress on), et al, our fabulous woman's team, MIT's Nationals representatives;
Barry Sussman, Isabel Pedraza, Theresa Sain, Shauneen Liu and Etchell Cordero, Cheryl Wapnick and Joanne Telegen, the BUDA folks that always made it so much fun.

This thesis is for the folks in Ashdown who have meant so much:
Erik Duerr, a kind and generous man, with whom I have shared way too many Clif bars;
Tal Malkin, a friend from early on, who hated that I had to kill cells every week;
Tara Arthur, Laura Adams and John-Paul Mattia, Laura Johnson, Juan Bruno, with whom I shared many a meal and story in the 4th-floor kitchen;
John Matz, an excellent suitemate with a great TV for watching the Olympics;
Derrick Tate, Cedric Logan, great next-door neighbors;
Sham Sokka, a person I have always admired for being so genuine;
Jenny Farver, Ronak Bhatt, and Manish Jethwa, the new-school Ashfun-ers;
Tom Burbine, Christina Manolatou, Rebecca Xiong, the old-school AHEC folks;
Gustavo Buhacoff, for all of those emails and everything else;
Wendy Yu, Emy Chen, Jane Woo, Mandy Mobley, Jenny Anderson, Joanna Au, and all the other Sigma Kappas, for giving the place a needed shot in the arm;
Jesse Hong, for taking the time to chat even when your thesis is looming;
Carl Kim and Dianne Keene, for so much sympathy and empathy and so many prayers;
Joe, Carmen, John, Pablo, Lenny, and the rest of the staff, for taking care of us in ways we never noticed;
Christine (Butts) Vardaro, for her dedication to the students and being a listening ear, for finding us all places to squeeze in every September ☺;
Beth and Vernon Ingram, who have shown me (and the rest of the students) a love that cannot be measured, you both will always have a special place in my heart.

This thesis is for the people at the Shriners Hospital who helped along the way:
Fran, Gloria, Steve, Darlene, Steve, Fran, for keeping me fed and alive;
Carol and Rosemary, for all those times I asked for anything;
Phil, for morning chats and Red Sox angst;
Al, for rides from Kendall, and anything and everything else;
Hannah, for keeping me in clean coats;
Ginny, Ciro, and Mike, for making sure all our stuff got to the right places.

To the people from Park Street Church and the Wednesday Bible study:
Daniel Harrell, for his teaching and listening, and for being there for our most important day;
Donald Crankshaw, for always having the Hebrew and Greek translations and providing stability in the face of our twists and tangents;
George Greco, for showing his humanity and his strength;
Shannon Stahl, for his example and strength of will;
Jason Heine, for his leadership, guidance, and educated perspective...and the folate.

Finally, this thesis is for my family:

My parents, who put up with not hearing from me more than once a week and seeing me more than once a year (but, maybe that was to their benefit ☺), for putting my grades on the fridge and driving me to college and grad school, for giving me their address and phone number when they moved, for giving me the chance to go to Las Vegas, for worrying about me working too much and running too little, for loving me as only parents can;

My brother, for reminding me that adversity can be a source of growth;

The Hyams family, for welcoming me and treating me as family;

Thomas Y. Lee (OK, not technically family, but can't you see the resemblance), for putting up with my mess for years without complaint, for making a place in his life for a new roommate, for the Volvo and his lost keys, for Ultimate and all his encouragement, for breakfasts and dinners in the kitchen, for runs to Costco, for late-nights and early mornings, for being there even when we were both so busy; for Jasper-Banff, Hood to Coast, Cabot Trail, and Winnepesaukee. No words will ever capture the place in my heart that you will always hold. I am the person I am in many ways because of him;

Deborah (Susan) Hyams Walton, my wife, my love; for all that we have shared and all that is to come; for Nomathemba and Rent; for *The American President* and *The Matrix*; for Ashdown/Myrtle St./Harvard St./Eastgate/Rainbow Dr./??; for New Mexico and the Houston Airport; for ducklings and koi; for "If I Stand"; for the Thirsty Ear; for Oscar and Cheeto, and Calico and Hat Head; for morning runs; for going to Taco Bell; for making up songs in the laundry room; for Touched by an Angel; for that smile, I like that one; for potstickers; for bike rides and strolls down Comm. Ave.; for dueling crosswords and solving them together; for ice-skating, in shorts; for Ankara's Café and Thai Dish II; for watching the Citgo sign come on; for cross-country skiing and grooming machines; for frisbee in the park; for AHEC meetings and coffee hours; for take-out Indian food; for The Matrix; for sharing my brain; for singing and praying and Park Street Church; for basketball lessons; for eggplant and liver and onions; for long-haired freaky people; for BigBrother 1 and 2; for Lincoln Center and a big coffee mug; for hearing my heart beat from 3000 miles; for support and encouragement even in the darkest times;...Thank you.

Biographical Note

Education:

1991 - 1994	Georgia Institute of Technology; B.ChE., With Highest Honors
1995 – 2001	Massachusetts Institute of Technology; M.S., Chemical Engineering Practice

Awards and Honors:

1995	Shell Foundation Fellowship
1999 – 2001	NIH Biotechnology Training Grant Trainee

Teaching and Research Experience:

1994 - 1995	Research Associate, Cardiovascular Fluid Mechanics Laboratory, Georgia Institute of Technology, Atlanta, GA.
1995 - Present	Research Assistant, Department of Surgical Research, Shriners Burns Hospital, Boston, MA.
1995 - Present	Research Assistant, Center for Engineering in Medicine, Department of Surgical Services, Massachusetts General Hospital, Boston, MA.
1998 - 1999	Teaching Assistant, Department of Chemical Engineering, Massachusetts Institute of Technology, Cambridge, MA.

Meetings and Presentations:

1995 "Three-dimensional integration of mitral inflow from digitized doppler color flow mapping: *in vitro* validation", American Heart Association, Anaheim, California.

1995 "Improving the accuracy of flow convergence calculations of valvular regurgitation: benefits of the hemi-elliptical formula for slit-like orifices", American Society of Echocardiography; Toronto, Canada.

1999 "Directed Discovery and Analysis of Antisense Oligonucleotides" (poster) United Engineering Foundation, Biochemical Engineering XI: Molecular Diversity in Discovery and Bioprocessing; Salt Lake City, Utah.

1999 "Prediction of Antisense Oligonucleotide Binding Affinity and Activity in Cell Culture", Biomedical Engineering Society/Engineering in Medicine and Biology Society Joint Meeting, Atlanta, Georgia.

1999 "Rational Selection of Antisense Oligonucleotide Therapeutics", American Institute of Chemical Engineers, Annual Meeting; Dallas, Texas.

2000 "Prediction of Antisense Oligonucleotide Binding Affinity and Efficacy", (poster) American Chemical Society, Annual Meeting; San Francisco, California.

2000 "Selection and Evaluation of Antisense Oligonucleotides", American Institute of Chemical Engineers, Annual Meeting; Los Angeles, California.

2001 "Thermodynamics and Kinetics of Oligonucleotide Binding" (poster), American Chemical Society, Annual Meeting; San Diego, California.

Publications

Original Reports:

1. Walker, P.G., Pedersen, E.M., Oyre, S., Flepp, L., Ringgaard, S., Heinrich, R.S., Walton, S.P., Hasenkam, J.M., Jorgensen, H.S., and Yoganathan, A.P. 1995. Magnetic resonance velocity imaging: a new method for prosthetic heart valve study. *J Heart Valve Dis.* **4**: 296-307.
2. Fontaine, A.A., Heinrich, R.S., Walker, P.G., Pedersen, E.M., Scheidegger, M.B., Boesiger, P., Walton, S.P., and Yoganathan, A.P. 1996. Comparison of magnetic resonance imaging and Laser Doppler Anemometry velocity measurements downstream of replacement heart valves: implications for *in vivo* assessment of prosthetic valve function. *J Heart Valve Dis.* **5**: 66-73.
3. Healy, T.M., Fontaine, A.A., Ellis, J.T., Walton, S.P., and Yoganathan, A.P. 1998. Visualization of the hinge flow in a 5:1 scaled model of the Medtronic parallel bileaflet heart valve prosthesis. *Experiments in fluids.* **25**: 512-518.
4. Walton, S.P., Stephanopoulos, G.N., Yarmush, M.L., and Roth, C.M. 1999. Prediction of Antisense Oligonucleotide Binding to a Structured RNA target. *Biotechnol. Bioeng.* **65**: 1-9.
5. Roth C.M., Kohen R.L., Walton S.P., and Yarmush M.L. 2001. Coupling of inflammatory cytokine signaling pathways probed by measurements of extracellular acidification rate. *Biophys. Chem.* **89**: 1-12.
6. Jayaraman, A., S.P. Walton, M.L. Yarmush, and C.M. Roth. 2001. Rational selection and quantitative evaluation of antisense oligonucleotides. *Biochim Biophys Acta* **1520**:105-114.
7. Walton S.P., Stephanopoulos, G.N., Yarmush M.L., and Roth C.M. 2001. Thermodynamic and kinetic characterization of oligodeoxynucleotide hybridization to a structured mRNA. *Biophys. J.* (in press).

Reviews and Book Chapters:

1. Walton, S.P., Roth, C.M., and Yarmush, M.L., "Antisense Technology", in *The Biomedical Engineering Handbook.* Volume II, Chapter 103, 1999, CRC Press LLC: Boca Raton, FL.

1. Introduction

1.A. Significance

Despite numerous advances in the prevention, diagnosis, and treatment of human disease, there remains a wide range of conditions for which no satisfactory therapeutic options exist. Currently, over 34 million people suffer with HIV/AIDS with roughly 5 million new infections each year [1]. In the United States, men have a 50% chance of developing cancer in their lifetimes; women have a 33% chance [2]. It is estimated that 600,000 people in America currently suffer from Crohn's disease/inflammatory bowel disease, annually [3]. Multiple Organ Dysfunction Syndrome (MODS) is the leading cause of death in post-burn patients [4, 5]. The promise of biotechnological therapeutics may lead to treatments for any or all of these diseases.

Many developing technologies are based on the hybridization of oligonucleotides for their targets. Two notable techniques, oligonucleotide microarrays for solid phase functional genomic applications and molecular beacons for solution phase diagnostics, typify the types of ways in which oligonucleotides are applied in biotechnology. Oligonucleotide and cDNA arrays have revolutionized the way in which cellular physiology is quantified. These microscale methods allow researchers to perform the equivalent of thousands of simultaneous Northern blots. However, use of oligonucleotide arrays is not without its pitfalls. In particular for oligonucleotide arrays, many oligonucleotides are chosen randomly to target each gene and the level of that gene quantified based on the ensemble average of all of the points. Variability in the hybridization levels for these oligonucleotides reduces the accuracy in assigning a level to the transcript, limiting the information content from these costly experiments. Further understanding of the impact of oligonucleotide sequence and mRNA target structure on the hybridization of the probes for their target would ensure that the most accurate calls are made and the most information extracted from every array.

Molecular beacons are hairpin oligonucleotides with a fluorescent molecule tethered to one end and a quenching molecule to the other. Upon binding of the targeted RNA, the hairpin unfolds and the fluorescent molecule signals the presence of the mRNA of interest. The rapid and high-affinity hybridization of these beacons for their target is central to their effectiveness in detecting potentially low-abundance transcripts, such as oncogene products in the detection of potentially cancerous tissue. Other solution-phase hybridization techniques, such as in the use of

ribozymes, rely on a strong interaction between the oligonucleotide and the target. If the complementary region on the transcript is a "poor" one, time and money will have been wasted on the synthesis and testing of a molecule that never had a chance of exerting its therapeutic effect.

A promising, but relatively young, technology that is being examined as a potential treatment for each of these diseases is termed antisense technology. The principle of antisense is based on the hybridization of short, DNA oligonucleotides to mRNA molecules to exert a desired effect. The simplicity of design of antisense molecules arises from the specificity of intermolecular Watson-Crick base-pairing. Though antisense mediated gene inhibition was first seen in the 1970's, development of commercial therapeutics began to proliferate in the 1990's with companies being founded or branching out into the field. A decade of research and development of antisense has produced hundreds of clinical trials of dozens of candidates but only one approved therapeutic, which has since generated only $560K worldwide in revenues [6]. With roughly 6 years of clinical research required to bring a single product to market, it has been estimated that bringing a single product to market costs approximately $500MM. Hence, product failure in late stage trials can doom a company. Methods for designing and selecting optimized candidate oligonucleotides would enhance the likelihood that clinically viable molecules will result.

Traditional *in vitro* and cell-culture screening methods are insufficient for confidently identifying the most active oligonucleotides, the desirable starting point for further optimization of stability and delivery. A strong need exists for rapid and quantitative methods for identifying those sequences with the highest likelihood for exerting a strong biological effect in the clinical setting. The structured methodology for selection and evaluation of antisense oligonucleotide candidates described here will reduce the number of sequences that must be tested *in vitro* while offering insight into the biophysics of antisense oligonucleotide interactions with its target mRNA.

1.B. Background

With the completion of the draft human genome [7], biomedical science is entering an era in which the knowledge and application of genomic information will be critical in the development of new therapeutics [8]. Antisense oligonucleotides (short 15-25 nt pieces of DNA)

take immediate advantage of this wealth of information. These molecules utilize Watson-Crick base-pairing to a target mRNA to achieve a therapeutic effect, typically by the reduction of protein expression from the targeted mRNA, as was definitively shown over 20 years ago [9]. While the use of antisense oligonucleotides has many attractive features as a novel molecular therapeutic, technical barriers have inhibited antisense drug development. A 1997 conference on antisense concluded with much discussion of a data gap that existed between industry and science, in particular, the need for fundamental understanding of the mechanism by which the molecules achieve their therapeutic effect [10-12]. The development of antisense therapeutics will follow from intense scientific study of the mechanisms by which these molecules exert their effect. Understanding the limitations to oligonucleotide efficacy will allow the directed engineering of their structure to achieve optimal activity with minimal non-specific effects.

1.B.1. Antisense Principle

Zamecnik and Stephenson were the first to use antisense DNA to modulate gene expression, inhibiting Rous sarcoma virus replication in chick embryo fibroblasts [9]. Surprisingly, the cells had internalized the antisense DNA, which was interrupting the viral life cycle. Natural antisense inhibition was first observed in bacteria as a means of regulating the replication of plasmid DNA [13, 14]. Antisense RNA, encoded on expression plasmids that were transfected into mouse cells, successfully blocked expression of target genes [15]. These early successes launched what is now a significant effort to expand the use of antisense molecules for research and therapeutic purposes, primarily with DNA oligonucleotides. When introduced to the target cells, they are internalized and hybridize with their complementary sequence, as shown in Figure 1-1. Translation of the target mRNA is inhibited by preventing ribosomal binding and procession and/or inducing cleavage by an enzyme, RNase H, that specifically degrades the RNA strand in an RNA-DNA hybrid [16]. While this mechanism is simple in concept, the challenges and outstanding issues in oligonucleotide development have slowed the development of viable therapeutics.

Antisense inhibition is based on the complementary hybridization of the oligonucleotide for its target mRNA. However, to achieve this effect, the oligonucleotide must negotiate a complicated path to reach its target (Figure 1-2). Oligonucleotides are typically administered to

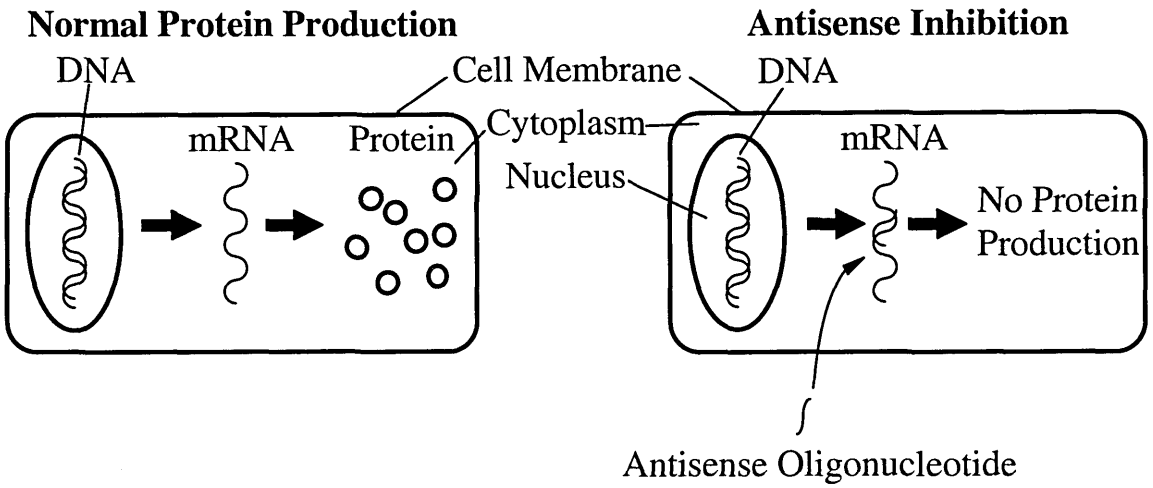

Figure 1-1: Antisense principle

Antisense oligonucleotides are administered to cells where they are internalized and gain access to the cytoplasm and nucleus. The oligonucleotides then hybridize specifically with their target mRNA to reduce or eliminate the translation of the gene product. Levels of protein are reduced subsequent to the reduction of mRNA levels via enzymatic cleavage. Alternatively, protein levels can be reduced by steric inhibition of ribosomal binding and progression.

the extracellular medium and must diffuse to reach the cell surface. *in vitro* experiments performed in the presence of serum will cause extracellular degradation of the oligonucleotides due to the presence of serum nucleases [17]. Upon reaching the cell surface, oligonucleotides will bind to either scavenger receptors or to adsorbed bovine serum albumin [18-21]. The mode of internalization is either via adsorptive endocytosis or receptor-mediated endocytosis [22-24]. Regardless, the oligonucleotides must escape vesicular structures to reach the cytoplasm, though the mechanisms for this process remain in doubt [25, 26]. Having finally accessed the cytoplasm, oligonucleotides can then diffuse to locate their intracellular target from among the RNAs in the cell, with the majority of the effect occurring subsequent to accumulation of the oligonucleotides in the nucleus, where the majority of RNase H activity is localized [27, 28].

Upon reaching its target mRNA, the oligonucleotide must then hybridize with sufficient affinity to exert an effect. Though oligonucleotides as small as 7 nt have been shown to exert an antisense effect [29], the general range of oligonucleotide length is 15-25 nt [8, 16]. This length balances the need for genomic uniqueness with possible partial hybridization of the oligonucleotide [30]. As RNase H activation requires hybridization of only 4-5 nt [31], oligonucleotides of excessive length have the potential to show marked non-targeted effects still based on specific interactions. The rate and affinity of the hybridization of the oligonucleotide to its specific target versus other targets will determine the therapeutic specificity as well as the efficacy of a particular oligonucleotide in a therapeutic context.

1.B.1.a. Molecular Aspects of Antisense Mechanism

In all of the phases of trafficking and binding of antisense oligonucleotides, particular molecules and intermolecular interactions determine the success of the oligonucleotides in achieving their desired effect. As is shown schematically in Figure 1-2, oligonucleotides encounter lipids, carbohydrates, proteins, as well as other nucleic acids in locating their target, and the interactions of the oligonucleotides with each of these different species affect them distinctly. Researchers have sought to take advantage of all of these molecular interactions and processes to enhance oligonucleotide efficacy. Any discussion of the principle of antisense, therefore, must begin with a discussion of the molecular aspects of the mechanism.

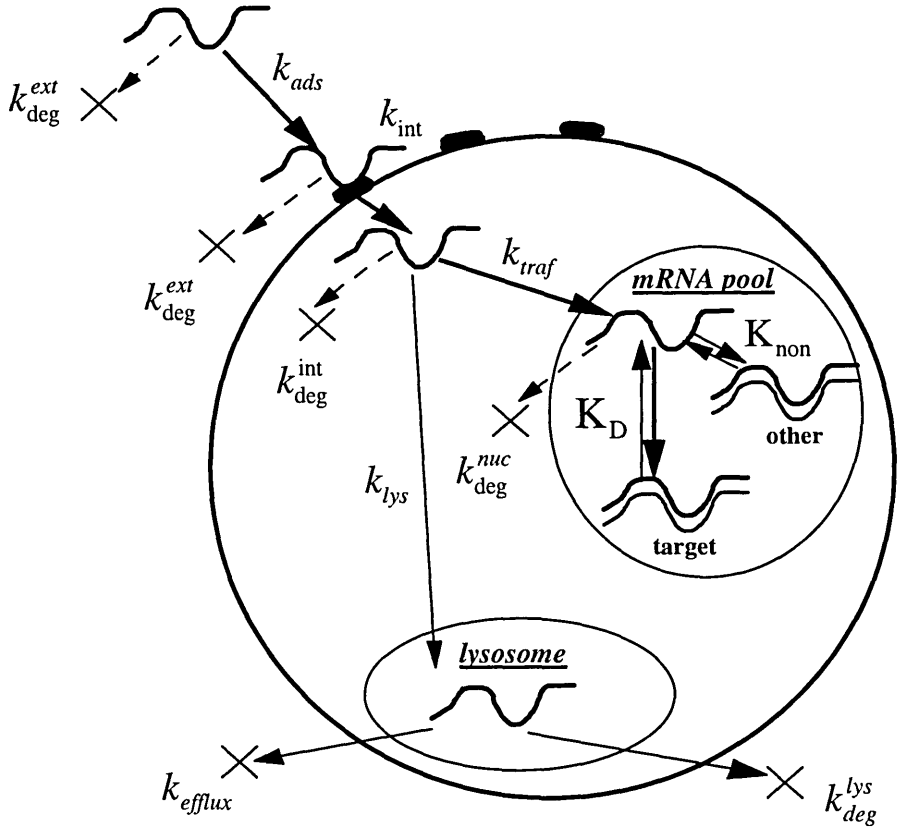

Figure 1-2: Processing of Antisense Oligonucleotides

Oligonucleotides are generally administered to the extracellular medium of cells and must avoid degradation to reach and adsorb on the cell surface whereupon it is internalized. Upon reaching the cytoplasm, intracellular nucleases degrade the oligonucleotide as it is trafficked to reach its target within the mRNA pool. If unable to escape the endocytic vesicle, the oligonucleotide will be trafficked to the lysosome where it will be either resecreted or degraded by lysosomal acid hydrolases. If able to reach the cellular mRNAs, it will then either hybridize with its target specifically or with an unintended target specifically or non-specifically. The selectivity will be a function of the length of the oligonucleotide and its affinity for its target. It is expected that the only step in the processing of antisense oligonucleotides that is largely sequence dependent is the hybridization reaction, with all other processes being somewhat equal regardless of the oligonucleotide sequence.

1.B.1.a.i. *Surface Adsorption and Uptake*

Antisense oligonucleotides when administered to cells are found to associate with cell membranes and membrane proteins prior to internalization [24]. Binding has been shown to occur with both specific cellular receptors and with non-specific proteins, such as bovine serum albumin (BSA), a molecule very relevant to cell culture studies [18, 32, 33]. Membrane association is followed by endocytosis via both temperature dependent and independent mechanisms [24, 34]. Liposomal release to the cytoplasm is inefficient and results in the majority of oligonucleotides being degraded in the endolysosomal compartments [35]. The exact mechanism for release in the absence of lipid delivery vehicles is not well-established and has been afforded little study due to its inherent inefficiency.

1.B.1.a.ii. *Intracellular Trafficking and Nuclear Localization*

Having escaped from the liposomal compartments, oligonucleotides then tend to move primarily by diffusion through the cytoplasm, though studies have shown that the process can be energy-dependent [36]. Trafficking of oligonucleotides is characterized typically using a two-compartment model, where the shallow compartment with half-life of 5-10 minutes and a deep compartment with half-life of 2-5 hours [37]. Nuclear localization generally occurs rapidly as the oligonucleotides associate with nuclear proteins and remain resident in the nucleus for long periods (> 2 days for nuclease stable analogues) [36, 38, 39]. The residence time in the nucleus is particularly critical to the activity of oligonucleotides, as it has been shown that mRNA reduction by RNase H primarily occurs subsequent to nuclear accumulation [27, 28].

1.B.1.a.iii. *Target hybridization and RNase H Cleavage*

Once resident in the nucleus, the oligonucleotide encounters a huge mixture of mRNA and DNA molecules and must interact specifically only with those transcripts to which it is targeted. Though it has been seen that single mismatches in complementarity can reduce binding affinity by 500-fold in some cases, non-specific hybridization is still a significant issue [40]. With the massive excess of mRNA targets relative to genomic DNA targets and the increased affinity of oligonucleotides for target RNA relative to complementary DNA, non-specific interactions with genomic targets are minimized [41].

Subsequent to hybridization, RNA strands hybridized to oligonucleotides are recognized and cleaved by a specific enzyme, RNase H [42]. This enzyme appears to recognize the

formation of A-B form duplex character, as 2'-methoxy and other modified oligonucleotides do not initiate cleavage by this enzyme [31]. A minimum of 5-6 bases are required to form a suitable substrate for the enzyme to act upon its target [31, 43]. RNase H cleavage of the target mRNA is often the dominant inhibitory mechanism, with steric contributions alone often being insufficient [31].

1.B.2. Antisense Oligonucleotide Development

Since the first published examples of antisense inhibition of protein expression [9], a wealth of research has been done into applying these molecules to the inhibition of many gene products. The work has primarily focused on those diseases that do not have satisfactory treatments from current methodologies, including many forms of cancer, viral infections, and others. In the course of these studies, a number of clinical trials have resulted, with FDA approval of one antisense therapeutic for the treatment of cytomegalovirus-induced retinitis in immune-compromised patients. The results of these studies have indicated that to produce oligonucleotides with the highest possible activity, it is necessary to optimize delivery to the appropriate organ/cells, to modify oligonucleotides for enhanced nuclease stability and target affinity, and to select the appropriate target site on the mRNA.

1.B.2.b. Oligonucleotide Delivery

In a therapeutic context, oligonucleotides must be delivered to the appropriate target tissue, associate with the target cells, and be internalized. *In vitro* studies using chemical and mechanical permeabilization support the hypothesis that cellular uptake limits oligonucleotide efficacy [36, 44-46]. Oligonucleotides must then negotiate the intracellular trafficking mechanisms to reach the cytoplasm and nucleus, with the majority of the effect resulting following localization in the nucleus [27]. Achieving the necessary oligonucleotide concentration to enact an effect is limited by many factors, including nuclease degradation, protein adsorption, and charge repulsion between the negatively-charged oligonucleotide and the negatively-charged cell surface. Issues of systemic and cellular delivery are being addressed by a number of different methods, including chemical modification of oligonucleotides to increase their hydrophobicity and nuclease stability; conjugation of oligonucleotides to molecules that

enhance biological half-life, cellular association, and endocytosis; and encapsulation of the oligonucleotide in various carriers, primarily cationic lipids or liposomes.

1.B.2.b.i. *Chemical Modification*

It was initially believed that increasing the hydrophobicity of oligonucleotides would enhance their association with lipid membranes as well as potentially allowing them to diffuse freely through the plasma membrane. This was accomplished using methylphosphonate backbone oligonucleotides. Despite their neutral backbone charge and their stability to nucleases [17], cellular uptake of MP oligonucleotides was shown to be very inefficient, with uptake primarily trapping the oligonucleotides in pinocytic vesicles with little or no nuclear accumulation after 4 h [24, 47].

1.B.2.b.ii. *Conjugation*

Early attempts at conjugation also focused on enhancing the oligonucleotide hydrophobicity. Oligonucleotides conjugated to cholesterol derivatives (chol-oligonucleotides) have improved association with cell membranes and internalization by cells [48-50]. Oligonucleotides conjugated with polycations such as poly-L-lysine (PLL) also have improved cellular uptake and efficacy [51, 52]. Conjugation to proteins can enhance the efficiency and specificity of delivery while potentially mitigating the toxicity of the PLL moiety [53]. Oligonucleotide-PLL complexes have been conjugated to transferrin to inhibit *c-myb* in human leukemia (HL-60) cells, with the expression of *c-myb* greatly reduced [54]. This approach has also been undertaken using specific cellular receptors, such as the asialoglycoprotein (ASGP) receptor, EGF receptor, or IGF1 receptor, with success [54-61]. Cellular signal peptide conjugates have also been used to mediate specific trafficking within cells. Nuclear targeting peptide was conjugated to an oligonucleotide to enhance its nuclear localization in *Paramecium* [62]. This strategy has also been tested with non-covalent conjugates of oligonucleotide with PLL conjugated to the signal import peptide from Kaposi fibroblast growth factor with positive results [63]. Recent success at the lipofection of non-dividing cells with plasmid using a nonclassical nuclear localization signal suggests another potential conjugate for oligonucleotide delivery [64].

1.B.2.b.iii. *Encapsulation into carriers*

A standard *in vitro* means to deliver oligonucleotides is lipofection. Oligonucleotides are mixed with cationic lipids that condense around the negatively charged oligonucleotide forming a lipid vesicle (liposome). The positively charged lipids reduce the electrostatic repulsion between the oligonucleotide and the cell surface. Oligonucleotides then separate from the liposomes following cellular internalization via adsorptive endocytosis [33, 57, 65-69]. Incorporation into liposomes has been shown to enhance efficacy by as much as 1000-fold in the inhibition of ICAM-1 and HIV-1 [70, 71]. Targeted liposomes have also been examined as a method for enhancing specific, cellular delivery [20, 72].

1.B.2.b.iv. Intracellular Trafficking

When material contained within vesicles enters the cell, it has two primary intracellular destinations: the cellular lysosomes and the Golgi apparatus. For the vast majority of species, the destination is the cellular lysosomes where acid hydrolases break down polymeric species such as proteins and nucleic acids to their monomeric constituents. One well-studied example of this mechanism is the LDL receptor [73]. Variants on this theme include many growth factor receptors in which both the ligand and receptor are destroyed upon internalization [74] and the mannose-6-phosphate receptor that binds lysosomal enzymes that were accidentally secreted and transports them to the lysosomes where they gain their hydrolytic function. Some free endocytic vesicles fuse with the *trans* Golgi body. Studies have shown that membrane proteins can be returned to the Golgi and become re-sialated [75, 76]. Ligands bound to membrane proteins could also be trafficked to the *trans* Golgi where they would re-enter the secretory pathway. Of these trafficking patterns, neither can completely describe the path oligonucleotides must traverse to achieve their therapeutic effect as neither provides a process whereby the vesicular contents are able to access the cytoplasm. Elucidation of the mechanism by which oligonucleotides enter the cytoplasm will substantially increase the understanding of their mechanism of action.

1.B.2.c. Oligonucleotide Modifications

To address the issues of stability to nuclease degradation and affinity for their target mRNA, natural phosphodiester (PO) oligonucleotides have been chemically modified in each of their primary functional regions, the phosphodiester backbone, the ribose ring, and the nucleoside base. It has been found that these modifications can affect the ability of the

oligonucleotide to activate RNase H. As such, the focus has been on using multiple modifications throughout the oligonucleotide as well as chimeric oligonucleotides that have different modifications along the length of the oligonucleotide to achieve the desired stability, affinity, and RNase H activation. Figure 1-3 shows some of the modifications that have been examined in antisense studies.

1.B.2.c.i. *Backbone Modifications*

Natural oligonucleotides have a phosphodiester backbone that is susceptible to nuclease degradation, having a half-life as short as fifteen minutes [80-84]. The need for oligonucleotides that are stable *in vivo* prompted the development of chemical derivatives of the phosphodiester backbone. The first derivatives were methylphosphonate and phosphorothioate backbone oligonucleotides. Over time, however, little attention has been afforded to methylphosphonates, as they appear less therapeutically viable due to their poor cellular uptake and the inability of their duplexes to be recognized by RNase H [82, 85].

Phosphorothioate (PS) oligonucleotides, with a sulfur atom substituted for a non-bridge backbone oxygen atom, are the current standard for antisense applications. PS oligonucleotides have half-lives > 5h [80]. However, this increased stability comes at the cost of reduced affinity, increased non-specific association with proteins, and greater toxicity and *in vivo* complications [86-88]. Nonetheless, all ongoing clinical trials utilize oligonucleotides with at least some of the bases having the PS backbone (http://www.clinicaltrials.gov).

Another backbone modification replaces one of the backbone oxygens by an amino group in what are called phosphoramidate (PN) oligonucleotides. These can take two forms, where either the non-bridging oxygen in the backbone or the 3' oxygen of the ribose ring is replaced by a nitrogen [89-94]. Though very stable to nuclease degradation [90], backbone PN molecules have lower affinity for their target mRNA molecules and have received little recent attention as N3'-P5' PN oligonucleotides have similar nuclease resistance with increased target affinity [93]. PN oligonucleotides also show reduced non-specific protein binding versus PS oligonucleotides [92]. In situations where RNase H activation is not required for antisense effect, it has been shown that PN oligonucleotides have greater efficacy than PS, and many other modified species [95].

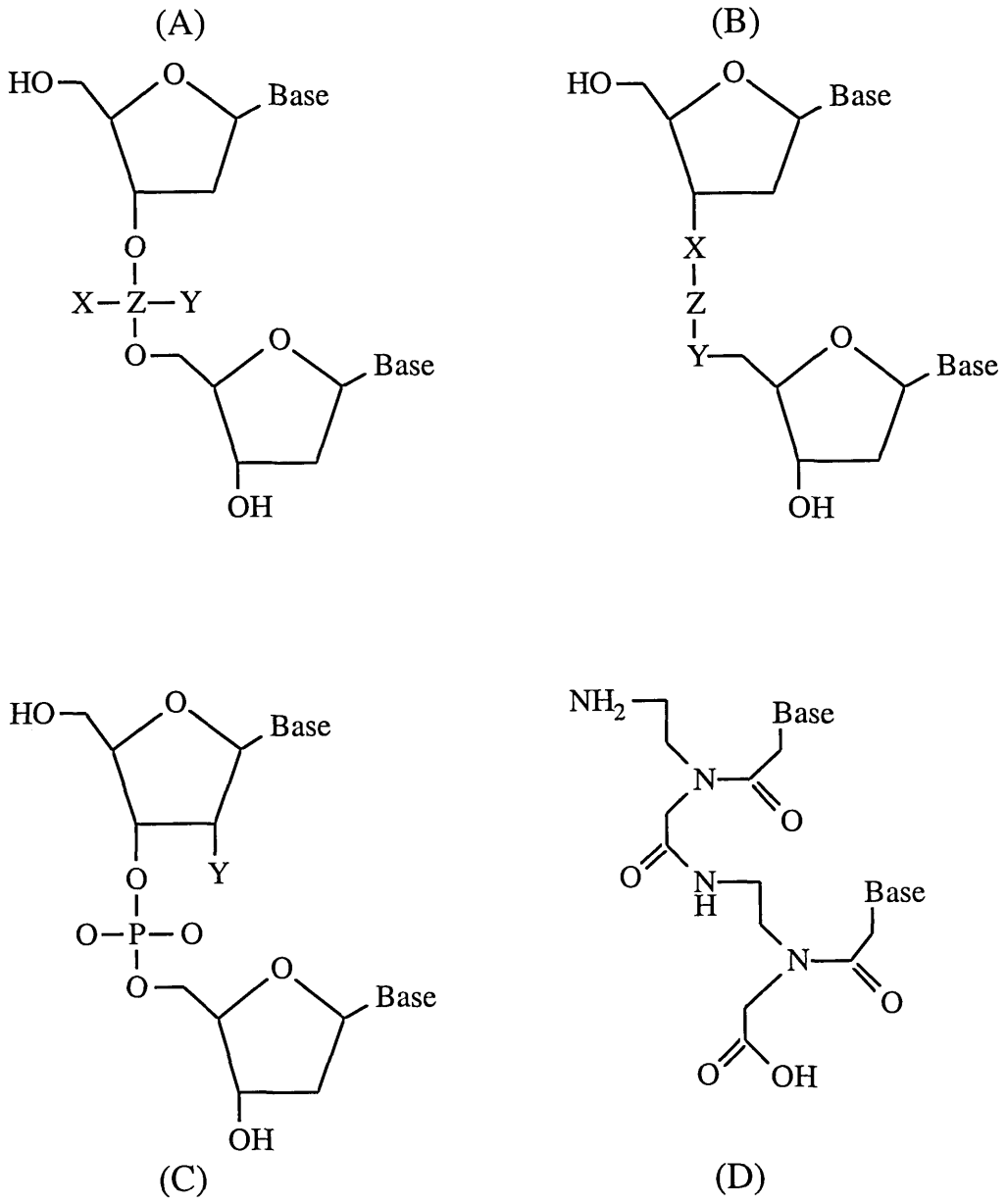

Figure 1-3: Analogues of natural oligonucleotides
(A) Backbone modifications in which the phosphorus bridge atom is retained. (B) Backbone modifications in which the phosphorus bridge atom is replaced. (C) 2' ribose modifications. (D) Peptide nucleic acids - the entire backbone is replaced with amino acids. See Table 1-1 for legend.

Table 1-1: The names and key characteristics of several oligonucleotide analogues
Columns X, Y, Z reference Figure 1-3. Replace the designated letter in Figure 1-3 with the molecule indicated in the Table 1-1 to determine the chemical structure of the oligonucleotide. [31, 40, 77-79]

Phosphorus Analogues (Fig 1-3A)	RNase H activation	Nuclease resistance	Chiral center	ΔT_M/Mod vs. PO [°C]	Charge	X	Y	Z
Phosphodiester (PO)	Yes	No	No	——	Negative	O-	O	P
Phosphorothioate (PS)	Yes	Yes	Yes	- 1	Negative	S-	O	P
Methylphosphonate (MP)	No	Yes	Yes	Negative[1]	Neutral	CH_3	O	P
Phosphoramidate (PN)	No	Yes	Yes	- 3	Neutral	NH-R	O	P
Phosphorodithioate	Yes	Yes	No	- 1+	Negative	S-	S	P
Phosphoethyltriester	No	Yes	Yes	Positive	Neutral	$O\text{-}C_2H_5$	O	P
Phosphoroselenoate	Yes	Yes	Yes	Negative	Negative	Se-	O	P
Non-Phosphorus Analogues (Fig. 1-3B)								
Formacetal	?	Yes	No	- 3	Neutral	O	O	CH_2
3' Thioformacetal	?	Yes	No	- 3	Neutral	S	O	CH_2
5'-N-carbamate	?	Yes	No	Either[2]	Neutral	O	NH	C=O
Sulfonate	?	Yes	No	Depends	Neutral	O	CH2	SO_2
Sulfamate	?	Yes	No	Negative	Neutral	O	NH	SO_2
Sulfoxide	?	Yes	No	Negative	Neutral	CH_2	CH_2	SO
Sulfide	?	Yes	No	Negative	Neutral	CH_2	CH_2	S
2' Modified Analogues (Fig. 1-3C)								
Fluoro	No	Yes	N/A	+ 2-3	N/A[3]	F		
Methoxy	No	Yes	N/A	+ 2	N/A[3]	$O\text{-}CH_3$		
Propoxy	No	Yes	N/A	+ 3	N/A[3]	$O\text{-}(CH_2)_2CH_3$		
Pentoxy	No	Yes	N/A	+ 2	N/A[3]	$O\text{-}(CH)_4CH_3$		
O-allyl	No	Yes	N/A	+ 2	N/A[3]	$O\text{-}CH{=}CH_2$		
Methoxyethoxy	No	Yes	N/A	+ 3	N/A[3]	$O\text{-}(CH_2)_2\text{-}O\text{-}CH_3$		
α-analogues	No	Yes	N/A[1]	Negative	N/A[3]	N/A[4]	N/A[4]	N/A[4]
Peptide Nucleic Acids (PNA) (Fig. 1-3D)	No	Yes	No	Positive	Positive[5]	N/A[6]	N/A[6]	N/A[6]

? = Unknown

[1] Depends on stereochemistry but affinities are generally lower than PO.

[2] Varies with buffer and other experimental conditions

[3] Chirality and charge depends on backbone structure used.

[4] Structure not drawn; the bond between the sugar and base (an *N*-glycosidic bond) of α-analogues has the reverse orientation (α-configuration) from natural (β-configuration) oligonucleotides.

[5] Typically, the C-terminus is covalently linked to a positively charged lysine residue, giving the PNA a positive charge.

[6] See Figure 1-3D for chemical structure.

1.B.2.c.ii. *Ribose Modifications*

Ribose modifications are used to generate oligonucleotides that have RNA-like character while not being as susceptible to nuclease degradation. Modifications to the sugar ring that have been tested have primarily focused on the 2' position, though the 4' position has received some minor attention [96]. Studies have investigated 2'-halide and 2'-*O*-alkyl substitutions, such as 2'-fluoro, 2'-*O*-methyl, 2'-*O*-propyl, 2'-*O*-pentyl, 2'-*O*-deoxy, 2'-*O*-allyl and 2'-*O*-methoxyethyl [31, 97-100]. Half-lives of 2' modified oligonucleotides have been found to approach that of PS oligonucleotides [81, 87, 101]. Fully 2'-modified oligonucleotides act only through steric inhibition, with no activation of RNase H, but have been found to be very effective despite this limitation [31, 100, 102].

A novel class of 2' modified oligonucleotides called locked nucleic acids have recently received attention. The structure is termed "locked" because the modification locks the furanose ring into a 3'-endo conformation by linking the 2' carbon to the 4' carbon [103]. The binding affinity of these molecules for their target has been reported to be the highest yet recorded, through decreased entropic costs of association with the target [104]. The specificity of this interaction remains in doubt, suggesting that therapeutics developed with this technology would need to be carefully chosen to avoid non-specific hybridization and potential side-effects. [103].

1.B.2.c.iii. *Base Modifications*

Modifications to the nucleoside bases have been tested primarily at the 5 and 6 positions of the base, e.g., 5-methyl, 5-bromo-2'-deoxycytidine and 7'-deazaguanosine and 7'-deazaadenosine, 5-propynyl, 5-methyl, 6-azathymidine, and 5,6-dimethyl-2'-deoxyuridine [29, 85, 105]. Increased nuclease stability from base modifications is typically exchanged for a loss of hybridization activity and/or duplex stability. Base modified oligonucleotides have shown some efficacy, including in the use of an oligonucleotide as short as a heptanucleotide [29], but have not received as much continuing attention as other modifications have proven more effective in enhancing oligonucleotide properties.

1.B.2.c.iv. *Chimeric Oligonucleotides*

Chimeric oligonucleotides take advantage of the properties of multiple modifications in the same molecule. Earlier chimeric oligonucleotides used end caps of nuclease resistant bases

with unmodified central bases [106]. It was found that oligonucleotides protected at their 3' ends resisted degradation more so than those protected at their 5' ends [107]. More recently, "mixed-backbone" oligonucleotides (also termed second-generation oligonucleotides) have been synthesized with both backbone (primarily PS) and sugar modifications [31, 108]. These molecules have improved binding affinity for their target over fully PS oligonucleotides while maintaining the ability to initiate RNase H cleavage of the RNA. When tested in the inhibition of c-fos, chimeric oligonucleotides with central PO linkages and capped PS linkages proved to have lower toxicity than fully PS oligonucleotides [109]. Circular "dumbbell" DNA/RNA chimeras have been shown to be active in the inhibition of HIV-1 replication [110].

1.B.2.c.v. *Other Modifications and Conjugates*

One of the most promising new antisense technologies utilizes a multiply modified oligonucleotide chemistry called morpholino antisense oligonucleotides [111]. These species replace the ribose sugar ring with a 6-membered morpholino ring and utilize the phosphoramidate backbone modification. With so many modifications, no cellular nuclease has been found that cleaves morpholino oligonucleotides [111, 112]. These molecules have shown activity in both cell culture and *in vivo* [113-116]. The mechanism of *in vivo* activity is not well understood, though, as it has been found that morpholino oligonucleotides do not enter cells easily and are typically administered by scrape or syringe loading [117, 118]. Though still limited as antisense molecules, morpholino oligonucleotides have already become established as a powerful biotechnological tool for functional genomics "knockdown" studies [112, 119-124].

Recent work with alternative modifications has sought to use new mechanisms of inhibition to generate a therapeutic effect. These alternative mechanisms seek to avoid "irrelevant cleavage" arising from RNase H cleavage of hybridization stretches as short as 5 – 6 nt [31]. In particular, 2'-5' linked polyadenylate (2-5A) has been shown to activate another cellular enzyme, RNase L [125]. In this case, the enzyme recognizes the (2-5A) sequence, so, the activity of RNase L can be directed at a particular transcript by conjugating to a specific oligonucleotide complementary to the target of interest, e.g., telomerase, bcr/abl mRNA, and cellular protein kinase mRNAs [125-128]. It has also been found that (2-5A) synthesized with PNA can stimulate RNase L activity and confer additional stability to the construct [129, 130].

Another "alternative mechanism" relies on the activity of the enzyme RNase P that cleaves pre-tRNA into its mature form. This enzyme, comprised of both protein and RNA components, recognizes the specific structure of the tRNA molecule in exerting its effect [131]. This structure is mimicked in application by synthesizing an oligonucleotide with a similar structure called the external guide sequence (EGS). When the arms of the EGS are hybridized by complementarity to the target RNA, the structure resembles that of a pre-tRNA, and the enzyme cleaves the targeted strand [132]. The EGS sequence is roughly 30 nt in length, however, so further development of this technology will depend on the ability to cheaply construct longer oligonucleotides for testing and to modify the EGS for nuclease resistance and affinity [131, 133].

Oligonucleotides covalently linked to active groups (e.g., intercalators such as acridine, photoactivated crosslinking agents such as psoralens and chelating agents such as EDTA-Fe) have also been investigated as potential antisense molecules [134]. The reader is directed to several reviews for a comprehensive treatment of chemically modified oligonucleotides [40, 134-137]. Oligonucleotides can also be conjugated to other species, such as proteins or lipids/cholesterol. This can enhance nuclease stability, membrane association, and internalization by cells [48, 50, 56, 138-141].

1.B.2.d. Target Site Selection

Choosing an appropriate target site in an mRNA has traditionally been a largely empirical process. Two primary factors determine whether a region within the target mRNA is a good target site: the sequence uniqueness and the ability of the oligonucleotide to exert the desired therapeutic effect. While specificity has been traditionally argued statistically, the ever-increasing availability of genome sequence information will permit direct comparison of potential target sequences to the entirety of the genome. To compare the efficacies of multiple candidate oligonucleotides, both experimental and theoretical metrics have been chosen. Of the experimental methods, both *in vitro* and cell-culture based screening assays have been developed. Theoretical metrics have evolved from satisfying basic heuristics to complex structurally-based affinity prediction methods.

1.B.2.d.i. Specificity of Oligonucleotides

The specificity of antisense-based therapeutic strategies is its most appealing aspect. The selection of a specific site was traditionally argued statistically based on the assumption of an even distribution of the 4 nucleotides throughout the genome [142]. Since each position in a given sequence can be occupied by any of four nucleotides (A, C, G or U), the total number of different possible sequences of length N bases is 4^N. Letting R equal the total number of bases in a given mRNA pool and assuming that it is a random and equal mixture of the four nucleotides, then the frequency (F) of occurrence in that pool of a sequence of length N is given by:

$$F = \frac{R}{4^N} \tag{1}$$

Assuming a typical human cell will have no more than 10^4 unique mRNA species with an average length of 2000 bases, R is approximately equal to $2x10^7$. Therefore, for a sequence to be unique ($F < 1$), N must be greater than or equal to 13 bases [142]. However, oligonucleotides cannot be made arbitrarily long, because longer oligonucleotides are more likely to contain internal sequences complementary to non-targeted RNA molecules. This has also been expressed mathematically [142]. The expected number of complementary sites (S) of length L for an oligonucleotide of length N in an mRNA pool with R bases is given by:

$$S = \frac{[(N - L + 1) \times R]}{4^L} \tag{2}$$

For example, an 18-mer (N = 18) has 6 internal 13-mers. Since a 13-mer is expected to occur 0.3 times in an mRNA pool containing 2×10^7 bases, the 18-mer is expected to match 1.8 (i.e. 6 x 0.3) 13-mers in the mRNA pool. Equation (2) also gives this result (N = 18, L = 13, and $R = 2 \times 10^7$; therefore, S = 1.8).

Woolf et al. have demonstrated that significant degradation of non-targeted mRNAs can occur [142]. They compared the effectiveness of three different 25-mers in suppressing the expression of fibronectin mRNA in *Xenopus* oocytes. Nearly 80% of the fibronectin mRNA was degraded after the oocytes were microinjected with a 25-mer in which all 25 of its bases were complementary to the mRNA. However, when the oocytes were microinjected with 25-mers that had only 17 or 14 complementary bases flanked by random sequences, greater than 30% of their fibronectin mRNA was still degraded. They also showed that a single mismatch in an oligonucleotide did not completely eliminate its antisense effect. Over 40% of the target mRNA was degraded when oocytes were treated with a 13-mer with one internal mismatch, though the

mismatch left a 9 base consecutive complementary sequence that showed nearly the same activity as a 13-mer with 10 complementary bases in succession.

The efforts to sequence the human genome have begun to provide more information about the actual specificity of oligonucleotides. It is possible to scan for sequences against all of the genomic information available using resources such as BLAST at the National Center for Biotechnology Information [143](http://www.ncbi.nlm.nih.gov). The results will determine the uniqueness of the oligonucleotide within the known database sequences. As the completeness of the databases grows, computational comparisons of target RNA sequences against the database will provide more reliable assessments of the uniqueness of these target sequences within the genome.

1.B.2.d.ii. *Oligonucleotide Evaluation and Comparison*

Active antisense oligonucleotides are typically identified from a group of candidates, perhaps 20-50 sequences, by trial and error using a cell-culture based screening assay [28, 144, 145]. The candidates are chosen with no *a priori* knowledge or guidance. The assays required to evaluate these oligonucleotides can require significant time and cost and often yield few active oligonucleotides, even outside of the context of cells [8]. Little guidance is available from the mRNA, either, given that active molecules have been identified in the 5' and 3' UTRs as well as around the start codon and within the coding sequence [146, 147]. Thus, random cell-culture based experimental screening has given way to *in vitro* experimental and theoretical evaluation of oligonucleotide binding affinity and target accessibility.

1.B.2.d.ii.a. *in vitro* Experimental Comparison

To test the affinity of oligonucleotides for their target mRNA *in vitro*, methods have been developed that can provide both detailed information of a few oligonucleotides or general information comparing a large-number of oligonucleotide candidates. One small-scale technique that is used to measure oligonucleotide hybridization strength is melting temperature measurement, where higher transition temperatures reflect increased hybridization strength [108]. This method only examines the intermolecular hybridization strength and only does so at non-physiologic temperatures. For these reasons, melting temperature is, at best, an incomplete metric for evaluating the relative hybridization strengths of oligonucleotides.

Though developed for evaluating the affinity of proteins for other proteins, nucleic acids, and small molecules [148, 149], the gel-motility shift assay is also a useful method for evaluating the affinity of oligonucleotides for their target mRNA [150, 151]. In this technique, radiolabeled oligonucleotide is hybridized with the target mRNA at different concentrations. After equilibrium has been reached, bound oligonucleotide is separated from free oligonucleotide by electrophoresis, the movement of the bound oligonucleotide being restricted by its association with the larger mRNA species. The affinity of each oligonucleotide is then extracted from the fractional binding data at each mRNA concentration (K_D = the [RNA] at which 50% of the oligonucleotide is bound). This assay is limited by the difficulty in analyzing a large number of samples as well as by the buffers that can be used. The most problematic weakness, though, arises from the fact that the signal for detection is a function of oligonucleotide concentration. With the small volumes that can be loaded onto an electrophoresis gel and the difficulty and expense in uniformly labeling oligonucleotides, the assay cannot measure the affinities of the highest affinity oligonucleotides ($K_D < 0.01$ nM), and there exists little flexibility to enhance the sensitivity.

Of the large-scale, combinatorial techniques that have been applied, these can be separated into two separate types, those that utilize RNase H screening and those that involve hybridization to arrays. Each of these techniques identifies those oligonucleotides that hybridize with high affinity for their target. Though RNase 1 cleavage of single stranded regions on the RNA has also been examined as a possible method for identifying accessible regions on the RNA [152], RNase H has proven a much more successful method. For RNase H screening experiments, semi-random libraries of oligonucleotides are hybridized with a target mRNA in the presence of the enzyme [153]. The resulting fragments are sequenced to locate those regions on the mRNA that are particularly susceptible to cleavage, typically showing significant cleavage in fewer than 30 minutes, the longest typical reaction time. This technique has been shown to identify reagents effective in cell culture and *in vivo* with roughly 30-50% accuracy [153, 154]. These results confirm the kinetic nature of the hybridization reaction and the need for oligonucleotides to bind quickly to exert a therapeutic effect. However, no judgment regarding the relative affinities of these molecules can be made, as hybridization has not been allowed to reach equilibrium for all the oligonucleotides.

In contrast, oligonucleotide array experiments are specifically designed to identify those oligonucleotides that bind most tightly at equilibrium conditions. Radiolabeled mRNA at a concentration that will discriminate among the oligonucleotides is hybridized to an array of oligonucleotides that have been immobilized on a solid substrate, e.g., a glass slide [155, 156]. Following incubation for an extended time, e.g., 16 hours, the slide is washed to remove non-specifically adsorbed material and exposed for radiographic detection of the bound mRNA. Those regions that show the highest radiographic intensity are the regions containing the oligonucleotides of highest affinity for the mRNA. The oligonucleotides of highest affinity have proven effective antisense reagents in cell culture and *in vivo* [156, 157]. The significant experimental cost of preparing the arrays precludes widespread use of this technique. Also, as the RNA is only applied at a single concentration and no measure of the fractional binding of the mRNA and oligonucleotide can be determined, measurement of exact binding affinities for each oligonucleotide is challenging, leaving the oligonucleotides to be grouped into classes of high, moderate, and low binding affinity.

1.B.2.d.ii.b. Theoretical comparison

The application of theoretical methods has progressed from simple techniques examining the primary sequence of the target mRNA to those that account for the role of structure in the hybridization process. Early studies applying these simpler metrics for selection have proven only slightly more successful that pure random choice. Over time, the sophistication of secondary structural prediction has been enhanced and the incorporation of and comparison to experimental data sets of sufficient size have proven that theoretical methods of selection can provide valuable guidance in selecting those oligonucleotides that will be most active in cell-culture and *in vivo*.

1.B.2.d.ii.b.i. Primary Sequence Motifs and G/C Content

The translational start codon is the initial primary sequence target chosen for many antisense screens, particularly those using cell-culture based screening assays. Oligonucleotides are chosen in the region of the start codon and slightly upstream and downstream with the expectation that prevention of translation initiation will most effectively prevent translation progression [58]. Also, it has been proposed that the region around the start codon tends to be more structurally flexible than the remainder of the RNA to avoid inhibiting ribosomal binding

[58]. However, the high rate of failure sequences and recent data from oligonucleotide array experiments [157] suggest that this proposal is not generally accurate, and, therefore, oligonucleotides in this region should be no more effective, in general, than oligonucleotides targeting any region along the mRNA.

In studies where large sets of experimental data have been reviewed and analyzed statistically, primary sequence motifs have been identified that are found to occur frequently in those oligonucleotides that show activity in cell culture experiments [158, 159]. These four-base motifs (CCAC, TCCC, ACTC, GCCA, CTCT) are C-rich and proposed to enhance the formation of A-form heteroduplexes and the recruitment of RNase H to cleave the target mRNA. Though the statistical analyses confirm the significance of these motifs, the correlation coefficients are at most 0.3, indicating that selection of oligonucleotides by this metric will still yield a large proportion of failures.

Another first-order method for selecting oligonucleotides with high affinity for the target mRNA is to select those with high GC content. The additional hydrogen bond in a G/C pair provides additional stability to the intermolecular complex and thereby results in a more stable hybrid. Success using GC selection is sporadic [160] and could also result in molecules that achieve their action through the formation of structural elements such as the tetra-guanine motif [161-163]. Also, use of this metric or any of the primary sequence techniques ignores the prominent role of RNA structure in the association of oligonucleotides with the RNA.

1.B.2.d.ii.b.ii. Secondary Structural Prediction

In comparison to primary sequence based comparison strategies, incorporation of secondary structure information provides additional complexity and enhanced accuracy in locating those regions on the mRNA that will be good target sites for antisense oligonucleotides. Secondary structures are those structures that form from the Watson-Crick base-pairing that occurs within the RNA molecule. Secondary structural features tend to form more quickly than tertiary features and have been shown to provide the majority of the three-dimensional character of RNA molecules [164], though in some cases, tertiary structure formation can alter existing secondary structures [165, 166]. Reasonably accurate predictions of the RNA secondary structure can be computed from free-energy minimization, and these predictions form the basis

of computational evaluation of oligonucleotide binding affinity and candidate oligonucleotide selection [167-169].

Prediction of RNA secondary structure was described in the literature as early as 1981 [170]. Using a dynamic programming algorithm, all possible structures are iteratively folded and their free energies calculated using nearest-neighbor thermodynamic parameters measured *in vitro* using small RNAs [171-173]. The resulting structures can be shown in tree diagrams for viewing a single structure (Figure 1-4) or in "dot-plot" format (Figure 1-5) to more completely describe the flexibility of the RNA and the reliability of the predicted structure and the overall flexibility of the molecular structure.

Several researchers have sought to use RNA structural predictions as a basis for selecting effective antisense oligonucleotides. The earliest methods focused on examining the structure of the target mRNA and identifying structural or energetic features that suggested a good target region for antisense inhibition, e.g., targeting regions predicted to be single-stranded [174]. When examining the 30 most energetically favorable folded structures, regions were identified that had a high probability of being unpaired [175]. This method was only found to be useful in identifying those oligonucleotides that were active in reducing *in vitro* translation when RNase H was present. The lack of inhibition in the absence of RNase H suggests that the oligonucleotides identified may form partial heteroduplexes of 4 or more bases in those regions that are kinetically accessible and will activate RNase H but do not form sufficiently stable complexes to prevent ribosomal binding and progression. Unpaired percentage, then, is not an effective metric for identifying those oligonucleotides that hybridize completely and can act through both inhibitory mechanisms. Also, it has been shown that regions predicted to be double-stranded are, in some instances, more susceptible targets for antisense inhibition than single-stranded regions [176, 177]. More sophisticated methods have since focused on incorporating the energies of folding into defining those regions that should be targeted by antisense.

A metric called "local folding potential" was proposed to identify those regions in the mRNA that showed structural flexibility in a large number of the most favorable, predicted structures [178]. The free energy of folding for 400 nt overlapping segments along the mRNA was calculated and averaged for each position along the mRNA. Correlation was found between low folding potential, i.e., regions very likely to be free of significant secondary structure, and

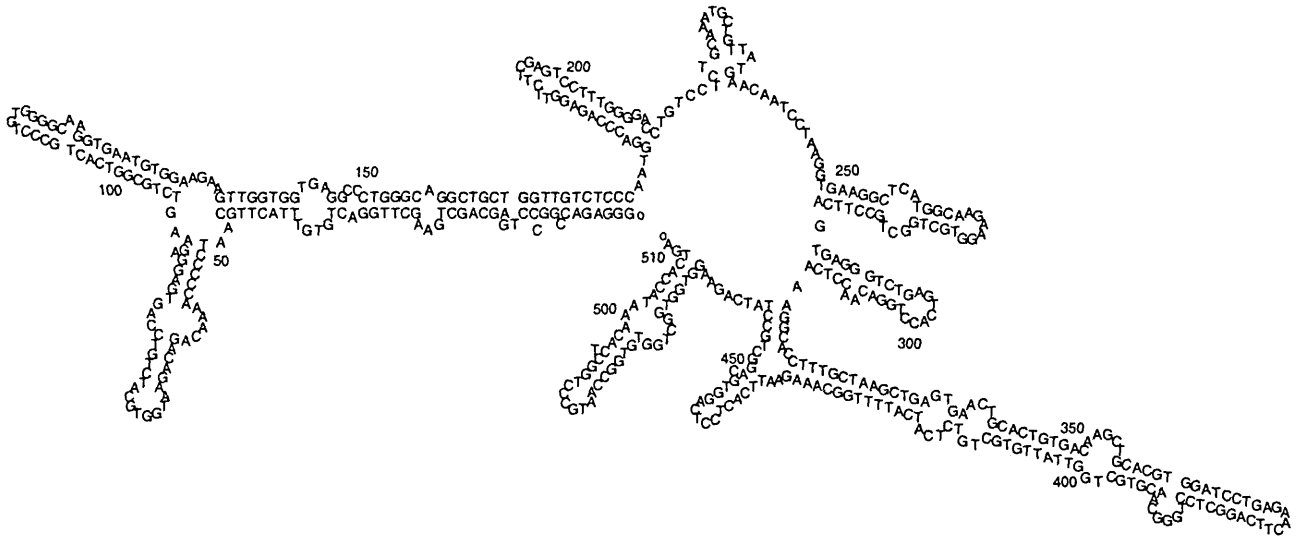

Figure 1-4: Predicted secondary structure of the RBG mRNA

The most-energetically favorable conformation of RNA molecules is highly folded. The majority of RNA folding results from intermolecular base pairing. For this 510 nt transcript, the longest single-stranded region is 12 nt. Any oligonucleotide of typical length (15-25 nt) will have to disturb native structure to exert its therapeutic effect. The accessibility of a region on the target will be a function of both its double-stranded and single-stranded regions and their interactions with the oligonucleotide.

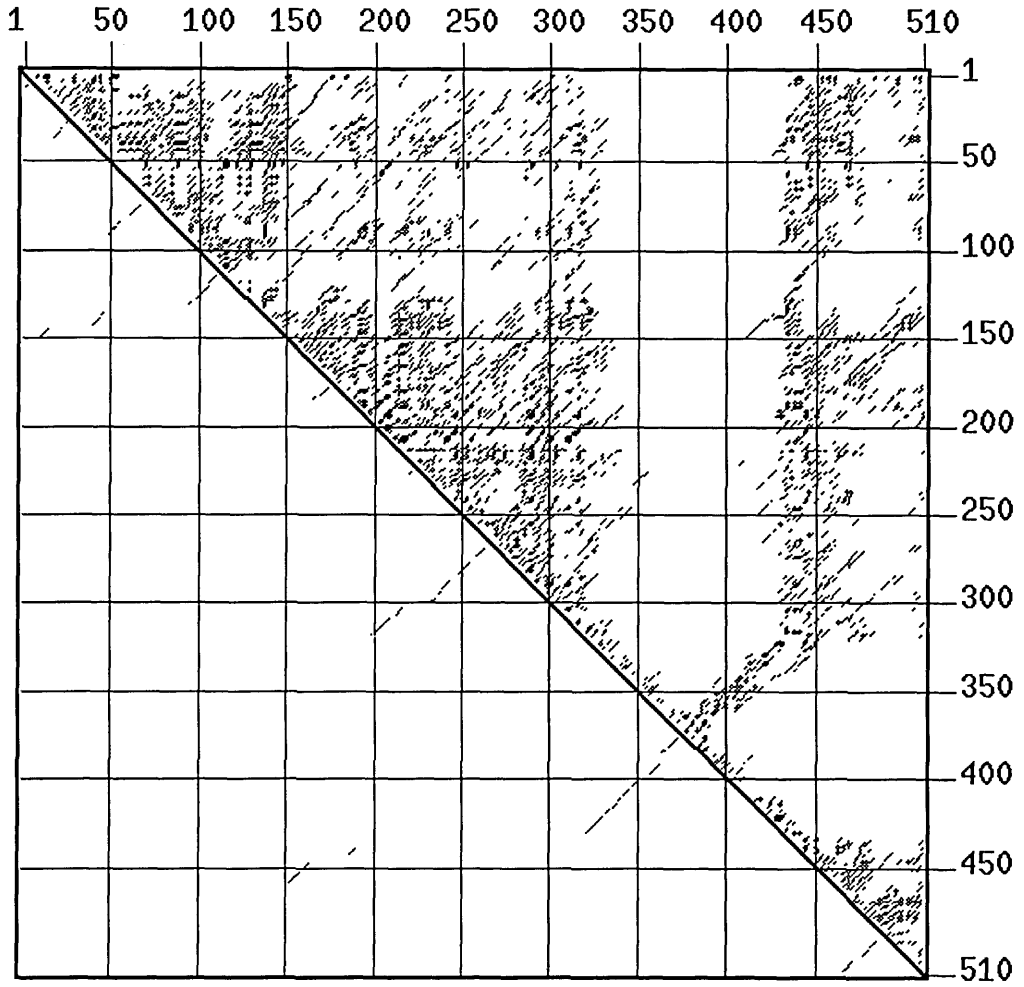

Figure 1-5: "Energy dot plot" of the RBG mRNA

In this depiction, a base pair between nucleotide X and nucleotide Y is indicated by a dot at the two corresponding positions on the grid, (X , Y) and (Y , X). The base pairs occurring in the minimum free energy (optimal) structure are shown alone in the lower triangle, while the upper triangle includes the optimal and suboptimal structures within a user-defined free energy interval of the minimum. Regions in the upper triangle that are densely spotted indicate significant structural flexibility while sparse regions indicate very stable structural elements.

those antisense RNAs that were found to be inhibitory. Concomitantly, regions of high folding potential were found to be poor antisense targets. This confirms the strong role of the structure of the target mRNA in determining those sequences that will show inhibitory activity. It is this highly ordered structure that provides the basis for establishing a rational framework for selection of oligonucleotides with high binding affinity described here.

1.C. Approach and Specific Aims

The objective of the work was to establish a methodology for the rational selection and evaluation of oligonucleotides to be used as antisense therapeutics. The selection method focused on applying a thermodynamic model to analyze the energetics of hybridization and identify those oligonucleotides that are predicted to have the highest binding affinity for their target mRNA. Despite the highly kinetic nature of the antisense mechanism, it was expected that the most discriminating step in the activity of oligonucleotides would be the hybridization interaction. If this interaction could be accurately predicted, it would provide a foundation for selection of optimally active oligonucleotides. Idealizations would be required in the development of any theoretical construct, and, therefore, *in vitro* testing would be required to support the continuing study of selected candidates. Subsequent cell culture testing of candidate molecules would confirm the reliability of the *in vitro* measurements and further support the use of the predictive methodology as a simplified method for the selection of candidate antisense oligonucleotides.

The Specific Aims of the project were to:

1. **Develop a method for selection of optimally active oligonucleotides against a candidate mRNA based on the molecular thermodynamics of the hybridization event.**

Theoretical techniques applied to this point have failed to recognize oligonucleotide hybridization as a stepwise process involving intermolecular interactions between the oligonucleotide and mRNA as well as structural rearrangements of both molecules and the heteroduplex. In most cases, the use of theoretical predictions has been dismissed as not helpful in identifying candidates or inaccurate in comparison to empirical measurements [156, 179]. Taking advantage of the ability to predict folded structures of mRNAs and oligonucleotides and

obtain the free energies for these folded structures, it was decided that molecular thermodynamics would accurately describe hybridization if based on a complete thermodynamic cycle. Results are shown to correlate well with data from the literature on two systems, particularly in the identification of those oligonucleotides measured to have the highest binding affinities.

2. **Measure *in vitro* binding affinities and kinetics and compare with thermodynamic predictions.**

The accuracy of the thermodynamic predictions was measured in idealized conditions *in vitro* using a novel centrifugal-based assay. The assay also proved useful in measuring the kinetics of hybridization. It was found that the binding affinity is primarily determined by the association kinetics and that those molecules that associate with the fastest kinetics also activate RNase H cleavage of the mRNA most quickly.

3. **Measure antisense inhibition in cell-culture to determine if selection of antisense oligonucleotides by thermodynamic prediction increases the success rate over random selection.**

Oligonucleotides of two different chemistries were selected using the thermodynamic method and applied to inhibit the expression of three genes, lactate dehydrogenase isozymes A and B, as well as cell-surface signaling receptor, gp130. In each case, mRNA levels and protein activity were measured. Of the 5 oligonucleotides expected to exert a biological effect, 4 showed significant inhibition of their target mRNA at sub-micromolar concentration. In all cases, reduced protein activity was associated with reduced mRNA levels. Nonsense oligonucleotides and oligonucleotides expected not to show activity did not significantly inhibit at either the protein or mRNA levels, reinforcing both the sequence specificity of the inhibition and the utility of the thermodynamic predictions for selecting active candidate molecules. The success rate was roughly 80% relative to 15% estimated for random selection.

2. *Development of Thermodynamic Model of Oligonucleotide Binding*

2.A. *Abstract*

Antisense oligonucleotides, which act through the pairing of complementary bases to an RNA target sequence, are showing great promise in research and clinical applications. However, the selection of effective antisense oligonucleotides has proven more difficult than initially presumed. We have developed a prediction algorithm to identify those sequences with the highest predicted binding affinity for their target mRNA based on a thermodynamic cycle that accounts for the energetics of structural alterations in both the target mRNA and the oligonucleotide. The model was used to predict the binding affinity of antisense oligonucleotides complementary to the rabbit β-globin (RBG) and mouse tumor necrosis factor-α (TNFα) mRNAs, for which large experimental data sets were available. Of the top ten candidates identified by the algorithm for the RBG mRNA, six were the most strongly binding sequences determined from an experimental assay. The prediction for the TNFα mRNA also identified high affinity sequences with ~60% accuracy. Computational prediction of antisense efficacy is more cost efficient and faster than *in vitro* or *in vivo* selection and can potentially speed the development of sequences for both research and clinical applications.

2.B. *Introduction*

Oligonucleotides, single-stranded DNA molecules typically 15-20 nucleotides (nt) in length, can be used as antisense molecules to affect gene expression upstream of protein synthesis. When exogenously added to cells, these oligonucleotides are designed to be internalized, bind to their complementary target by Watson-Crick base pairing, and inhibit the production of the protein encoded by the target mRNA. Currently, antisense oligonucleotides are being developed as clinical therapeutics against refractory diseases such as cancer and HIV, but they are also powerful tools for analyzing and manipulating gene expression in applied biotechnology research [180].

The ideal antisense oligonucleotide would have the greatest specific inhibition of gene expression at the minimum possible concentration. To date, active oligonucleotides have been chosen empirically by trial-and-error using an *in vitro* or *in vivo* assay. The sequences of the oligonucleotides are often selected using heuristics such as targeting the start codon of the mRNA. However, only a small proportion of attempted antisense oligonucleotides provide sequence specific inhibition at reasonable concentrations [160, 181, 182]. As a result, the selection of effective antisense sequences based on affinity for their target RNA has received increasing attention.

Binding affinity can be measured by a number of empirical screening approaches based on the direct hybridization of candidate oligonucleotides to target mRNA. These include small scale methods, including gel shift assays [150] and melting temperature measurements [108], and large scale techniques, such as incubation of the target mRNA with combinatorial libraries [177, 183] or oligonucleotide arrays [156, 184]. These screens have also found a relatively low proportion of antisense sequences to exhibit high affinity for their target, suggesting that affinity is indeed a limiting factor in antisense effectiveness. Though these screens can identify oligonucleotides with high target affinity, they are quite elaborate, and concerted searches of all possible oligonucleotides remain a major experimental challenge. Hence, theoretical strategies are also being considered.

The first such strategy focuses on selecting oligonucleotides with high GC content. However, this simple rule has proven only marginally successful [160]. Also, this method of selection could also result in molecules that achieve their action non-specifically, e.g., by acting

through a tetra-guanine structural motif [161]. Predictions of RNA folding structures have been used in design strategies that are based on finding locations on the mRNA predicted to be single-stranded, and, presumably, accessible to oligonucleotide binding [175, 178]. However, it has been shown that regions predicted to be double-stranded are, in some instances, more susceptible targets for antisense inhibition than single-stranded regions [176, 177]. Therefore, considering the RNA target alone is insufficient to identify good binding sites for oligonucleotides.

We have developed a method that uses the RNA secondary structure prediction algorithm, *mfold* [167, 168], and an appropriate thermodynamic cycle to predict the free energy of hybridization between an antisense oligonucleotide and its target mRNA. The key feature that is distinct from previous approaches is that the method described here accounts for restructuring of the RNA after being bound by the antisense oligonucleotide. Using the rabbit β-globin (RBG) and mouse tumor necrosis factor-α (TNFα) mRNAs as model systems for which sufficiently large experimental data sets were available, we have used this method to identify, theoretically, those oligonucleotide sequences which most strongly bound their RNA targets. We found that the model accurately predicted the general trend in binding affinity for all oligonucleotide sequences and clearly distinguished the highest affinity sequences from those of low affinity. Furthermore, we found that accounting for all of the steps in the thermodynamic cycle was necessary for the most accurate predictions.

2.C. *Theory and Methods*

The goal of our model was to predict the free energy of hybridization of an antisense oligonucleotide to its target RNA, given the sequence of the RNA. The sequence of the RBG mRNA was provided by the investigators of the experimental study [156]. The TNFα mRNA sequence was obtained from GenBank (Accession #: M13049). As the free energy is a thermodynamic state variable, any free energy change can be represented as the sum of all steps required to make the change, regardless of whether the steps correspond to the path followed in the actual process. The basic framework of the decomposition is shown in Figure 2-1. In this case, the processes are the unfolding of the structured RNA and any oligonucleotide structure, which have unfavorable free energies of ΔG°_{UN} and ΔG°_{OS}, respectively, and the binding of the oligonucleotide to the exposed target sequence followed by the refolding of the RNA to a new

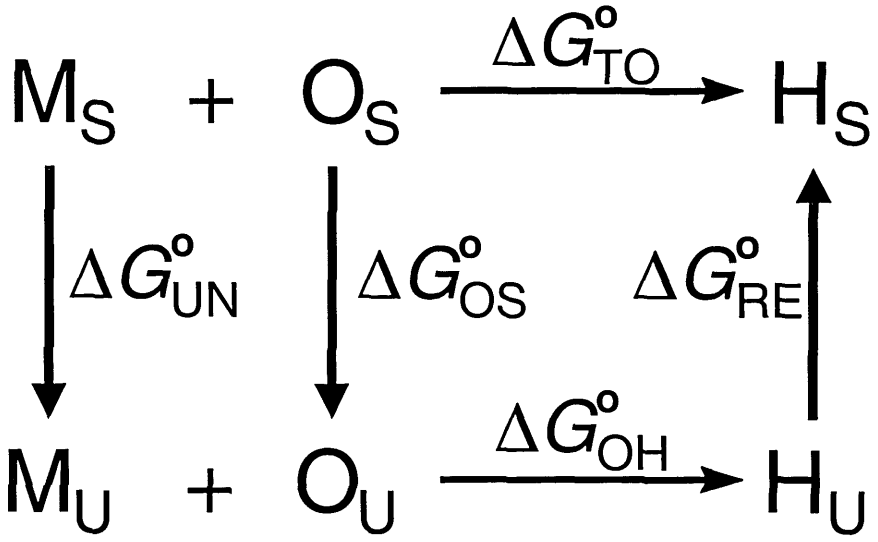

Figure 2-1: Thermodynamic construct describing oligonucleotide:mRNA hybridization
M = mRNA; O = *oligonucleotide*; *H* = *oligonucleotide*:mRNA hybrid. S = structured; U = unstructured. In the hybridization process, structured mRNA molecules hybridize to oligonucleotides that may or may not have some stable intermolecular folding to form a hybrid with the most favorable, constrained folded structure. In the first conceptual steps, these two molecules are "unfolded" to make the target site on the mRNA and the oligonucleotide single-stranded, with associated free energy costs ΔG°_{UN} and ΔG°_{OS}. These molecules can then hybridize with free energy ΔG°_{OH}. Finally, the unstructured hybrid refolds to the most energetically favorable conformation available with free energy ΔG°_{RE}. The sum of these energy terms, ΔG°_{TO}, is related to the intermolecular dissociation constant by $\Delta G^\circ_{TO} = RT\ln(K_D)$.

minimum energy structure, which have favorable free energies of ΔG°_{OH} and ΔG°_{RE}, respectively. The summation of these energy terms yields the total energy for the hybridization, ΔG°_{TO}.

An RNA molecule is folded into a minimum energy structure that is dictated primarily by the intramolecular base-pairing configuration. The structural energies for unfolding and refolding were found using the secondary structural prediction algorithm, *mfold* [167, 168]. The dynamic program generates the minimum free energy folded mRNA structure by calculating, using established thermodynamic parameters, the energy for all possible configurations of intramolecular base pairs in the mRNA [168]. The first part of the calculation, the fill algorithm, calculates the folding free energy of the base-pairing that occurs between any two pentanucleotides. It then recursively calculates the energies for the possible hexanucleotide hybridization patterns, and so on. The traceback algorithm then searches all of the accumulated free energies and constructs the minimum free energy structure from the possible base-pairing patterns identified. Suboptimal free energy structures can then be constructed by selecting base-pairing motifs that are not contained in the global minimum free energy structure. The limits on the allowed suboptimality and the number of tracebacks are user-specified, as is the parameter dictating how "close" in final structure folding computations are allowed to be. In addition to locating the optimal folded structure, the dynamic program allows user-specified constraints to the structure, permitting incorporation of chemical and enzymatic structural information into the predictions to ensure the greatest accuracy of the prediction.

The mRNA folding free energies, ΔG°_{UN} and ΔG°_{RE}, were calculated using the minimum free energy structures predicted from *mfold* at 37°C. ΔG°_{UN} was taken to be the negative of the folding free energy for the sequence without constraints (98.2 kcal/mole) and is independent of the targeted sequence in the mRNA. For each 17mer oligonucleotide within the first 122 nt of the RBG mRNA, ΔG°_{OH} was calculated by summing the individual nearest neighbor components for each base pair using parameters correlated for DNA:RNA hybridization [185]. Any oligonucleotide dimerization was ignored. To determine ΔG°_{RE} for each oligonucleotide:RNA hybrid, the "Single Prohibit" function of *mfold* was used to specify the targeted bases of the mRNA as being unavailable for intramolecular base pairing. Thus, ΔG°_{RE} corresponds to the

minimum free energy structure computed under these constrained conditions. ΔG°_{OS} accounts for any secondary structural features of the 17-mer oligonucleotides and was determined for each oligonucleotide using the *mfold* program with nearest-neighbor parameters for DNA [186]. Only positive ΔG°_{OS} values (i.e., favorable oligonucleotide folding energies) were included in ΔG°_{TO} calculations. The total free energy for binding of the oligonucleotide to the mRNA, ΔG°_{TO}, was calculated as the sum of the unfolding (RNA and oligonucleotide), hybridization, and restructuring energies:

$$\Delta G^{\circ}_{TO} = \Delta G^{\circ}_{UN} + \Delta G^{\circ}_{OS} + \Delta G^{\circ}_{OH} + \Delta G^{\circ}_{RE} \quad (1)$$

Though in reality the structural changes of the RNA will not follow the path assumed in the model, this representation of the process accounts for the energetics of any structural changes that will occur, if both the initial and final structures of the RNA are the ones that are thermodynamically most favored.

In calculating ΔG°_{UN} and ΔG°_{RE}, the whole RNA sequence was not used. The sequence was segmented into separate domains, and only the domain containing the oligonucleotide target sequence was refolded to a new structure. Domains of short-range interactions were chosen from the "energy dot plot" created by *mfold* (Figure 2-2). The domains are characterized by a large density of potential folding structures between the endpoints of the domain with few intramolecular interactions outside of this region [187]. For the 608 nt RBG mRNA, three domains were observed, the first consisting of the first 314 nt. Since the sequences investigated using the oligonucleotide array assay [156] and in our predictions here were all within the first 122 nt, only this first domain was used in the folding calculations.

For the RBG mRNA, the model predictions were compared to experimental data generated by incubating radiolabeled RBG mRNA with a glass slide on which were immobilized all possible complementary oligonucleotides of length 1-17 nt [156]. The radiographic intensity, I, measured with a PhosphoImager, is proportional to the number of hybrids, H, over a large range, and we assume that this proportionality held in their experiment. To develop a correlation between our predictions and these results, we use the equilibrium relationship between binding affinity K_H of a particular oligonucleotide sequence with surface concentration O to the target

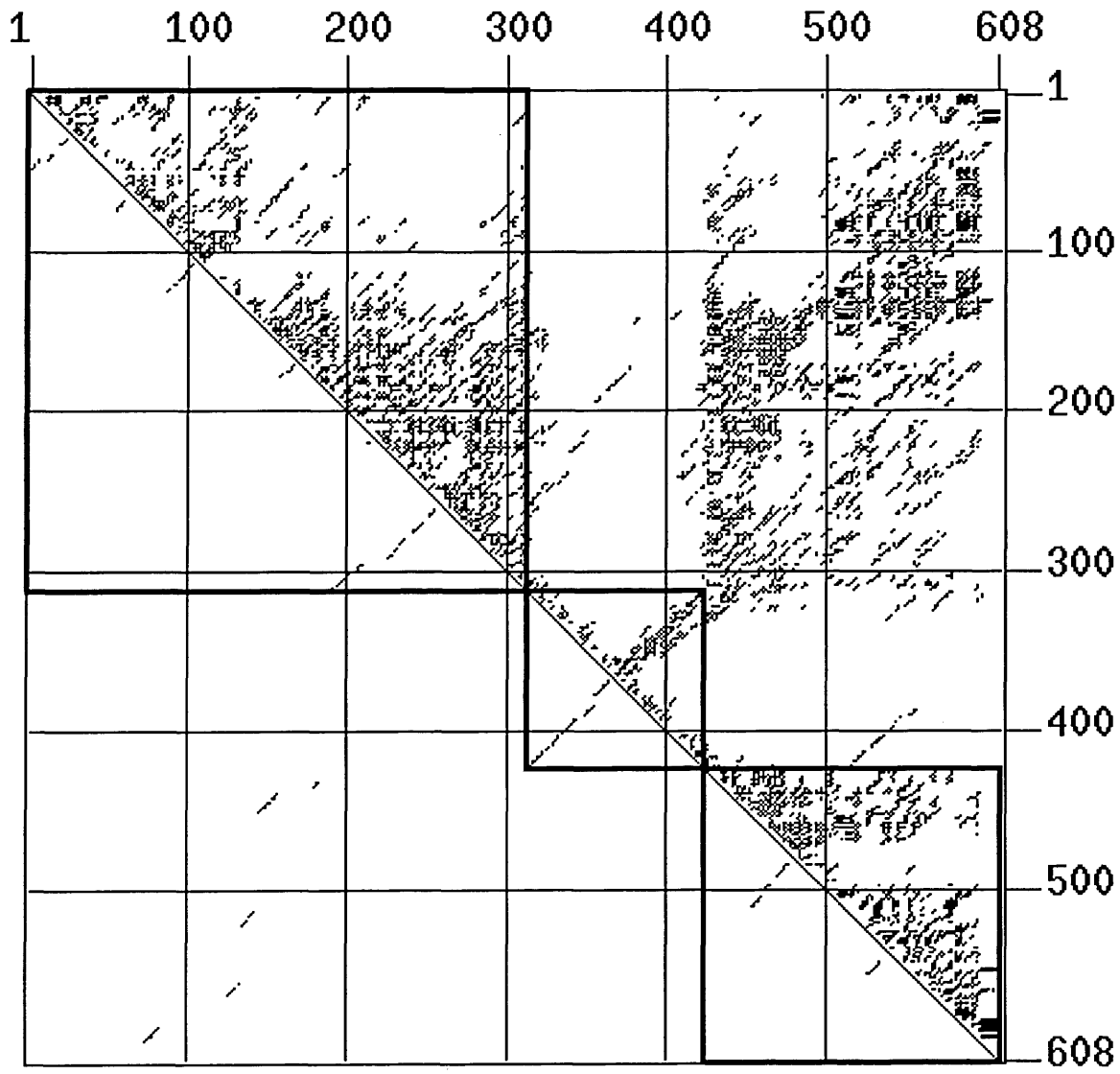

Figure 2-2: "Energy dot plot" for Southern transcript of the RBG mRNA
Each dot represents a potential base pair that can occur in any structure with a calculated folding free energy within 12 kcal/mole of the minimum folding free energy. Dots appearing in the lower triangle are those base pairs that occur in the minimum free energy structure. Long-range base pairing has been ignored by defining regions of primarily self-contained folding as delineated by the thick black lines at nt 314 and 425. The region of folding between nt 314 and 425 is particularly stable, showing few if any alternative foldings.

RNA, present at bulk concentration M:

$$K_H = \frac{H}{OM} = e^{-\frac{\Delta G_{TO}}{RT}} \tag{2}$$

At equilibrium, the bulk concentration of mRNA may be less than at the beginning of the experiment but nonetheless has some finite value. The total amount of oligonucleotide O_T is distributed between unbound oligonucleotide O and hybridized species H. Thus, equation (2) can be rearranged to give an expression for H:

$$H = \frac{O_T M K_H}{1 + M K_H} \tag{3}$$

Furthermore, no saturation of oligonucleotide binding was observed. For low concentration of mRNA relative to the dissociation constant ($MK_H << 1$), the concentration of hybrids is approximately:

$$H \cong O_T M K_H . \tag{4}$$

The concentration of RBG mRNA used was very low (100 pM), so this may be justified for $K_H < 10^{10}$ M^{-1}. The fact that the intensities displayed in Figures 2-3 and 2-4 do not show a clustering at high values suggests that the oligonucleotides are not being saturated and, therefore, that these assumptions are approximately correct. Even if this condition is not strictly accurate (for high affinity binding), the general correlations of this paper and the ranking of predicted energies will still be valid.

Combining (2) and (4) yields the relationship between the free energy and the number of hybrids:

$$-\Delta G^{\circ}_{TO} = RT \ln H - RT \ln(O_T M) \tag{5}$$

As a result, the computational results are presented as $-\Delta G^{\circ}_{TO}$ versus $\ln(I)$, since the intensity on the radiograph should be proportional to the number of hybrids formed.

Predictions were also compared to binding affinity data for 12-mers complementary to the TNFα mRNA [150]. These data were generated using a gel-shift assay to determine K_D, the concentration of mRNA at which 50% of the oligonucleotide was bound to the mRNA. The

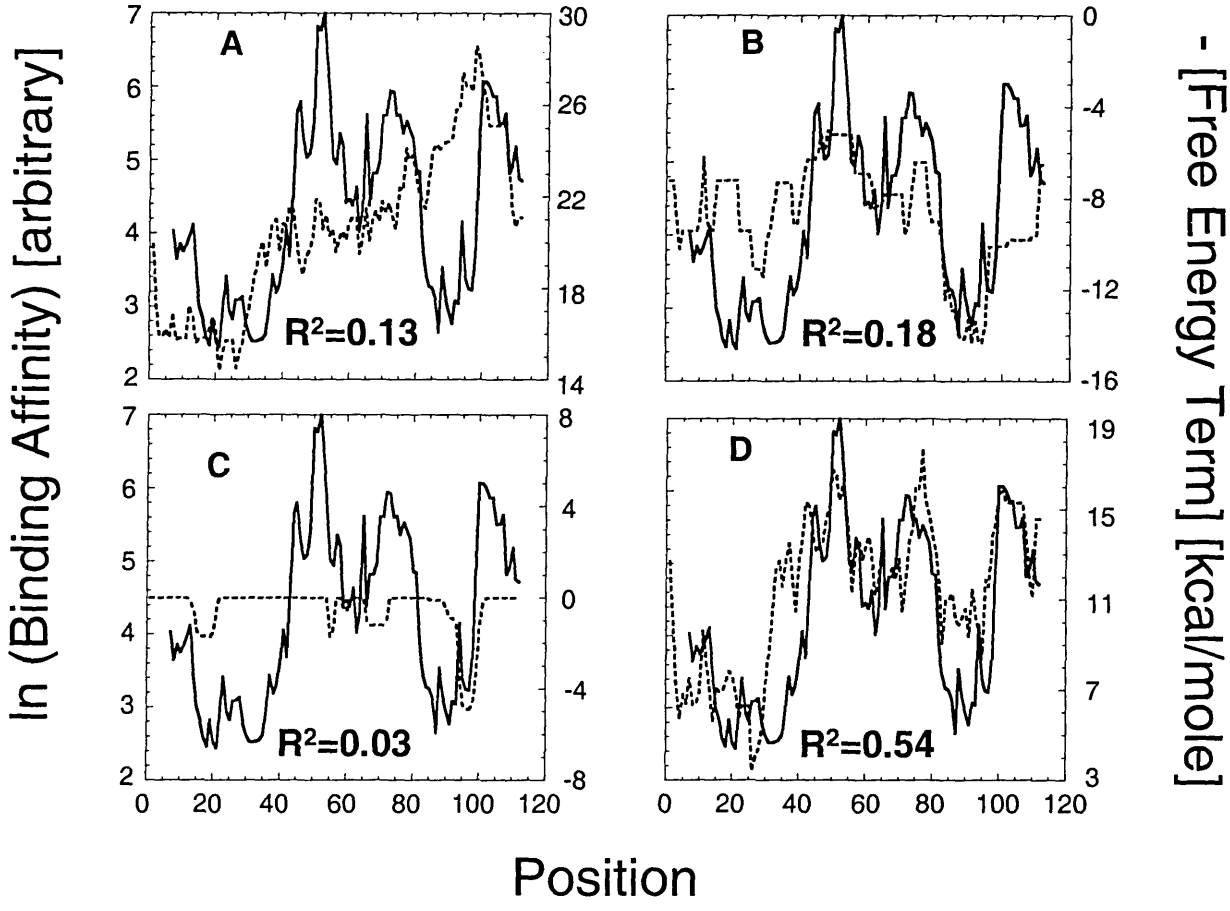

Figure 2-3: Comparison of experimental (ln(Intensity)) and predicted free energy terms
All of the figures show the negative of the free energy component.
a) $-\Delta G^{\circ}_{OH}$, b) $-\left(\Delta G^{\circ}_{UN} + \Delta G^{\circ}_{RE}\right)$ c) $-\Delta G^{\circ}_{OS}$, and d) $-\Delta G^{\circ}_{TO}$. Listed position is the 5'-terminal base of the mRNA to which the 3'-terminal base of the oligonucleotide hybridizes. —— ln(Intensity), ------- $-\Delta G^{\circ}$. R^2 values calculated from curve fits of plots of negative free energy versus ln(Intensity) for each component. Each component contributes to the accuracy of the model. However, no component as accurately models the data as the overall free energy, $-\Delta G^{\circ}_{TO}$ (Figure 2-3d).

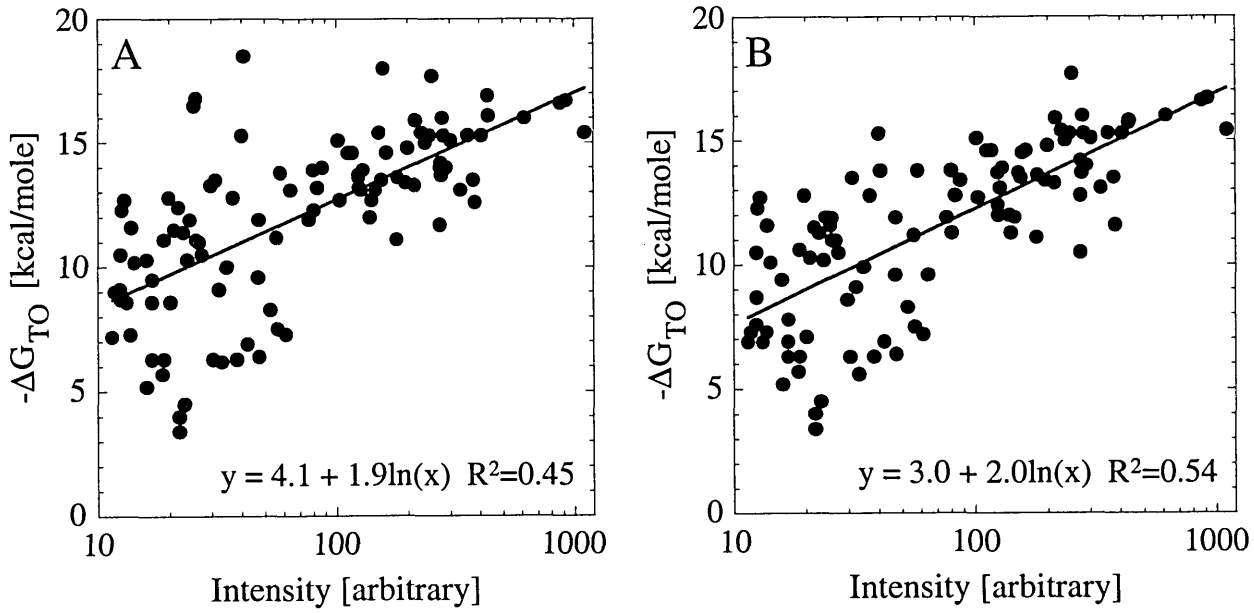

Figure 2-4: Correlation of experimental (ln(Intensity)) and predicted ($-\Delta G_{TO}$) binding) A). Without considering oligonucleotide structure contribution. B.) Including oligonucleotide structure contribution. The contribution from oligonucleotide structure only affects the predicted free energy values for a fraction of the oligonucleotides, but correlation is noticeably improved.

"energy dot plot" indicated that the mRNA consisted of 2 domains (808 and 524 bases). The corresponding ΔG°_{UN} values for the 808 base and 524 base segments were 241.9 and 136.7 kcal/mole, respectively.

2.D. *Results*

2.D.1. Correlation of predictions with oligonucleotide array for RBG mRNA

Initially, we compared the model predictions to the most extensive set of antisense oligonucleotide:mRNA binding affinity data available [156]. The data set was produced using a glass slide on which were immobilized all oligonucleotides complementary to 1-17 nt segments of the first 122 bases of the RBG mRNA. To this array, radiolabeled mRNA was added and its binding to each oligonucleotide quantified using a PhosphoImager and image analysis software. Under the conditions of the experiment, the natural logarithm of the measured intensity, I, can be considered to be roughly proportional to the equilibrium constant for the hybridization (see Methods). Binding was found to be strongest for the longest oligonucleotides, with no marked variation of the loci of binding with length.

As a result, we focused our efforts on the prediction of ΔG°_{TO} for each 17mer oligonucleotide fully complementary to segments within the first 122 bases of the RBG mRNA. The measured $\ln(I)$ and the predicted free energy components are plotted as a function of position along the mRNA in Figure 2-3. The position values correspond to the 5' base of the targeted sequence on the mRNA. Each component of the free energy correlates with some portions of the intensity profile (Figures 2-3a - 2-3c). However, the aggregate, ΔG°_{TO}, most closely mimics the form of the intensity profile, both in the locations and relative magnitudes of the local maxima and minima (Figure 2-3d). The correlation between ΔG°_{TO} and the $\ln(I)$ is shown explicitly in Figure 2-4. Indeed, there is a statistically significant positive correlation between the two quantities, as determined by a t-test with $\alpha = 0.0005$ [188]. From Equation 5, the slope of the line in Figure 2-4 should equal RT, which is ~0.6 kcal/mole at 37°C. The curve fit has a slope of 2.0 ± 0.6, which is somewhat higher but reasonable given the simplifications in the derivation of the equation.

2.D.2. Predictions applied to selection of candidate oligonucleotides

For use as biological research tools and as candidate therapeutic molecules, antisense oligonucleotides should have the highest possible affinity for their target. As shown in Table 2-1, the six highest affinity sequences located by the oligonucleotide array assay [156] were among the ten lowest predicted total free energies (ΔG°_{TO} values). More generally, the assay identified three loci of high affinity binding (ca. nt 50, 75, and 100), and each of these is represented among the top ten predictions. Taken alone, the direct hybridization free energy (ΔG°_{OH}) is a relatively poor predictor of the observed binding, though it does predict that the locus around nt 100 should have high affinity (Table 2-1, Figure 2-3a). The sum of the unfolding and refolding free energies, which we term the restructuring free energy, is also an important contribution to the overall free energy (Table 2-1, Figure 2-3b). The restructuring free energy is overall a much better predictor of the overall energetics and high affinity binding sites. In particular, this quantity is most favorable for the sequences exhibiting the highest affinity binding, in the region around nucleotide 50 (Table 2-1, Figure 2-3b). Though not an important contribution for the highest affinity binding positions, the oligonucleotide structural energy (ΔG°_{OS}) greatly reduces the affinity of some other oligonucleotides (Tables 2-1 and 2-2, Figure 2-3c, and Discussion). A common rule of thumb is to select candidate antisense sequences based on their GC content. This was also a poor predictor of observed binding affinity, capturing only one high affinity sequence at position 100 (Table 2-2).

The results for the TNFα mRNA further support the need to include each of the free energy components (Table 2-3). In the case of this limited data set, none of the component free energies shows an identifiable trend mimicking the trend in the K_D values. However, the predicted values of ΔG_{TO} still effectively identify high affinity binding sequences, identifying four of the most strongly bound sequences among those tested. Importantly, the sequences found to have poor binding affinity experimentally (K_D >10000 nM) were ranked as fourteen of the lowest twenty in free energy among the tested sequences (data not shown).

Table 2-1: Calculated energetics of high affinity sequences*

Position	Intensity	ΔG°_{TO} ‡	$(\Delta G^{\circ}_{UN} + \Delta G^{\circ}_{RE})$	ΔG°_{OH}	ΔG°_{OS} †	Rank	GC content
52	1101	***-15.4***	5.2	-20.6		9	8
50	919	***-16.7***	5.2	-21.9		2	8
51	870	***-16.6***	5.2	-21.8		3	8
53	613	***-16.0***	5.2	-21.2		4	8
101	433	***-15.8***	10.1	-26.2	0.3	7	11
100	431	***-15.7***	10.1	-27.0	1.2	8	12
102	405	-15.3	9.8	-25.1		11	10
72	381	-11.6	9.1	-21.7	1.0	60	9
73	376	-13.5	7.6	-21.1		36	9
104	355	-15.3	9.8	-25.1		11	10

**All energies in kcal/mole. Position corresponds to the 5'-terminal base of the targeted region on the mRNA (3'-terminal base of the oligonucleotide). GC content indicates the number of G and C nucleotides in the 17mer oligonucleotide. Rank indicates the order of the predicted ΔG°_{TO} values among the 106 sequences tested experimentally, with the lowest free energy #1. Intensity data from Milner et al (1997).*

† Only positive energies were considered in accounting for ΔG°_{OS}.

‡ Bold, italicized values are among the top ten sequences according to model predictions.

Table 2-2: Analysis of sequences with high GC content*

Position	Intensity	ΔG°_{TO}	$(\Delta G^\circ_{UN} + \Delta G^\circ_{RE})$	ΔG°_{OH}	ΔG°_{OS}	GC content
86	23	-11.3	12.9	-24.3	0.1	12
88	35	-9.9	14.2	-24.2	0.1	12
90	19	-10.6	13.3	-24.4	0.5	12
91	16	-9.4	14.3	-24.6	0.9	12
92	22	-11.5	13.4	-25.8	0.9	12
93	21	-10.3	14.3	-25.8	1.2	12
94	64	-9.6	14.3	-27.4	3.5	12
95	30	-8.6	13.5	-26.8	4.7	12
97	25	-11.6	10.1	-26.6	4.9	12
98	41	-13.8	10.1	-28.6	4.7	12
99	157	-14.5	10.1	-28.1	3.5	12
100	431	-15.7	10.1	-27.0	1.2	12

**All energies in kcal/mole. Position corresponds to the 5'-terminal base of the targeted region on the mRNA (3'-terminal base of the oligonucleotide).*

Table 2-3: Calculated energetics of high affinity mouse TNFα sequences*

Name	K_D	ΔG°_{TO} ‡	$(\Delta G^\circ_{UN} + \Delta G^\circ_{RE})$	ΔG°_{OH}	ΔG°_{OS} †	Rank	GC content
8-12-PD	90	-5.8	8.3	-14.2	0.1	18	7
25-12-PD	150	-12.4	7.0	-19.4	0	3	10
5-12-PD	500	-11.3	8.3	-19.6	0	6	10
13-12-PD	1500	-11.4	2.1	-13.5	0	5	7
11-12-PD	1600	-14.2	5.2	-19.4	0	2	10

**All energies in kcal/mole. GC content indicates the number of G and C nucleotides in the 12mer oligonucleotide. Rank indicates the order of the predicted ΔG°_{TO} values among the 26 sequences tested experimentally, with the lowest free energy #1. Oligonucleotide names and K_D data from Stull et al. (1996).*

†*Only positive energies were considered in accounting for ΔG°_{OS}.*

‡*K_D values in nM.*

2.E. *Discussion*

The task of simply and accurately selecting potent antisense oligonucleotides, without conducting costly and time-consuming experiments, is one of the many barriers that inhibits the rapid development of antisense constructs in the clinical setting. The work described here provides a method by which candidate oligonucleotides can be chosen from the entire population of possible sequences. The majority of successful studies published in the literature describe experimental evaluation of a number of oligonucleotides (typically $n > 5$) before locating a sequence that demonstrates the desired biological activity [160, 181, 189]. Even in such cases where an active sequence can be located, there are no guarantees that this sequence provides optimal activity, i.e., that it is maximally active at a lower dose than all other candidates. Though cellular uptake, intracellular trafficking, and degradation also greatly affect the activity of oligonucleotides, binding to the target is critical to ensuring the activity of antisense oligonucleotides, whether through ribonuclease H mediated or steric events [190]. Using the computational strategy outlined, six of the ten sequences that were selected for the RBG mRNA had the strongest binding to their target under the experimental conditions. For the TNFα mRNA, the model also effectively distinguished between the highest and lowest affinity sequences identified experimentally. Successful prediction of antisense oligonucleotide binding affinity has previously been unsuccessful and is commonly considered beyond current capabilities [179, 190]. In this light, the success reported here is a significant improvement over the predictive and heuristic methods that have been used previously.

The binding of an antisense oligonucleotide to its target mRNA is a structurally complex event. As can be seen from the predicted secondary structure of the RBG mRNA (Figure 2-5), the molecule is able to form an intramolecular base pairing structure with no contiguous stretches of greater than 8 single-stranded nucleotides. In order for a 17mer antisense oligonucleotide to bind to its target mRNA, some segment of the native structure must first unfold. Binding of the oligonucleotide to the mRNA creates a constraint on the intramolecular base pairing such that the original base-pairing configuration (of the remaining nucleotides) may no longer be the thermodynamic minimum. Our thermodynamic cycle accounts for this entire process by incorporating the RNA unfolding and refolding free energies (ΔG°_{UN} and ΔG_{RE}), in addition to

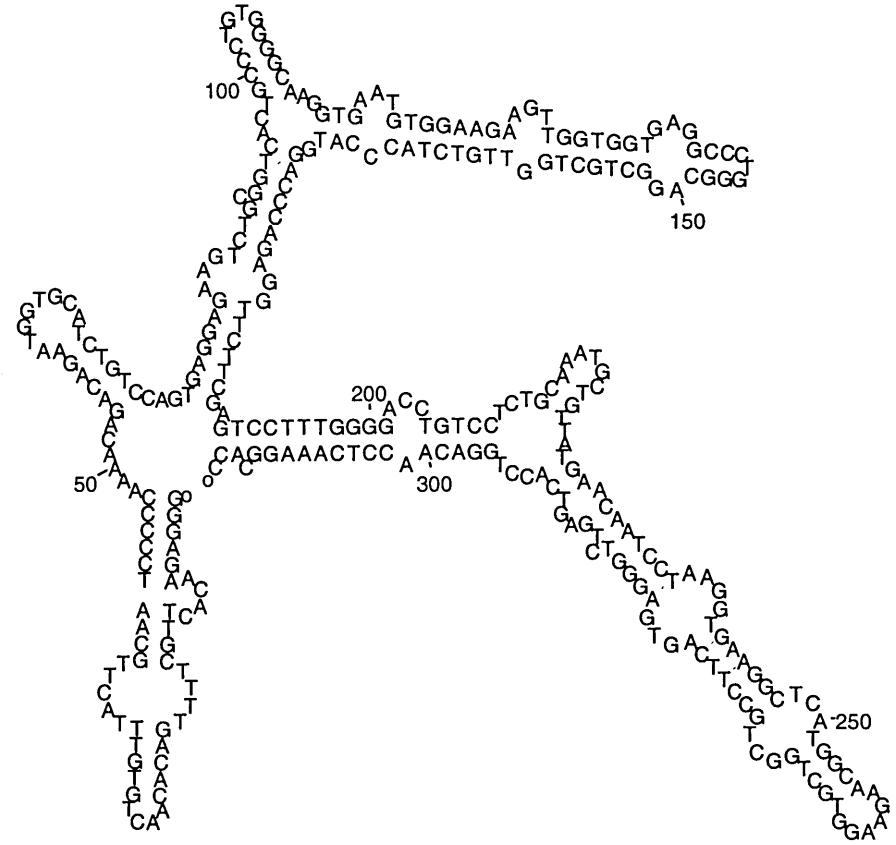

Figure 2-5: Minimum free energy structure of the first 314 bases of rabbit β-globin mRNA
The structure was generated using the program *mfold* with the following parameters: percent suboptimality = 10, window = 0, folding temperature = 37°C, and salt concentration = 1 M NaCl (no divalent ions). The folding free energy ($-\Delta G_{UN}$) was -98.2 kcal/mole. The folding structure is characterized by very few single-stranded regions. Subsequent rearrangements due to oligonucleotide hybridization will result in the formation of a new optimal structure constrained by the presence of the oligonucleotide.

the hybridization free energy (ΔG°_{OH}) of the oligonucleotide:RNA complex. Because the mfold program computes the energies of complete folding and unfolding, the values of the ΔG°_{UN} and ΔG°_{RE} terms are individually large in magnitude and not meaningful, but their sum provides a measure of the energetic cost of restructuring the mRNA to accommodate the oligonucleotide. Indeed, we find that the restructuring free energy ($\Delta G^{\circ}_{UN} + \Delta G^{\circ}_{RE}$) can be an important determinant of the overall affinity (Table 2-1, Figure 2-3b). It is the incorporation of the energetics of RNA restructuring that distinguishes our model from others.

Interestingly, in the paper from which the RBG data set was derived, the authors note that the results did not correlate with thermodynamic predictions [156]. Though details were not offered in the paper, it appears that their calculation only accounted for the hybridization of the oligonucleotide and the mRNA (ΔG°_{OH}). With no other energetic contributions and predicted ΔG°_{OH} values typically -30 to -15 kcal/mole, the binding of the mRNA to the oligonucleotide should have K_D values of 10^{-22} to 10^{-11} M; in practice, binding with this affinity is not observed, suggesting that other contributions must also be important. Adding $\Delta G^{\circ}_{UN} + \Delta G^{\circ}_{RE}$ (~10 kcal/mole), the overall K_D should be 10^{-15} to 10^{-4} M, which compares favorably with the range found experimentally (Table 2-3 and [150]). Additional contributions from oligonucleotide structure (0 - 5 kcal/mole) could reduce the binding affinity further, completely preventing oligonucleotide binding at reasonable concentrations.

One heuristic technique for antisense sequence selection is to test oligonucleotides that bridge the start codon. For the RBG mRNA, the start codon is at positions 60-62. From the experimental data, the four most strongly binding oligonucleotides all cross the start codon, indicating that using this heuristic here could result in selection of very good candidate sequences. Yet, among the fifteen 17-mers which bridge the start codon, only those four are among the highest affinity oligonucleotides. Therefore, it is quite possible that in a random selection of, e.g., five sequences, none of these would have been chosen. For the TNFα mRNA, the start codon also contains high-affinity sequences, 8-12-PD and 5-12-PD (Table 2-3), but the 3'-UTR contains the second highest affinity sequence, 25-12-PD. Also, in other cases, oligonucleotide analogues targeting either of the two start codons of a fusion protein proved less

effective than an analogue targeting the 5'-UTR [191]. Clearly, both the experimental data and our predictions show that loci outside of the start codon region should also be considered.

Another heuristic technique often employed for the selection of candidate antisense oligonucleotides is to explore the target RNA for regions of high GC content, on the notion that GC and CG base pairs are stronger than TA or AU pairs. There are twelve sequences in the RBG mRNA of seventeen bases in length containing a total of twelve guanines and cytosines. Of these twelve sequences localized around the GC-rich region between bases 90 and 102, only one was among the ten strongest binding (Table 2-1). As expected, the DNA-RNA hybridization (ΔG°_{OH}) is strongest in this region (Table 2-1, 2-2), but it is among the most costly for restructuring the mRNA ($\Delta G^{\circ}_{UN} + \Delta G^{\circ}_{RE}$) (Table 2-1, 2-2). The oligonucleotides targeting this region also have the highest cost for oligonucleotide structure (Table 2-2), greatly reducing their ability to bind to the RNA target. In this context, it is plausible that high GC content may be somewhat contra-indicative of antisense affinity, because intramolecular (both RNA-RNA and oligonucleotide-oligonucleotide) GC (or GU/T) pairs need to broken to allow for the formation of RNA-DNA pairs (i.e., ΔG°_{UN} and ΔG°_{OS} are particularly unfavorable). Although several of the highest affinity TNFα sequences have high GC content (Table 2-3), GC content is an imprecise predictor of oligonucleotide affinity.

Others have used mRNA secondary structure predictions as a basis for predicting effective antisense sequences. The simplest approach is one in which the minimum free energy structure predicted by *mfold* or a similar algorithm is used to select antisense sequences complementary to single stranded regions. An extension of this approach was applied by Jaroszewski, et al. [175], who considered the 30 lowest free energy structures of RBG mRNA as an ensemble and identified those bases that were least likely to form intramolecular base pairs. The effectiveness of phosphorothioate antisense oligonucleotides against RBG seemed to correlate with the unpaired base percentage of the target for an *in vitro* translation assay using wheat germ extract but surprisingly not in a similar one using rabbit reticulocyte lysate. However, their data set was small, and unpaired base percentage is at best a qualitative index for the antisense binding process. A more quantitative approach was developed by Sczakiel, et al. [178], who considered the folding free energy (dubbed local folding potential, but essentially –

ΔG_{UN} in our model) of short segments of RNA and used the rankings of those as a basis for predicting the effectiveness of antisense RNA target sequences. However, this approach does not account for the energetics of the direct DNA:RNA interactions (ΔG°_{OH}). As our method accounted for both the flexibility of the target structure and the binding affinity of the oligonucleotide to the target, it more accurately models the hybridization than these other techniques.

Initially, contributions to the energetics of either intramolecular (hairpin) or intermolecular (dimer) structure formation on the part of the oligonucleotide were ignored, with the expectation that short (17-mer and 12-mer) molecules would not have significant structural features. Though it appears that this assumption was sufficient for the 12-mers from the TNFα data set (Table 2-3, column 6), incorporation of the energetics of hairpin formation improved the accuracy of the model formulation for the oligonucleotides in the RBG system. The formation of oligonucleotide dimers was considered to be unlikely and ignored in this system, as the array experiment used covalently immobilized oligonucleotides. Incorporation of the unfolding energy for the 38 (of 112) sequences with a positive ΔG°_{OS} resulted in higher correlation with ln(I) (Figure 2-4b vs. Figure 2-4a) and better prediction of the highest affinity sequences. For those sequences in the GC-rich region between bases 90 and 102, ΔG°_{OS} exceeded 3 kcal/mole for five oligonucleotides (Table 2-2) with hairpins of up to 5 base pairs. A number of these sequences were identified as strong candidates when considering only the structural features of the RNA. However, the measured intensities are in the background of the experiment, with the exception of oligonucleotide 100, which has only a 1.2 kcal/mole (3 base pairs) ΔG°_{OS} contribution (Table 2-2), suggesting that the binding of the RNA to the oligonucleotide was prevented by the stable intramolecular structure formed by the oligonucleotide. Because of the increased relative importance of end-effects, prediction of ΔG°_{OS} may not be as accurate for short oligonucleotides as it would be for longer single-stranded species, e.g., primers, so further refinement of the energies from this contribution may be possible. This may improve the overall success rate, as two more of the ten highest affinity sequences were ranked in a tie at 11th in the predictions (Table 2-1).

While the success of our model in predicting oligonucleotide binding affinity for these systems is notable, agreement between the model and experiments is imperfect, suggesting that elements of the binding process are not being taken into account or are not being treated accurately by the model. The correlation is best for sequences with the highest binding affinity, presumably where the measurements are the most accurate. However, even at the high intensities, there are regions where the model and measurements are not in agreement. The model formulation does not account for any effects of tertiary structure on the accessibility of the target sequences by the oligonucleotides. Though base pairing and stacking have been shown to be the main components of the folded structure of RNA [192], the formation of tertiary structural features in the presence of Mg^{2+} ions has been shown to result in secondary structures that disagree with thermodynamic predictions [165]. In particular, the lack of information regarding the potential formation of pseudoknots could have enough of an effect on the energetics to influence the agreement between model and experiment. It is also possible that an antisense oligonucleotide could "cross react" with non-targeted regions of the mRNA. However, a homology analysis of the RBG mRNA indicated that nonspecific binding is unlikely for this experimental system. Interestingly, the sequences for which the prediction was unsatisfactory, positions 72 and 73 in Table 2-1, were ranked very highly in predictions for shorter oligonucleotides. As such, it is possible that the local concentration of mRNA in the vicinity of these positions was enhanced by the binding of the mRNA to shorter oligonucleotides immobilized adjacent on the array, resulting in an increased binding to the 17mers at this position. Alternatively, stable binding could have been achieved with partial hybridization, a factor not taken into account by the model predictions. Additional effects that could influence agreement between theory and experiment include those arising from the buffer composition (principally its pH and ionic strength) as well as ones relating to the definition of folding domains (see Methods).

The success rate in this study – ~60% accuracy in prediction of active oligonucleotides – is a solid advance over commonly used heuristics, though applicability of our methodology to a wide spectrum of mRNA remains to be proven. Providing such validation requires large experimental data sets, which are generally lacking. In addition to filling this void, we are working towards addressing the question of whether high affinity binding in cell free assays

corresponds to high affinity binding within a living cell. In the few cases where extensive comparison has been made, agreement between *in vitro* experiments and intracellular data suggests that binding affinity is a useful predictor of antisense activity [193]. The computational strategy described here provides a convenient, inexpensive method for selecting candidate oligonucleotides to guide further exploration. If the high affinity sequences predicted by this method prove effective *in vivo*, this approach could positively impact the development of antisense oligonucleotides for diagnostic and therapeutic purposes.

3. *Analysis of* in vitro *Binding Affinity and Kinetics*

3.A. *Abstract*

Antisense oligonucleotides act as exogenous inhibitors of gene expression by binding to a complementary sequence on the target mRNA, preventing translation into protein. Antisense technology is being applied successfully as a research tool and as a molecular therapeutic. Yet, a quantitative understanding of binding energetics between short oligonucleotides and longer mRNA targets is lacking, and selecting a high affinity antisense oligonucleotide sequence from the many possibilities complementary to a particular RNA is a critical step in designing an effective antisense inhibitor. Here, we report measurements of the thermodynamics and kinetics of hybridization of a number of oligonucleotides complementary to the rabbit-β-globin (RBG) mRNA using a novel binding assay. A wide range of equilibrium dissociation constants were observed, and association rate constants within the measurable range correlated strongly with binding affinity. In addition, a significant correlation was observed of measured binding affinities with binding affinity values predicted using a thermodynamic model involving DNA and RNA unfolding, oligonucleotide hybridization, and RNA restructuring to a final free energy minimum. In contrast to the behavior observed with short oligonucleotides, the association rate constant increased with temperature, suggesting that the kinetics of association are related to disrupting the native structure of the target RNA. The rate of cleavage of the RBG mRNA in the presence of ribonuclease H and oligonucleotides of varying association kinetics displayed apparent first-order kinetics, with the rate constant exhibiting binding-limited behavior at low association rates and reaction-limited behavior at higher rates. Implications for the rational design of effective antisense reagents are discussed.

3.B. *Introduction*

With ever increasing amounts of genome sequence information becoming available, the potential exists to use antisense oligonucleotides for the inhibition of gene expression in a wide variety of therapeutic and biotechnological applications. Antisense oligonucleotides hybridize to their target mRNA by Watson-Crick base pairing and inhibit translation of the mRNA by enzymatic and steric means [195]. Traditionally, active antisense oligonucleotides have been identified by trial and error of a number (20-50) of sequences [28, 144], and this practice continues [196]. These methods are time consuming and typically suffer from a low rate of success. Although the criteria for activity are somewhat subjective and depend on the system and application, most estimates are that fewer than 15% of tested oligonucleotides are sufficiently active to warrant further investigation [28]. While extensive research has identified barriers presented by cells to oligonucleotide entry and activity, even tests outside of the context of cells do not often yield oligonucleotides with sufficient efficacy [8]. Recent efforts have focused on applying RNA and oligonucleotide structural information as a means of identifying those sequences that should be particularly active against a target mRNA [144].

Whereas understanding of molecular recognition in protein-protein interactions has been aided by structural information determined by X-ray crystallography and NMR, no such information is available for the understanding of oligonucleotide:mRNA interactions. In the absence of direct structural data, inferences regarding RNA structure have been derived from minimum free-energy theoretical predictions of RNA folding, which are in turn validated using indirect comparative, enzymatic, and chemical methods, in some cases also using oligonucleotides as structural probes [171, 183, 187, 197-200]. Several researchers have sought to use RNA structural predictions as a basis for selecting effective antisense oligonucleotides, but simple inspection of folded structure does not reveal any general relationships with antisense effectiveness. A more productive approach is to use this information in a thermodynamically consistent model, which accounts for unfolding of oligonucleotide and RNA molecules to expose bases need for hybridization, the base pairing between the deoxyribonucleotides of the antisense molecule and the ribonucleotides of the target, and restructuring of the bound target to a new free energy minimum [169, 201]. Summing the free energies of each of these steps gives a total free energy for antisense binding to a particular sequence on a target mRNA. Predictions are then

generated for many possible antisense oligonucleotides binding to particular mRNA species. To date, such predictions have been compared to several data sets, with significant correlations observed between predicted free energy and measured binding, RNase H activation, and antisense efficacy [147, 169, 201]. These promising results point to the role of RNA structural flexibility as a key factor in determining the accessibility of RNA to antisense binding but highlight the importance of accounting for the whole process simultaneously. Nonetheless, there clearly exists a need for more thorough investigation, both experimental and theoretical, of the biophysics involved in the interaction of short oligonucleotides with their full-length mRNA targets.

Towards this end, we chose to study the affinity and kinetics of hybridization of 17-mer DNA oligonucleotides complementary to *in vitro* transcribed rabbit β-globin (RBG) mRNA, a well-studied mRNA found to exhibit considerable variability in both oligonucleotide binding affinity and *in vitro* antisense efficacy depending on the complementary oligonucleotide sequence chosen [156, 202, 203]. To measure binding in solution quantitatively and rapidly, we developed an assay that uses the rapid and efficient separation of free oligonucleotide from hybridized oligonucleotide by centrifugation through size-selective membranes. We used this assay to investigate the affinities and kinetics of binding of a panel of oligonucleotides targeting regions of various characters (base composition and predicted structure) on the RBG mRNA. In addition, we studied the dynamics of RBG mRNA cleavage in the presence of oligonucleotides of varying association kinetics and a constant level of ribonuclease H, which recognizes DNA:RNA duplexes and is believed to play a significant role in the antisense mechanism *in vivo*. Confident prediction and measurement of hybridization affinity and kinetics will reduce the number of failure sequences tested in antisense assays and improve the likelihood of identifying those sequences that will be active most rapidly at the lowest possible concentrations.

3.C. Materials and Methods

Oligonucleotide:mRNA hybridization free energy prediction. The method used for free energy predictions was described in detail in an earlier publication [201]. Briefly, and in general terms, the energies of folding for the target mRNA and oligonucleotide were calculated using the nearest-neighbor algorithm developed by Zuker et al, *mfold* [167, 168]. The algorithm was

applied using thermodynamic parameters available with *mfold 2.3*, using the "N Best" program with a sort percentage of 10, 1 traceback, and a window size of 0, at a temperature of 37°C.

The energies of folding were used to calculate the overall free energy of antisense binding (ΔG^{o}_{total}) by considering: the free energies of RNA unfolding (ΔG^{o}_{unfold}), the negative of which was computed by *mfold*); the corresponding energy of oligonucleotide unfolding (ΔG^{o}_{oligo}), computed analogously, except with DNA rather than RNA parameters [186]; the free energy for the intermolecular interaction of the oligonucleotide and the mRNA (ΔG^{o}_{hyb}), which was computed using nearest-neighbor parameters for DNA:RNA hybrids [185]; and the energy to refold the mRNA into a new minimum energy structure with the constraint of the antisense oligonucleotide bound to its complement ($\Delta G^{o}_{restruct}$). Thus, ΔG^{o}_{total} is given by the sum:

$$\Delta G^{\circ}_{total} = \Delta G^{\circ}_{unfold} + \Delta G^{\circ}_{oligo} + \Delta G^{\circ}_{hyb} + \Delta G^{\circ}_{restruct} \quad (1)$$

The path by which free energies are calculated (i.e., involving complete unfolding of the RNA) does not correspond to the physical situation, but the thermodynamic cycle will provide the correct total free energy, if equilibrium is truly attained and the assumed before and after states are correct. For the purposes of comparing the ability of various target regions on the mRNA to accommodate an oligonucleotide, the sum ($\Delta G^{o}_{unfold} + \Delta G^{o}_{restruct}$) is used and termed the "RNA structure cost". Because the initial RNA folded state is at its minimum free energy, the RNA structure cost is always non-negative. The ΔG^{o}_{oligo} term is likewise non-negative, though frequently zero, and the ΔG^{o}_{hyb} is always negative. Thus, there is a balance between unfavorable (costs) and favorable (gains) contributions to ΔG^{o}_{total}.

Oligonucleotide preparation. Oligonucleotides were obtained from Life Technologies, prepared at 200 nmol scale and purified by HPLC. Before use, the lyophilized oligonucleotides were resuspended to 100 μM concentration in Tris-EDTA (TE, pH = 8.0) buffer per the manufacturer's instructions. Prior to labeling, all oligonucleotides were stored at -20°C. Oligonucleotides were 5'-labeled with ^{33}P-γ-ATP (NEN Life Science Products, Boston, MA) using T4 polynucleotide kinase (PNK) and standard forward reaction conditions (Promega, Madison, WI). Unincorporated label was removed from the reaction by separation on a Chroma-Spin 10+STE column (Clontech Laboratories, Palo Alto, CA). Oligonucleotides were then

phenol-chloroform extracted and ethanol precipitated with ammonium acetate to ensure complete removal of PNK and any other contaminating buffer components. If necessary, an additional purification was performed using NucAway Spin Columns (Ambion, Austin, TX). Oligonucleotides were resuspended in TE and the purity verified by electrophoresis. Labeled oligonucleotides were stored at 4°C for daily use. Position label refers to the 5' base of the mRNA to which the 3' base of the oligonucleotide is complementary.

cDNA preparation and in vitro *transcription:* The pSV2RbetaG clone was obtained from ATCC (ATCC#: 37646). The RBG encoding insert was extracted by double digestion with *Hind*III and *Bgl*II. The gel-purified insert was ligated into the pSP73 vector (Promega). The new vector was transformed into competent cells, and vector-carrying clones were selected from individual colonies growing on agar-amp50 plates. Clone 73-10-1-1 was grown into large-volume cultures, as needed, and the plasmid purified by Maxi-prep (Qiagen, Valencia, CA). The insert sequence was verified by positive and negative strand sequencing (Massachusetts General Hospital DNA Sequencing Core Facility). The plasmid was linearized using *Bgl*II, and the mRNA was transcribed with the MegaScript *in vitro* transcription system (Ambion), per the manufacturers instructions. RNA was distributed into aliquots and stored at -80°C. RNA purity was confirmed by denaturing PAGE using TBE-Urea Ready Gels (Bio-Rad, Hercules, CA).

Hybridization Reactions: Hybridization reactions were performed in 96-well, Non-Binding Surface plates (Corning, Acton, MA). This minimized adsorption of the nucleic acids, which was observed when microcentrifuge tubes were used to perform the hybridizations. All hybridization reactions were performed in 1M NaCl, 0.5 mM EDTA, and 20 mM sodium cacodylate, pH 7.0. Equilibrium hybridization reactions were performed for at least 16h, but no more than 20h; no differences were seen in the degree of hybridization for any of the oligonucleotides throughout this time period. Kinetic hybridization reactions were performed at a concentration of mRNA sufficient to generate 100% binding of the oligonucleotide at equilibrium. In each case, an mRNA-containing and an oligonucleotide-alone control hybridization were performed for the same time period (see Data Analysis). Oligonucleotides were used at the minimum detectable concentration, typically within 2 weeks of the calibration date of the radioactivity. This resulted in oligonucleotide concentrations of 2-4 pM. In situations where minimum oligonucleotide concentrations were required (where the measured K_D

was close to 0.01 nM), ^{33}P-γ-ATP at or before its calibration date was used to ensure maximal sensitivity.

Gel-Shift Separation: Following hybridization, 15 µl of the hybridization reaction was added to 3 µl of 6X loading buffer (30% glycerol, 0.25% bromophenol blue, 0.25% xylene cyanole). From this mixture, 15 µl were then loaded onto a 4-20% gradient acrylamide gel and electrophoresed until the bromophenol blue front reached ~75% of the length of the gel. The location of the mRNA was verified using SYBR Gold nucleic acid gel stain (Molecular Probes, Eugene, OR). Gels were then dried on Whatman filter paper at 80°C for 45 minutes under vacuum. The dried gels were exposed to imaging screens for 40 h, and accumulated signal from ^{33}P-γ-oligonucleotide was measured using the Molecular Imager (Bio-Rad). Band densities were quantified using the Multi-Analyst software package (Bio-Rad). The fraction bound was calculated as the signal in the band corresponding to bound oligonucleotide divided by the total signal of the bound and free bands.

Centrifugal Separation (Figure 3-1): Following hybridization, 100 µl of the hybridization reaction was loaded onto a Microcon-50 centrifugal concentrator (Millipore, Bedford, MA). The concentrators were loaded into an Eppendorf 5415C centrifuge and centrifuged for ~40-60 s at 8,200 g (10,000 rpm). The membranes were then inverted into a new centrifuge tube and centrifuged for ~20 s at 10,000 rpm. The initial centrifuge time was adjusted to generate a permeate fraction of roughly 50% of the added volume. The volumes in each fraction were measured using a micropipette, and each fraction was counted by liquid scintillation (counter: Beckman 6000IC; fluid: Ultima Gold, Packard Biosciences). To ensure that a constant concentration of oligonucleotide was added to each reaction and that the retentate was fully recovered from the membrane, the radioactivity on the separator membrane was also measured.

RNase H Cleavage Experiments: RNase H cleavage experiments were performed in a buffer suitable for maintaining enzymatic activity, 0.1 M KCl, 10 mM $MgCl_2$, 1 mM DTT, and 50 mM Tris-HCl (pH 8.0). The standard hybridization buffer (i.e., 1 M NaCl) eliminated enzyme activity and could not be used. Oligonucleotide and mRNA were each used at a concentration of 50 nM. Equilibrium and kinetic hybridization experiments were performed

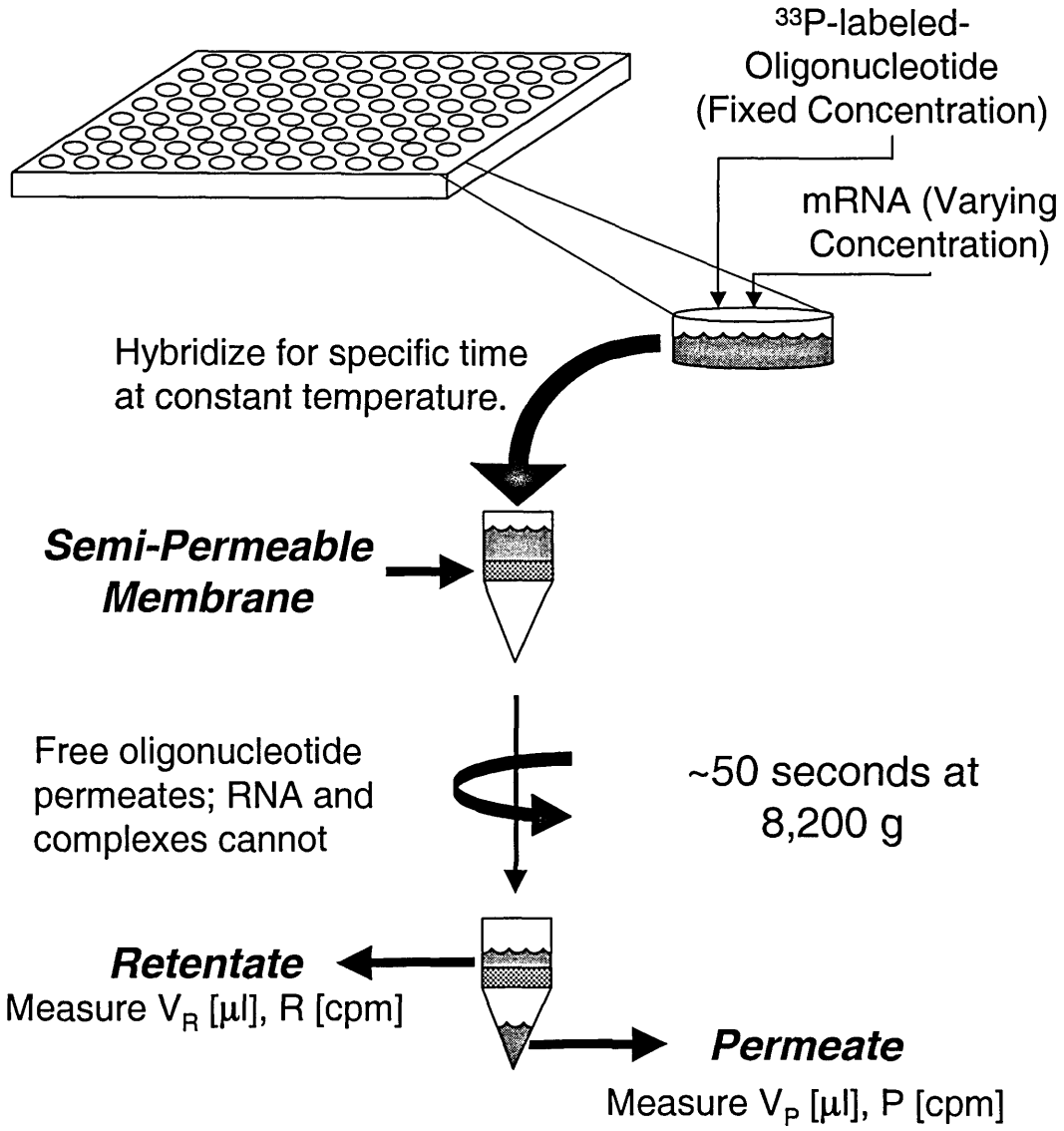

Figure 3-1: Centrifugal separation assay

Solutions of varying concentration of mRNA and a fixed concentration of 5'-^{33}P-oligonucleotide are added to individual wells of a non-binding surface plate, which is maintained at constant temperature during the incubation time. 100 µL of hybridization volume are added to the centrifugal membrane and centrifuged for a time sufficient to separate fractions into approximately equal volumes. After collecting the permeate, the membrane is inverted into a new centrifuge tube and centrifuged again to collect the retentate. The volumes and cpm of the retentate and permeate fractions are then measured, and the fraction bound determined by material balance.

under these conditions with selected oligonucleotides to ensure that equivalent K_D and k_a values were achieved in the RNase H and hybridization buffers (data not shown). Three units of RNase H was added to the oligonucleotide solution, after which RNA was added and an initial sample taken, defining time 0. Subsequently, six aliquots were taken at various times and added to formamide-containing gel-loading buffer to stop the cleavage reaction. The samples were then run on a 10% TBE-Urea Ready Gel (Bio-Rad) and post-stained using SYBR Gold nucleic acid gel stain (Molecular Probes). Fluorescence was measured using the Fluor-S system and quantitated using the Multi-Analyst software package (Bio-Rad). The band intensities were expressed as a fraction of the maximum measured band intensity (maximum amount of cleaved product) to normalize for differences in staining and exposure.

Data analysis: Following centrifugal separation, the radioactivity (cpm) and volume of each fraction were measured. Two key principles are necessary to quantify the fraction of oligonucleotide bound to mRNA from these measurements. First, the permeate fraction is assumed to contain only free oligonucleotide, while the retentate contained free oligonucleotide and any bound oligonucleotide. This assumption was verified by electrophoresis. Therefore, the (radioactive) label in the retentate (R) and permeate (P) is distributed as

$$R = R_{bound} + R_{free} \tag{2}$$

$$P = P_{free} \tag{3}$$

where the subscripts "bound" and "free" refer to the state of the oligonucleotide. Second, the separation is assumed to occur rapidly, such that dissociation of bound hybrids does not occur during the separation. The concentrations of free oligonucleotide in the retentate and permeate after centrifugal separation are then assumed to be related by a membrane distribution coefficient, K_{memb}:

$$K_{memb} = \frac{[\text{free oligo}]_{retentate}}{[\text{free oligo}]_{permeate}} = \frac{R_{free}/V_R}{P/V_P} \tag{4}$$

where V_R and V_P are the volumes of the retentate and permeate fractions, respectively. The value of K_{memb} is determined experimentally in each sequence of measurements on a labeled oligonucleotide sample in the absence of RNA. This quantity reduces to unity if the concentrations in each fraction are exactly equal, as should be the case for a membrane pore size much larger than required for the oligonucleotide. Indeed, the measured values of K_{memb} ranged from 0.95-1.10. For kinetic experiments, the K_{memb} was measured for each distinct time point, though no consistent variation was observed with time.

The fraction of bound oligonucleotide (in the hybridization reaction, before separation) is given by:

$$f = \frac{R_{\text{bound}}}{R+P} \tag{5}$$

Combining Eq.2-4 and 2-5 provides the expression used to determine fraction bound, in terms of measured quantities:

$$f = \frac{R - V_R\left(P/V_P\right)K_{memb}}{R+P} \tag{6}$$

The equilibrium dissociation constant, K_D, for the binding of each oligonucleotide to the RBG mRNA (at total concentration M_T) was determined by applying a mass action law. The data reported were calculated by fitting the fraction bound data to:

$$f = \frac{M_T}{M_T + K_D} \tag{7}$$

Fits were made to composite data sets for at least two independent experimental runs, resulting a total of 12-25 data points per K_D value. It is assumed that the concentration of free mRNA remains unchanged throughout the experiment. Since this requires the mRNA concentration to be substantially greater than the oligonucleotide concentration (the practical minimum for which was about 2 pM), we estimate that the lower limit on the range of measurable K_D values is approximately 0.005-0.010 nM. To ensure an accurate fit, fraction bound data were normalized to 100% by dividing by the maximum measured fraction bound (typically 0.96 – 0.98) before being fit by Eq. 7.

Kinetic data were fit using a second-order rate law for the formation of duplexes (D) from oligonucleotides (O) and mRNA (M). As in the equilibrium experiments, it was assumed that mRNA concentration remains unchanged over time such that a pseudo-first order condition occurs:

$$\frac{dD}{dt} = k_a OM - k_d D \cong k_a' O - k_d D \tag{8}$$

where k_a is the second order association rate constant, k_d is the first order dissociation rate constant, and the pseudo-first order rate constant, k_a', is equal to $k_a' = k_a M_T$. Applying the condition $k_d = K_D k_a$, imposing an initial condition of no bound oligonucleotide, and solving for fraction bound gives:

$$\frac{f}{f_{eq}} = 1 - e^{-k_{fit} t} \tag{9}$$

where f_{eq} is the equilibrium value given by Eq. 7, and k_{fit} is given by:

$$k_{fit} = \frac{k_a'}{f_{eq}} = \frac{k_a M_T}{f_{eq}} \tag{10}$$

Therefore, the fraction bound was measured over a range of times during two independent experimental runs, the composite data fit to Eq. 9, and the second-order association rate constant, k_a, determined using Eq. 10.

The cleavage of RNA by ribonuclease H in the presence of antisense oligonucleotide was observed to follow first order kinetics, as can be derived from mechanistic arguments (See Appendix 3-1.). Because the appearance of cleavage product could be quantified more accurately than the disappearance of full-length RNA, the former was used and fit to an equation of the form:

$$X = 1 - e^{-k_{eff} t} \tag{11}$$

where X is the fractional increase in cleavage product and k_{eff} is the effective first order rate constant.

All data fits were performed using Kaleida Graph software (Synergy Software, Reading, PA).

3.D. Results

3.D.1. Centrifugal assay description and validation

To date, a paucity of experimental data exists regarding the interactions between antisense oligonucleotides and their complementary, but structured, messenger RNAs in solution. To measure the binding of an oligonucleotide for its target mRNA, it is important to be able to separate hybridized oligonucleotides from free. Traditionally, this is accomplished with a gel-motility shift assay. However, limited sample volumes and constraints of usable buffers make this technique relatively inflexible. We have developed a centrifugal separation method (Figure 3-1) designed to separate bound oligonucleotide from free in a faster, more quantitative, and more sensitive fashion than the gel-shift assay. The basic premise of the assay is to perform a rapid separation, such that free oligonucleotides pass through a semi-permeable membrane, while bound oligonucleotides are prevented from permeating due to the size of the RNA to which they are bound; the fraction bound is then computed from measurements of label in each compartment with equilibrium and mass balance relationships (see Materials and Methods).

After verifying that oligonucleotides completely permeated and that the rabbit β-globin (RBG) mRNA was completely rejected by the membrane under use, we compared the binding curves measured with the centrifugal separation technique with those from a gel-shift assay. Figure 3-2a shows a typical gel-shift assay using a 17-mer oligonucleotide targeting position 259on the RBG mRNA (in this paper, we refer to position as the 5'-end of the mRNA, thus, 3'-end of the oligonucleotide). In the gel-shift assay, radiolabeled oligonucleotide that is bound to RNA experiences a decrease in electrophoretic mobility and is retained at the top of the gel. As expected, with increasing mRNA concentration, the quantity of radioactivity in the bound fraction increases. The fraction bound was calculated from the band intensities and compared with the binding curve measured for the same oligonucleotide-mRNA interaction using the centrifugal separation assay (Figure 3-2b). The slight (log scale) discrepancy between the two methods was consistent for a range of binding curves, with the centrifugal technique measuring higher K_D values (by a factor of 1.2 - 3). The slightly higher K_D values for the centrifugal assay could reflect incomplete equilibration between the retentate and permeate (though our results in the absence of mRNA suggest this is unlikely) or the difference in buffer conditions used for the gel-shift assay, where the samples were mixed with loading buffer before electrophoresis.

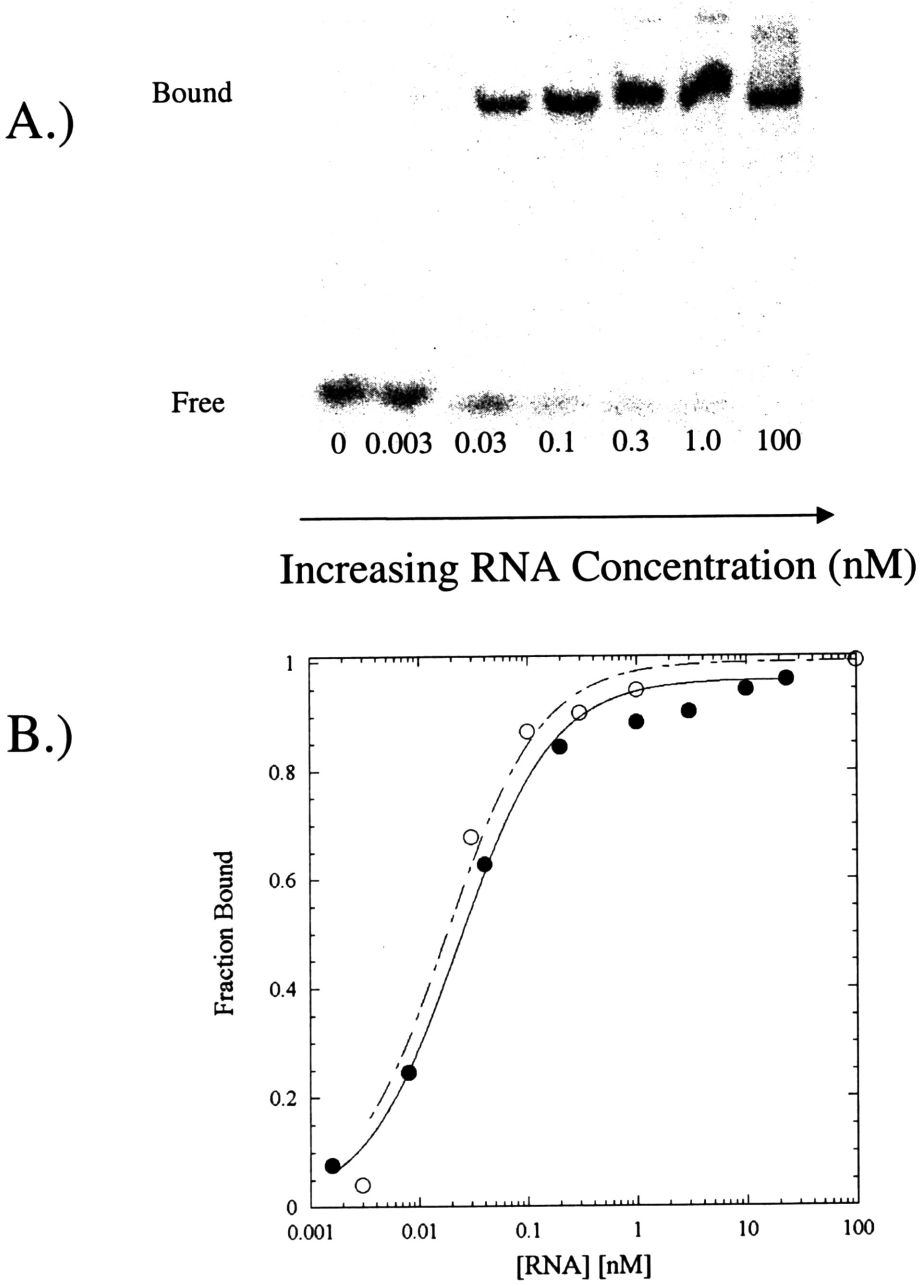

Figure 3-2: Comparison between gel-shift and centrifugal assays
A.) Radiographic image of a 4-20% gradient polyacrylamide gel showing bound and free oligonucleotide with increasing concentration of RBG mRNA. b.) Fraction of oligonucleotide bound as measured by each assay vs. free mRNA concentration (assumed unchanged from initial concentration). Data points normalized to maximum binding, typically 96-98% (see Methods). (●) gel-shift assay, (○) centrifugal assay. Curves show the fits of Eq. 7 to each of the data sets. The K_D values obtained from curve fits are given in Table 3-1.

Next, we used the centrifugal assay to study the binding of a panel of oligonucleotides complementary to the RBG mRNA. These included a selection of those previously studied in an oligonucleotide array (Milner et al., 1997) and several more chosen to provide a diversity of predicted affinities and predicted structural characteristics. A range of K_D values spanning nearly five orders of magnitude was accessible with this binding assay (Table 3-1). As a control, we also measured the binding curves for several nonsense oligonucleotides, which are identical in base composition to their antisense counterparts but are in scrambled sequence and hence should not hybridize to their target. Indeed, binding was not seen for nonsense sequences corresponding to oligonucleotides 33, 58, 59, 103, and 107 at the highest tested mRNA concentration, confirming the requirement of sequence complementarity for binding of oligonucleotides to their target mRNA.

3.D.2. Correlation of predicted free energies with measured binding affinities

Also listed in Table 3-1 are the K_D values calculated from the free energies of binding predicted with our molecular thermodynamic model (Methods and [201]). While not in quantitative agreement with measured values, the predictions generally distinguish between oligonucleotides with large differences in affinity. When the predicted affinity values are ranked and assigned a percentile score (the sequence of highest affinity is at 99 and the median is 50), this score correlates fairly well with measured affinity (Figure 3-3a). When examining those oligonucleotides with measured K_D values less than 0.1 nM, in only one case was the percentile score less than 78, with two of these oligonucleotides within the highest 2%. From these results, we infer that using model predictions as a means to select high affinity oligonucleotides is likely to result in a fraction of false positives and false negatives, but overall should reduce greatly the number of sequences to be tested.

3.D.3. Correlation of predicted free energies with solid-phase binding intensity

Previously, the loci of binding of labeled RBG mRNA were determined by exposure to an oligonucleotide array on which were immobilized all antisense sequences up to 17 nucleotides in length spanning the first 121 bases of the particular RBG transcript employed [156]. The results were reported for each oligonucleotide in terms of a radiographic intensity, roughly proportional to amount bound, which ranged from ~11 to 1000 arbitrary intensity units with a

Table 3-1: Equilibrium binding of oligonucleotides to the RBG mRNA at 37°C

Target Position	Measured K_D (nM)	Predicted K_D (nM)	Percentile*
58	0.011 ± 0.001	0.0014	84
59	0.012 ± 0.002	0.010	78
49	0.015 ± 0.002	$2.1x10^{-5}$	98
259	0.019 ± 0.002	0.0024	82
84	0.021 ± 0.002	0.0062	79
79	0.031 ± 0.004	15	30
139	0.072 ± 0.006	$3.6x10^{-6}$	99
448	0.10 ± 0.02	$2.4x10^{-4}$	92
438	0.22 ± 0.02	$7.8x10^{-5}$	95
217	0.22 ± 0.02	0.11	62
107	0.54 ± 0.07	1.8	42
33	1.1 ± 0.3	4.8	34
98	2.7 ± 0.4	200	22
147	7.3 ± 0.9	$2.9x10^{-4}$	91
103	310 ± 30#	240	21
407	550 ± 50#	>10000	2
33Non	>>150	N/A§	
58Non	>>150	N/A§	
59Non	>>150	N/A§	
103Non	>>150	N/A§	
107Non	>>150	N/A§	

*Rank of predicted affinity out of 494 sequences. An oligonucleotide with the highest predicted affinity would have percentile score of 99, i.e., the oligonucleotide would be in the 99th percentile.

#Extrapolated values, based on the fractional binding curve at mRNA concentrations < 150 nM. For nonsense sequences, no extrapolation could be made as no measurable binding was detected at any concentration tested.

§N/A – No value could be predicted as no specific binding interaction could be defined.

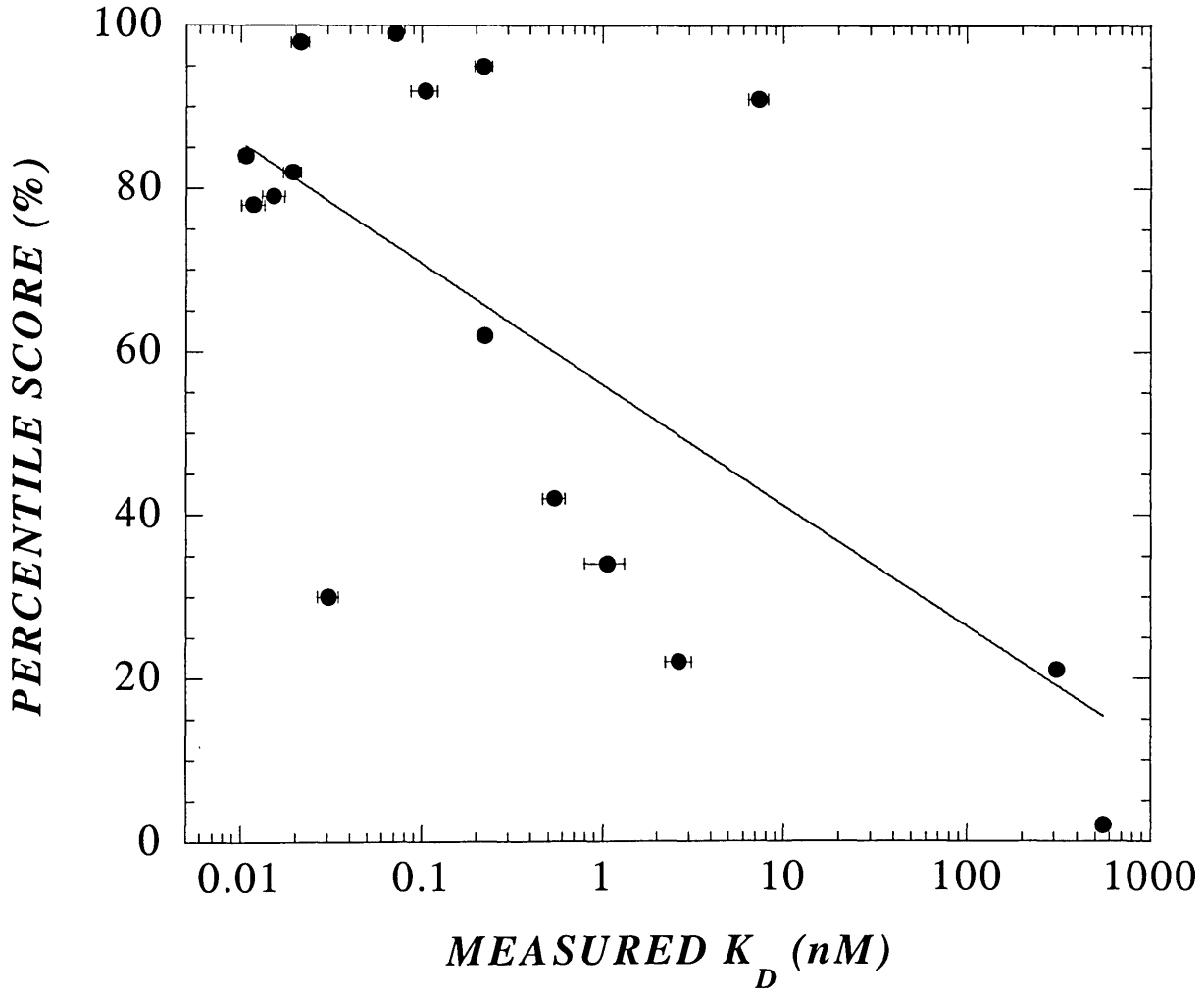

Figure 3-3a: Equilibrium dissociation constant correlations

Correlation of percentile score (see text for definition) from thermodynamic binding affinity predictions with measured K_D values. Error bars represent the uncertainty for the nonlinear fit of each K_D value based on a composite data set of 12-25 points each. The logarithmic curve fit to the data has equation: $y = -14.5\log(x) + 56.7; R^2 = 0.44$. The utility of the thermodynamic predictions in identifying high-affinity oligonucleotides is demonstrated, despite the lack of strong correlation between the predicted percentile score and the measured affinities.

mean intensity of ~150. In the array experiment, an mRNA concentration of 0.1 nM was used. Because of the relationship between fraction bound and dissociation constant (Eq. 7) the array experiment probably only distinguishes among equilibrium dissociation constants in the range 0.01 nM < K_D < 1.0 nM. In comparing nine oligonucleotides whose binding was measured by each assay, a general correlation is observed between equilibrium dissociation constant and binding intensity (Figure 3-3b). In general, the highest affinity oligonucleotides in our measurements correspond to those exhibiting high binding in the array format, though the more limited dynamic range of the latter prevents a solid quantitative comparison. Specifically, the oligonucleotide in the lower right corner appears to be out of line, but this is because its binding intensity in the array format is in the background. Another cause of variation could be due to altered mRNA structure resulting from somewhat different 5' and 3' sequences of the *in vitro* transcript used in the solid phase assay versus that used in our measurements. This could be particularly important for oligonucleotide 49 (the point in the lower left quadrant of Figure 3-3b), whose target sequence is predicted to interact with the 5' end of the transcript used in the array assay but not in the transcript used in the present study. Differences could also be due to slight variations in the hybridization buffers and temperatures used, or to enhanced oligonucleotide-oligonucleotide interactions in the context of the solid phase.

3.D.4. Measurement of oligonucleotide binding kinetics

The kinetics of oligonucleotide binding to target mRNA may also be quite important in antisense applications. The dynamics of delivery and degradation dictate that oligonucleotides must not only bind with sufficient affinity but also with sufficiently rapid kinetics to have an effect in living cells. Particularly stable intramolecular structure within the target regions on the mRNA would limit oligonucleotide accessibility and result in a much slower approach to equilibrium, if equilibrium is ever reached. The components of the free energy of binding that we compute include the free energies of unfolding the native RNA molecule, unfolding the native oligonucleotide molecule, binding the oligonucleotide to the RNA, and refolding the RNA to a final minimum energy conformation (Eq. 1). The sum of the first and last of these is always non-negative and is the RNA structure cost, the second is the oligonucleotide cost, and the third is the energetic gain from hybridization. These three net contributions are summarized in Table

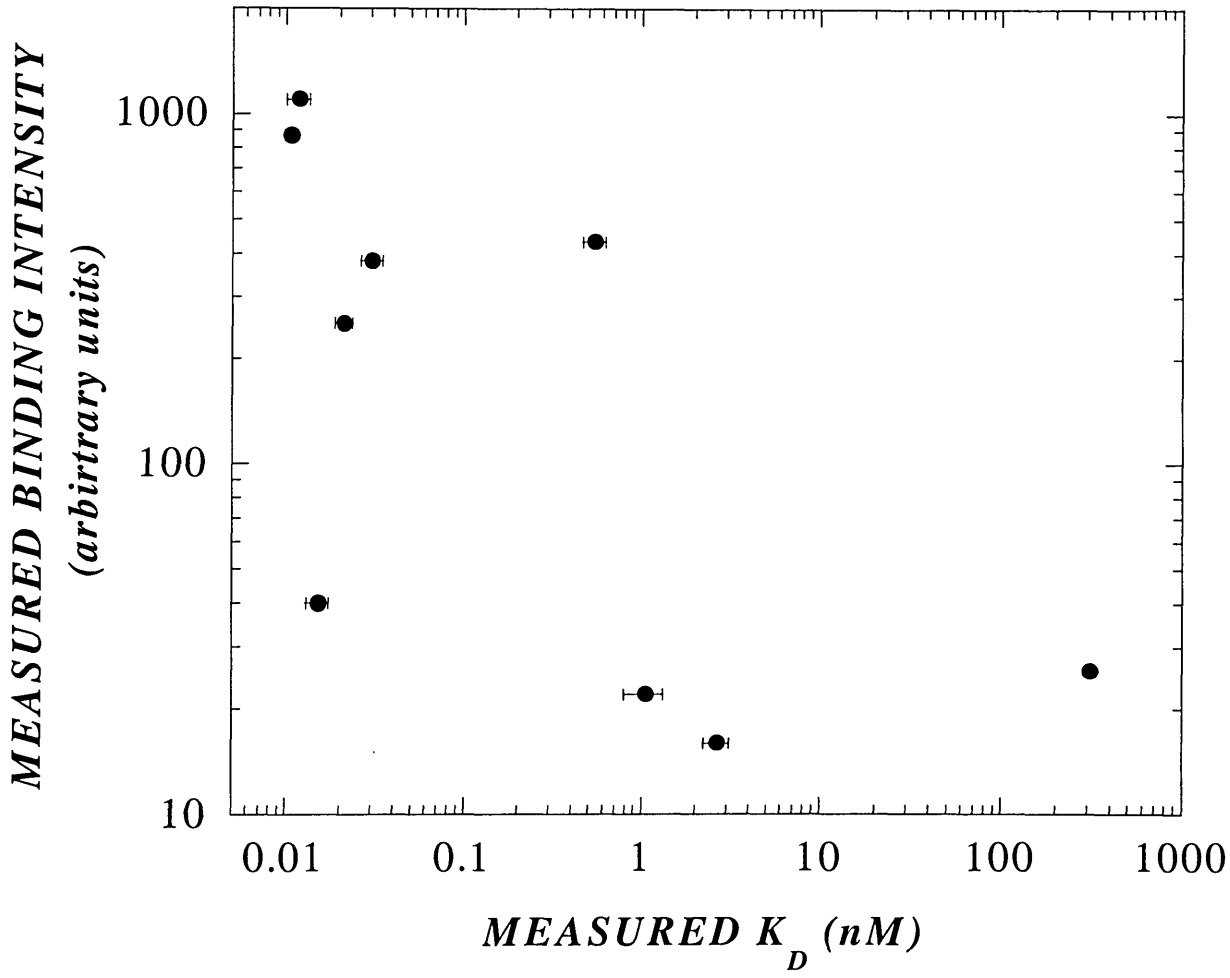

Figure 3-3b: Equilibrium dissociation constant correlations

Correlation of solution-phase binding affinity measurements with binding intensity of RBG mRNA to a solid-phase oligonucleotide array. Binding intensity data was obtained from Milner, et al [156] and is in arbitrary units. The correlation between the measured intensities using the solid-phase oligonucleotide array and the solution-phase reinforces the reliability of the centrifugal assay. Also, the overall agreement suggests that use of solid-phase measurements is a reliable predictor of solution-phase affinities.

3-2 for all of the intermediate affinity oligonucleotides, on which kinetic experiments were subsequently performed.

To determine the role of mRNA structure in controlling the hybridization kinetics, eight oligonucleotides with varying predicted RNA structure costs and energetic gains, but generally intermediate affinities (as we found these were most amenable to accurate kinetic determination) were chosen for kinetic study. Association kinetics for each of these oligonucleotides were measured using the centrifugal assay for a number of time points leading up to equilibrium. Because the RNA concentration was much greater than the oligonucleotide concentration, the fraction bound vs. time profiles followed pseudo-first order behavior (Figure 3-4a and Eq. 9), from which second-order rate constants were obtained with knowledge of the RNA concentration and equilibrium fraction bound (Eq. 10). For all of the oligonucleotides studied, the association rate increased with temperature. Since duplex stability decreases with temperature, the increase in k_a with temperature can be interpreted as the decrease in intramolecular RNA base pairing, thus making target sites more accessible to hybridization by oligonucleotide. The rate constants appeared to obey an Arrhenius law over the temperature range studied, although not enough data points were generated to obtain accurate values for the activation energy (Figure 3-4b).

Second-order association rate constants were found to correlate strongly with overall affinity (Figure 3-5), and the values are similar to those measured in previous studies of oligonucleotide hybridization [204, 205]. Because of the correlation between association rate constant, k_a, and equilibrium dissociation constant, K_D, the dissociation rate constant, k_d ($=k_aK_D$), is relatively constant for almost all of the oligonucleotides studied (Table 3-3). The one exception is oligonucleotide 33, which exhibited unusually rapid association kinetics. RNA folding calculations suggest that this might be explained by the very low energetic cost of altering the RNA structure, combined with no cost for altering oligonucleotide structure (i.e., no hairpins or other stable secondary structures are formed).

3.D.5. Measurement of RNase H cleavage kinetics

The importance of RNase H in the action of antisense oligonucleotides in cell culture is well-established [206]. To understand the relationship between the kinetics of hybridization and the dynamics of RNase H-mediated cleavage of oligonucleotide:mRNA duplexes, hybridization experiments were performed in the presence of RNase H at 37°C. As can be seen for

Table 3-2: Predicted thermodynamics for oligonucleotides to the RBG mRNA at 37°C

Target Position	Total*	RNA Structure Cost ($\Delta G^o_{unfold} + \Delta G^o_{restruct}$)	Oligonucleotide Structure Cost (ΔG^o_{oligo})	Intermolecular Hybridization Gain (ΔG^o_{hyb})
259	-16.5	8.8	1.4	-26.7
139	-20.5	8.8	0	-29.3
448	-17.9	2.6	0.9	-21.4
438	-18.6	5.4	0.7	-24.7
107	-12.4	13.4	1.2	-27
33	-11.8	2.7	0	-14.5
98	-9.5	14.2	0.9	-24.6
147	-17.8	11.3	2.1	-31.2

*All energies listed in kcal/mole.

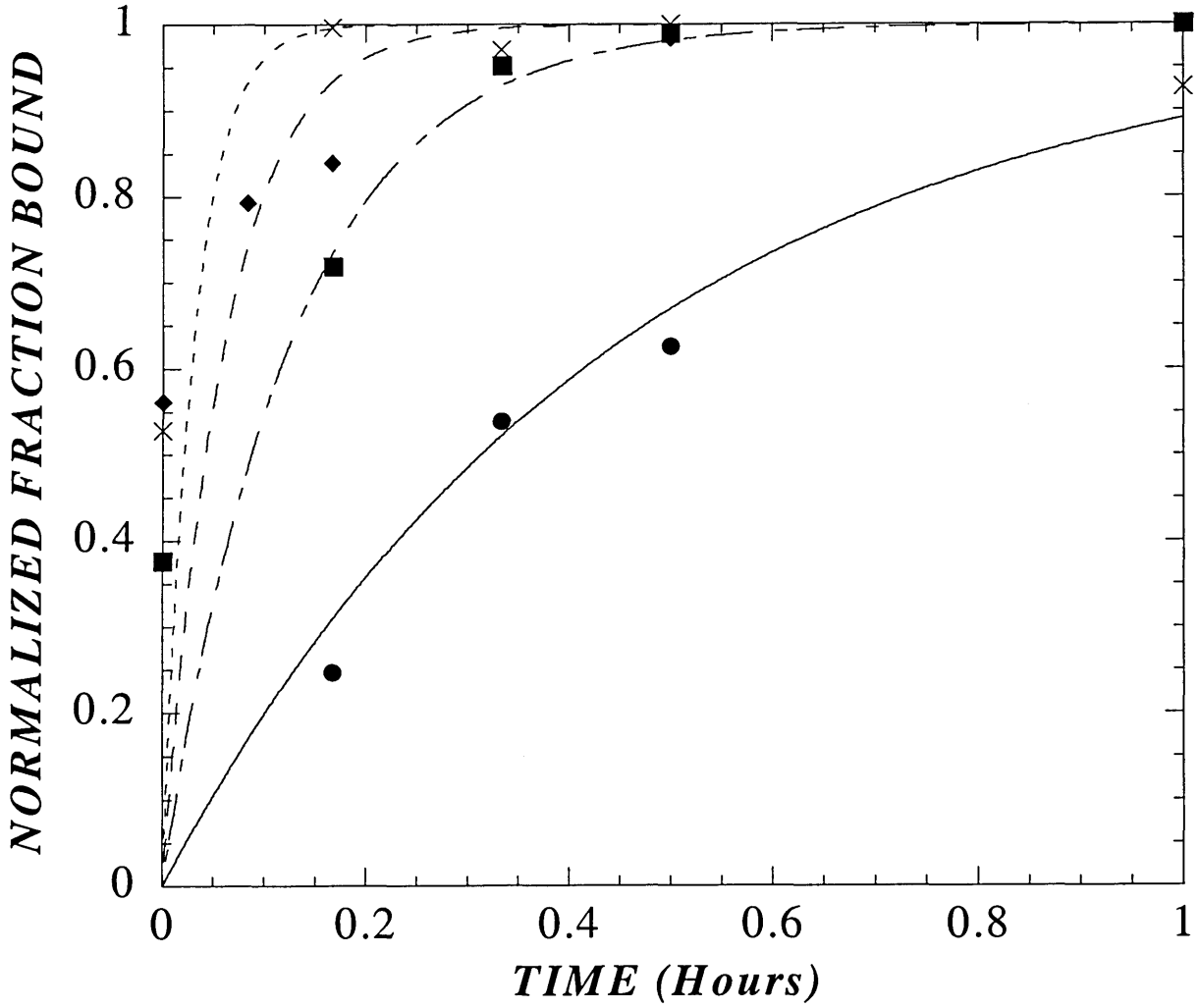

Figure 3-4a: Kinetics of hybridization vary with temperature
Kinetics of hybridization are shown for oligonucleotide 259 binding to the RBG mRNA at (●) 4°C, (■) 25°C, (◆) 37°C, and (X) 50°C. Curves represent the fits to Eq. 9. Increases in temperature (e.g., in melting temperature measurements) destabilize intermolecular hybridization. Increased hybridization, then, points to the destabilization of the native mRNA structure to allow enhanced oligonucleotide association.

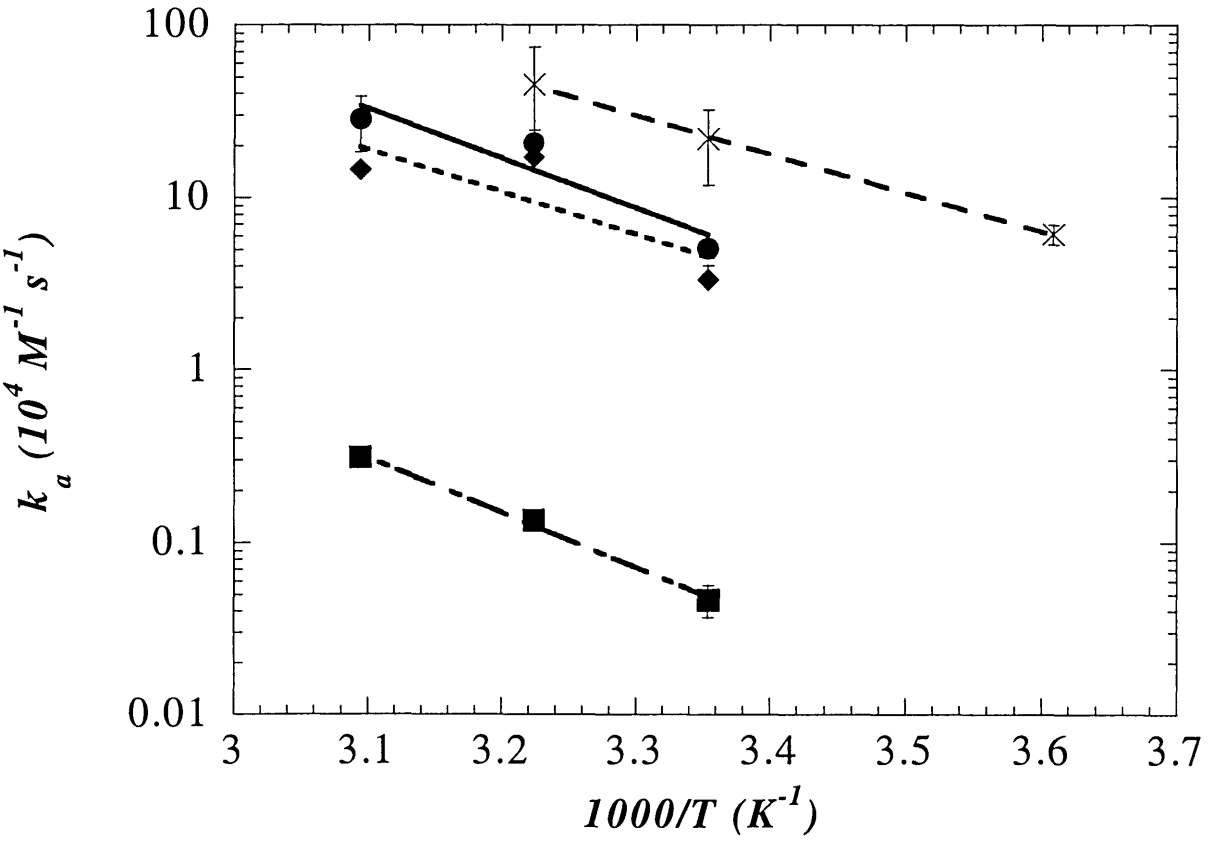

Figure 3-4b: Kinetics of hybridization vary with temperature
Arrhenius plot for oligonucleotides (●) 139, (■) 147, (X) 259, and (◆) 448. For all of the oligonucleotides tested, the association rate increased with temperature in agreement with a typical Arrhenius law. However, too limited a temperature range was used to provide accurate measurement of the associated activation energies.

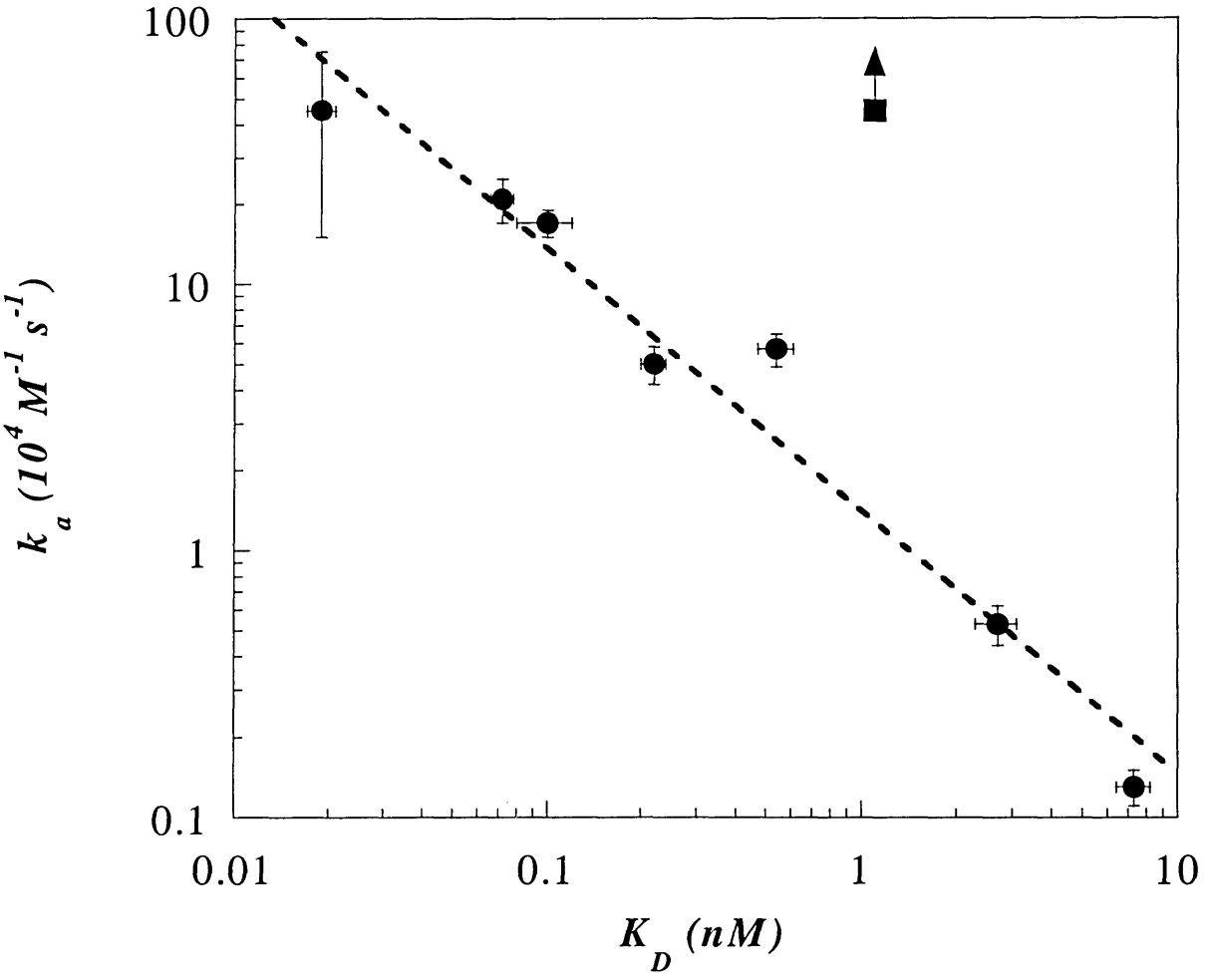

Figure 3-5: Correlation of association rate constant with equilibrium dissociation constant
Second-order association rate constants and equilibrium dissociation constants were determined as described in the text for a panel of oligonucleotides targeting regions of the RBG mRNA with varying predicted structural characteristics. The dotted line is the power law regression: $k_a = 1.4K_D^{-0.99}$ ($R^2 = 0.94$). The square symbol and arrow represent oligonucleotide 33, for which binding was very rapid and k_a could only be bounded. Strong correlation between association kinetics and equilibrium affinity demonstrates the importance of the mRNA secondary structure in defining the strength of the intermolecular interaction.

Table 3-3: Association and RNase H cleavage kinetics of selected oligonucleotides at 37°C

Target Position	K_D (nM)	k_a (10^4 $M^{-1} \cdot s^{-1}$)	k_d* (10^{-5} s^{-1})	RNase H k_{eff} (10^{-4} s^{-1})
259	0.019 ± 0.002	45 ± 30	0.87	4.6 ± 0.9
139	0.072 ± 0.006	21 ± 4	1.5	4.1 ± 1
448	0.10 ± 0.02	17 ± 2	1.8	3.0 ± 0.3
438	0.22 ± 0.02	5.0 ± 0.8	1.1	3.8 ± 0.5
107	0.54 ± 0.07	5.7 ± 0.8	3.1	1.8 ± 0.4
33	1.1 ± 0.3	> 45#	> 50	6.5 ± 2
98	2.7 ± 0.4	0.53 ± 0.09	1.4	0.48 ± 0.05
147	7.3 ± 0.9	0.13 ± 0.02	0.99	0.47 ± 0.07

*Estimated from measured K_D and k_a values.

#Kinetics too rapid for accurate correlation; listed as higher than the highest value that was reliably measured.

A.)

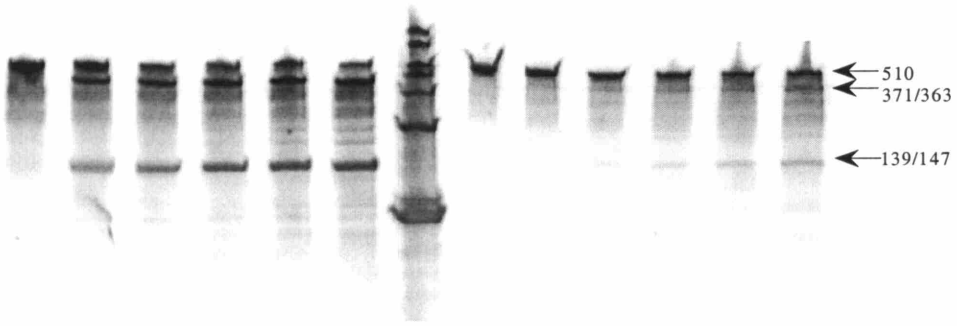

B.)

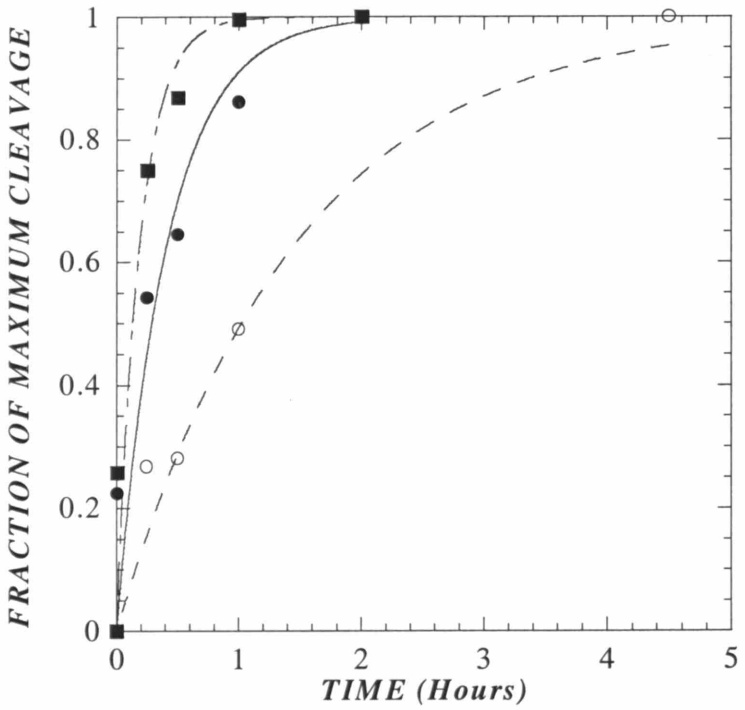

Figure 3-6: Kinetics of RNase H cleavage in the presence of oligonucleotides
A.) Typical RNase H cleavage pattern showing the full-length mRNA (510 nt), and the two cleavage products (139 nt, 371 nt, left; 147 nt, 363 nt, right). In each case, the lanes from left to right represent time points of 0, 15 minutes, 30 minutes, 1 hour, 2 hours, 4 hours. Markers (from bottom) 100, 200, 300, 400, 500, 750, 1000 nt. B.) Rates of cleavage of the full-length mRNA. Points show normalized intensity (see Methods) of the smaller cleavage product band for oligonucleotides (■) 33, (●) 259, and (○) 147. First-order initial cleavage rate constants, k_{eff}, obtained from the fits of the data to Eq. 11, are shown in Table 3-3.

oligonucleotides 139 and 147, cleavage by RNase H results in the formation of two bands corresponding in each case to the length of the regions upstream and downstream of the target site of the oligonucleotide (Figure 3-6a). For all oligonucleotides tested, the appearance of cleavage product followed first-order kinetics (Figure 3-6b), but complete degradation was never observed, possibly due to loss of enzyme activity or product inhibition. The effective rate constants for RNase H cleavage, k_{eff}, are listed in Table 3-3. Although there is some scatter, the k_{eff} values are relatively insensitive to the association rate constants, except at low values of k_a (Figure 3-7); this behavior is predicted by the putative reaction scheme (Appendix 3-1) and corresponds to binding-limited and reaction-limited cases at low and high k_a, respectively.

3.E. Discussion

There has been relatively little study of the interactions between long mRNA molecules (500-4000 nt) and short oligonucleotides (12-25 nt). In mechanistic studies of hybridization, such as those from which nearest-neighbor parameters are determined, short oligonucleotides (typically 6-8 nt) of similar length have been used [200, 207]. This situation is quite different from that for antisense hybridization, where a highly structured mRNA hybridizes with a minimally structured and much shorter oligonucleotide. The selection of hybridization site becomes critical, as each oligonucleotide encounters a different structural landscape on the mRNA. Using our centrifugal assay, we have shown that a panel of 17 nt oligonucleotides complementary to the RBG mRNA exhibits affinities (or, equivalently, equilibrium dissociation constants) spanning nearly five orders of magnitude. Furthermore, for oligonucleotides targeting regions overlapping by as many as 13 out of 17 nt, affinity can vary over 100-fold (e.g., Table 3-1, oligonucleotides 103 and 107). Similarly, association rate constants were found to vary over several orders of magnitude, and in general these mirror the variation in affinity. It is to be expected that such drastic differences in affinity and association kinetics will lead to the types of variability in antisense efficacy often seen in the data from oligonucleotides selected randomly from the target sequence, even if the search is constrained to a small region of the target mRNA.

We and others have found that thermodynamic prediction of the binding affinity of oligonucleotides for their target mRNAs increases the likelihood of finding antisense sequences of high affinity, ribonuclease H activity, and efficacy in cell culture [169, 201]. In this paper,

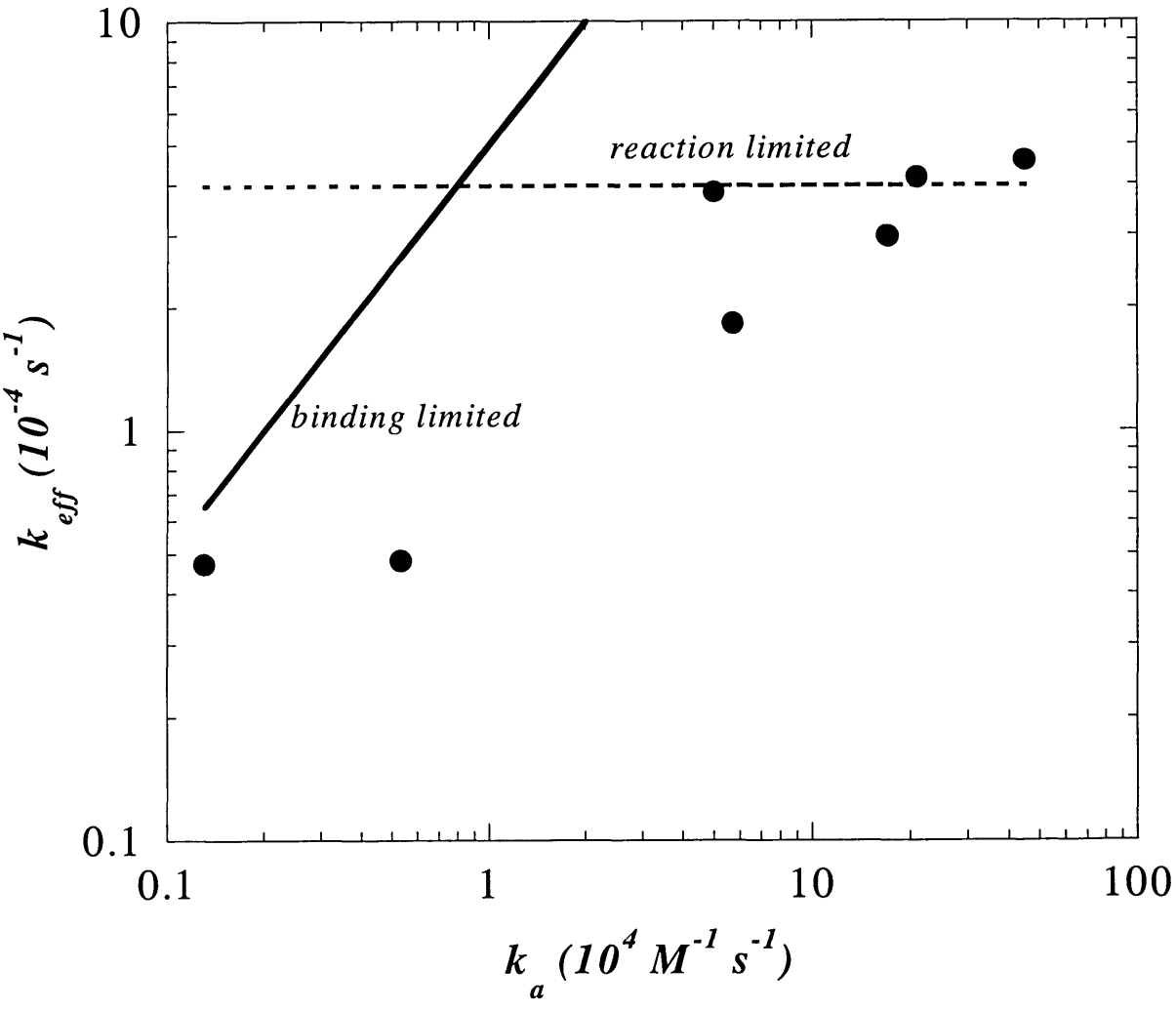

Figure 3-7: Correlation of RNase H cleavage with association rate constant
The association rates and RNase H cleavage kinetics were measured for a panel of antisense oligonucleotides. The solid line represents the expected variation in k_{eff} in the binding limited regime (Eq. 17, Appendix 3-1, no adjustable parameters), and the dotted line represents a constant k_{eff} in the reaction limited regime (Eq. 21, Appendix 3-1, with the maximum fit to the data at the three highest k_a values.

thermodynamic predictions, which correspond to free solution conditions under 1 M NaCl, were tested for the first time with experimental measurements made under comparable conditions. The range of dissociation constants observed experimentally ($0.01 \leq K_D \leq 550$ nM) was significantly smaller than the range predicted from the model ($4x10^{-6} \leq K_D \leq 10^4$ nM), though for a number of oligonucleotides the predictions were indeed of the right order of magnitude (Table 3-1). In light of the unrealistically wide range of predicted dissociation constants, it seemed more reasonable to express the predictions as a ranking, or percentile score, which indicates those oligonucleotides that should have lower and higher affinity on a relative scale. On this basis, there is a positive correlation with solution binding affinity (Figure 3-3a), but the correlation is of moderate power, similar to comparisons of our predictions with binding measured by an oligonucleotide array [201], or with ribonuclease H susceptibility [169] and activity in cell culture [147]. Taken together, these results suggest that the limitation in using binding affinity predictions to select antisense reagents is not the differences in binding in solution vs. in cells [193] or the sequence-dependent processing of oligonucleotides by cells, but the imperfect ability to predict affinity itself.

Binding affinity predictions are limited by the accuracy of structural descriptions. In structural prediction alone, 70-80% accuracy as compared to phylogenetically determined structures is sufficient to predict the major features of the native mRNA structure [200]. However, when looking at oligonucleotides that might target at most 5% of the mRNA structure (a 25-mer targeted to a 500 nt mRNA), greater accuracy will be required to increase the reliability of oligonucleotide hybridization energy predictions. Efforts to extend these predictions have focused on predicting pseudoknot formation and combining free energy predictions with other methods such as a comparative analysis or statistical sampling [208-211]. However, the lack of detailed experimental data with which to validate folding algorithms is likely to limit the development of major improvements in the near future.

When secondary structural features can be more accurately predicted and tertiary interactions can be accurately modeled and understood [165], it will be possible to further reduce the fraction of oligonucleotides that should be tested *in vitro* to be considered viable antisense candidates. For the time being, predictions of binding affinity will be useful in concert with accurate *in vitro* assays. A useful metric for rational selection may be the percentile score

(Figure 3-3a). For example, the group of oligonucleotides measured to have K_D values less than 0.1 nM had average percentile scores of 79%. For the 0.1-1.0 nM and greater than 1.0 nM groups, respectively, the average scores are 73% and 34%. Selection of potential candidates from among the set expected to be highest in affinity will enhance considerably the likelihood of identifying sequences that have high affinity and are expected to have antisense activity [193]. For example, we have experienced marked success testing *in vitro* sequences selected from the highest percentile scores (> 95%) [147].

Although we have found that the calculated free energy of binding is a better predictor of binding affinity than the RNA structure alone, or the free energy of folding the RNA into its structure, one might expect the structure to be more indicative of association kinetics. The predicted structure of the RBG mRNA is shown in Figure 3-8, with the highlighted regions representing those targeted by oligonucleotides used in the kinetics experiments. In general, the oligonucleotides that exhibited the most rapid binding kinetics (33, 259, 139, and 448) target regions with less structure than those exhibiting slower kinetics. Oligonucleotide 33 exhibited unusually rapid binding relative to its affinity (Table 3-3). This oligonucleotide is predicted target a region spanning a bulge and a joint in the RBG RNA, with several non-canonical base pairs included among the structured region in between. Others have posited that unstructured regions of the RNA should provide necessary accessibility for oligonucleotide binding [178, 211], and this has been shown nicely in a case where the target was carefully genetically engineered [212]. One study of the correlation between predicted structure and cell culture effectiveness [174] suggests that an unstructured 5' end of the RNA is particularly important for initiating hybridization.

Kinetic effects, such as the bias towards nucleation from one side of the oligonucleotide that is suggested by the results described above, could complicate thermodynamic prediction of oligonucleotide:mRNA affinity, but the close correlation between association kinetics and affinity suggests that this is probably not a serious limitation. Other effects could alter the agreement between theoretical prediction and experimental observation of affinity. For example, it has been suggested that a single minimum free energy structure may not accurately describe RNA and, instead, an ensemble of structures should be evaluated [169, 213]. We have found that an ensemble-average free energy is no better predictor of binding affinity in the RBG system

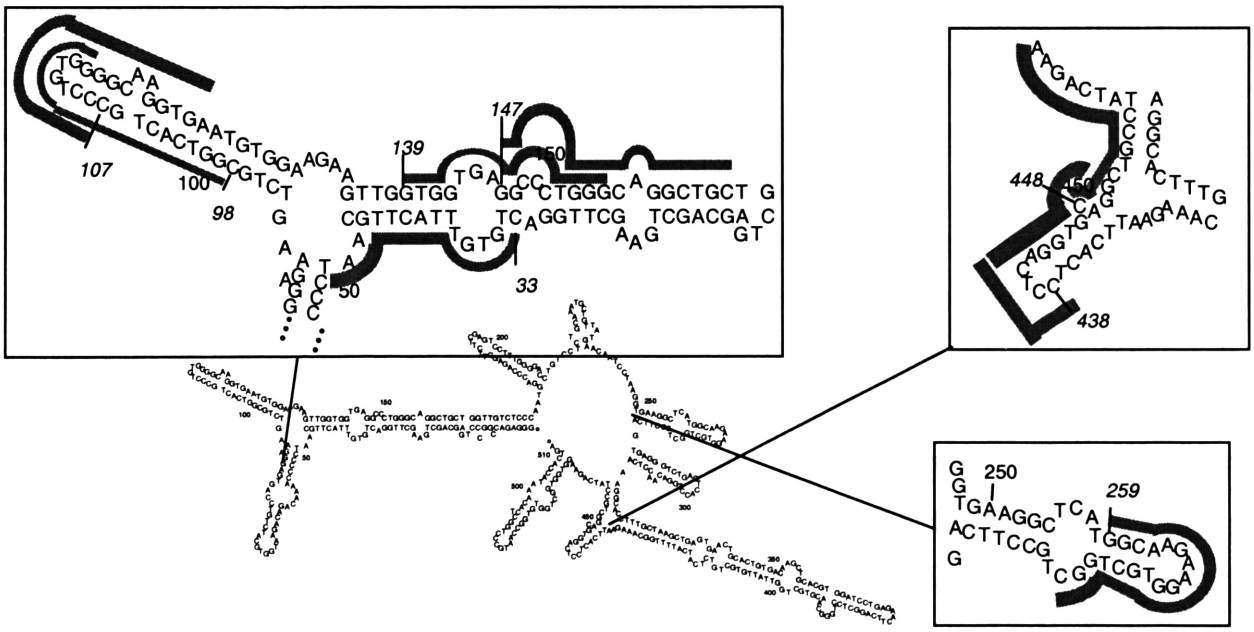

Figure 3-8: Predicted RBG mRNA structure

The predicted structure of the RBG mRNA was determined using *mfold*, as described in the Materials and Methods. The complementary region for each oligonucleotide on which kinetic experiments was performed is indicated by a gray bar. Particular structural features, for instance, hairpins as targeted by oligonucleotide 259, tend to be targeted by the fastest binding oligonucleotides. However, the presence of a great deal of intramolecular structure does not prevent rapid association kinetics (e.g., oligonucleotide 139). The discrepancy in binding kinetics between oligonucleotides 139 and 147 suggests a minimum of 3 single-stranded bases required for heteroduplex initiation.

(unpublished results), but qualitative use of structural ensembles has been shown to exhibit moderate utility in identifying accessible binding sites on the RBG mRNA [211].

The thermodynamic model for antisense binding results in calculation of the binding affinity for an oligonucleotide:mRNA interaction under conditions that may or may not be relevant for antisense efficacy in cells. In the latter case, activity is complicated by the need for rapid kinetics, possible differences in binding thermodynamics and kinetics in the cellular environment (e.g., presence of RNA binding proteins), and the role of ribonuclease H in mediating destruction of targeted transcripts in living cells. The interplay among these different events and phenomena has not been explored extensively and quantitatively. We have sought to connect prediction of dissociation constants with their measurement, and measured dissociation constants (K_D) with association rate constants (k_a), and association rate constants with RNase H cleavage (k_{eff}). A very strong correlation was observed between K_D and k_a, with the notable exception of oligonucleotide 33, which exhibited unusually rapid kinetics. The region of the RBG mRNA targeted by this oligonucleotide (Figure 3-8) is extremely flexible (RNA structure cost 2.7 kcal/mole), and the oligonucleotide itself has no stable structure (Table 3-2); therefore, a structural origin for such anomalous behavior is suggested.

A correlation between RNase H cleavage and oligonucleotide:RNA association rate is also indicated by our results, albeit not a uniform linear correlation. Kinetic analysis of the interplay between oligonucleotide:RNA binding and RNase H-catalyzed cleavage of duplexes shows that in the binding-limited case, the effective rate constant is equal to the product $k_a O_T$ (Appendix 3-1). For the lowest values of k_a measured, the corresponding values of k_{eff} appear to approach this limit (Figure 3-7 and Table 3-3). In the other limit of slow catalysis, the observed cleavage rate is expected to be independent of k_a (Appendix 3-1). Indeed, this was observed (Figure 3-7), although it was necessary in this case to fit the maximum value of k_{eff}.

In vitro RNase H assays can be reliable predictors of antisense efficacy in living cells. Several researchers have reported that antisense oligonucleotides that induce cleavage of a target RNA in the presence of RNase H tend to be effective antisense reagents in cell culture [177, 214]. In RNase H mapping experiments, the amount of both oligonucleotide and RNA is quite high, resulting in a high rate of binding, and perhaps increasing the number of oligonucleotides that mediate cleavage. However, many antisense targets *in vivo* are transcripts expressed in

relatively low abundance, which will present a much more stringent condition to the association of oligonucleotides; thus, controlling the oligonucleotide library concentration may help select for the fastest binding members. It is not yet clear whether measured affinity, binding kinetics, or RNase H cleavage rates correlate most strongly with effectiveness in cell culture.

The optimization of antisense efficacy with minimal non-specific effects will result from concerted efforts in oligonucleotide chemistry, delivery, and target site selection. With the ability to predict high affinity sequences that bind with rapid association kinetics, it is possible to optimize the target site selection so that downstream modifications and conjugations can be explored with the greatest hope for success. Modifications that destabilize native mRNA structure may prove a fruitful avenue for enhancing antisense efficacy, as structural factors appear to determine which oligonucleotides have the highest binding affinities. With the coupled dynamics of nuclease degradation and intracellular diffusion acting as kinetic traps for the effectiveness of antisense oligonucleotides, the ability of an oligonucleotide to access rapidly its target site becomes even more critical to its activity. While further exploration of these effects *in vivo* is required, it may become increasingly possible to rationally engineer highly effective antisense oligonucleotides for therapeutic and other applications.

4. *Demonstration of Model Applicability to Cellular System*

4.A. *Abstract*

Antisense oligonucleotides are an attractive therapeutic option to modulate specific gene expression. However, not all antisense oligonucleotides are effective in inhibiting gene expression, and currently very few methods exist for selecting the few effective ones from all candidate oligonucleotides. The lack of quantitative methods to rapidly assess the efficacy of antisense oligonucleotides also contributes to the difficulty of discovering potent and specific antisense oligonucleotides. The development of a prediction algorithm for identifying high affinity antisense oligonucleotides based on mRNA-oligonucleotide hybridization has been previously described. In this study, the antisense activity of these rationally selected oligonucleotides against three model target mRNAs (human lactate dehydrogenase A and B and rat gp130) in cell culture is reported. The effectiveness of oligonucleotides was evaluated by kinetic RT-PCR, allowing quantitative evaluation of mRNA levels and thus providing a measure of antisense-mediated decreases in target mRNA, as occurs through RNase H recruitment. Antisense oligonucleotides that were predicted to have high affinity for their target proved effective in almost all cases, comprising tests against three different targets in two cell types with phosphodiester and phosphorothioate oligonucleotide chemistries. This approach should aid the development of antisense oligonucleotides for a variety of applications.

4.B. *Introduction*

Antisense oligonucleotides are being used to modulate gene expression in a variety of research, biotechnology, and therapeutic applications [8]. Despite a number of notable successes, the application of antisense oligonucleotides to modulate gene expression has proven to be more difficult than originally estimated. The most frequently noted barriers to efficacy involve issues of oligonucleotide stability and delivery, which are being addressed in many laboratories by modified oligonucleotide chemistries and by derivatization and/or encapsulation of the oligonucleotides [16]. In contrast, selection of a highly active oligonucleotide sequence towards a particular target has only recently been recognized to be a major barrier and, thus far, has proven to be a much more significant challenge. The most widely utilized strategy for selecting active oligonucleotides is to synthesize a large number of candidate oligonucleotides complementary to different regions of the target mRNA and test them all empirically for activity in an appropriate model system [190, 216].

An alternate approach to oligonucleotide selection is the use of a combinatorial screen, which typically involves the use of RNase H and a library of oligonucleotides to map the accessible portions of the target mRNA [177, 183]. The results of these types of experiments, as well as more detailed studies, increasingly support the view that the activity of antisense oligonucleotides in cells is related to the structure of the targeted mRNA [174, 175, 212-214]. However, a quantitative understanding of the relationship between structure and activity is lacking to date, and the resolution of the mechanistic details would greatly aid in the design of active antisense sequences. At the simplest level, certain sequence motifs have been found to correlate with antisense activity [158, 159], though it is unclear why such a relationship exists or whether the correlation is adequate for rational design. Some researchers have argued that a short run of unpaired nucleotides in a native RNA structure is necessary to initiate binding of the complementary oligonucleotides [174, 212]; this view essentially says that hybridization is kinetically limited. We [201] and others [169] have adopted a thermodynamic approach, in which we account for the complete thermodynamic cycle involved in oligonucleotide binding to a structured RNA target: unfolding some of the native RNA structure to accommodate the antisense oligonucleotide, hybridizing the oligonucleotide to the RNA, and rearranging the bound structure after binding. This approach has been justified on the quality of correlations of

predictions made with the thermodynamic model to binding data and RNase H mapping results, and also on observed correlations between affinity and effectiveness in cell culture [193].

In this work, we have used the thermodynamic modeling approach to select antisense oligonucleotides that are predicted to have high affinity for their targets as candidates for the inhibition of target gene expression in cell culture. One of the problems with developing correlations between effectiveness in cell culture and theoretically derived quantities is that measurements of the former are typically not very sensitive, and the extent of inhibition observed may be slight relative to the expression level. The need for quantitative differential mRNA measurement is addressed by kinetic reverse transcription polymerase chain reaction (kRT-PCR), which is an extremely sensitive technique that allows analysis of expression levels from very small amounts of RNA [217-219]. In this report, we utilize a kinetic PCR assay to assess the ability of our prediction algorithm to identify antisense oligonucleotides that are effective inhibitors of gene expression in living cells. The selection algorithm has been applied to predict high affinity antisense oligonucleotides complementary to the human lactate dehydrogenase (LDH) A and B mRNA and the rat gp130 mRNA. The *in vitro* inhibition of gene expression for each of these targets by these rationally selected antisense oligonucleotides has been demonstrated. Furthermore, changes in protein expression were observed to correspond to those in mRNA for those systems that are transcriptionally controlled.

4.C. Materials and Methods

Cell Culture and Reagents: A sub-clone of the H35 rat hepatoma cell line selected for its acute-phase responsiveness [220] was grown and maintained in T25 flasks containing Dulbecco's modified eagles medium (DMEM, Life Technologies, Long Island, NY) supplemented with 10% fetal bovine serum (Life Technologies) in the presence of Penicillin 200 U/mL, Streptomycin 200 μg/mL specific activity, and Gentamycin 10 U/mL in a humidified 5% CO_2 incubator at 37°C. Primary cultures of fibroblasts were isolated from human foreskin [221] and grown on 100 mm dishes in DMEM supplemented with 10% bovine calf serum (Life Technologies) in the presence of Penicillin 200 U/mL and Streptomycin 200 μg/mL specific activity. For both cell types, the growth medium was replenished 24 hours prior to the experiment (after the cells had reached confluence).

Rational selection of antisense oligonucleotides: In this study, the human lactate dehydrogenase (LDH) A and B mRNA isoforms and the rat gp130 mRNA were used as the target molecules. The prediction of the binding affinity of oligonucleotides complementary to target mRNA was performed as described elsewhere [201]. Briefly, the free energy (ΔG°_{total}) of antisense binding to a structured mRNA target was computed from a sum of free energy terms of the form:

$$\Delta G^{\circ}_{total} = \Delta G^{\circ}_{oligo} + \Delta G^{\circ}_{unfold} + \Delta G^{\circ}_{hyb} + \Delta G^{\circ}_{restruct} \quad (12)$$

The negative of the unfolding energy (ΔG^{o}_{unfold}) was computed as the minimum free energy secondary structure for the target mRNA as predicted using *mfold* v2.3 [167, 168] and was a constant for any target RNA regardless of the oligonucleotide candidate. The energy required to break up secondary structure in the oligonucleotide (ΔG°_{oligo}, which frequently is negligible due to the short size of the oligonucleotides) was computed in the same manner, except with DNA rather than RNA parameters [186]. Folding calculations were performed using a temperature of 37°C without correction for ionic strength. The free energy for the intermolecular interaction of the oligonucleotide and the mRNA was calculated using nearest-neighbor parameters for RNA:DNA hybrids [185]. The available parameters are based on phosphodiester oligonucleotides while, in some of our experiments, phosphorothioate oligonucleotides were used. The energy to refold the RNA with an antisense oligonucleotide bound ($\Delta G^{\circ}_{restruct}$) was calculated using *mfold* by constraining the bases bound by oligonucleotide not to participate in intramolecular base pairing. Except for $\Delta G^{\circ}_{unfold}$, each term was computed for each 15-mer oligonucleotide complementary to the target mRNA, the sums ΔG°_{total} determined for each candidate oligonucleotide, and the resulting table of free energies sorted to choose (rationally design) the most effective (and in some cases, least effective) antisense candidates based on predicted overall free energy of binding.

A panel of oligonucleotides complementary to the mRNA for rat gp130 was chosen, including ones among the best (Good1, Good 2, and Good 3) or worst (Bad1 and Bad2) in the ranking of 3039 possible oligonucleotides (Table 4-1). The gp130-targeting oligonucleotides were selected from clusters that appeared among the highest and lowest affinity predictions. For example, oligonucleotides targeting positions 2046 (Good1), 2055, and 2053 were predicted to

Table 4-1: Properties of candidate oligonucleotides for cellular assays

Target	Name	Sequence	Position*	Target Region	Rank#	ΔG_{TO} (kcal/mol)
LDH-A	AS-A	GGCGGTCGTCGGGGG	44	3'-UTR	1	-22.5
LDH-B	AS-B	CGCCATGTTCCCCCA	656	Coding	1	-19.6
LDH-A	NS-A♣	GCGTGGGCGGCGGGT				
LDH-B	NS-B♣	CGCTCACTCGCACTC				
gp130	Good1	GGGGGTGTGAGGTGA	2046	Coding	1	-20.3
gp130	Good2	CCCGCAGGAGCCGGT	2812	Coding	32	-18.1
gp130	Good3	TCTGGCCGCTCCTCG	2414	Coding	11	-19.0
gp130	Bad1	GTATAGCCCATCATG	593	Coding	3039	2.2
gp130	Bad2	TCCTTATTCAAGATG	22	3'-UTR	3028	0.7
gp130	NS-G1♣	GTGGAGTGGGAGTGG				
gp130	NS-G2♣	CCCGCAGGAGCCGGT				

* Position corresponds to the 5'-terminal base of the targeted region on the mRNA (3'-terminal base of the oligonucleotide).

The rank of the oligonucleotide is out of all the possible oligonucleotides generated for any particular transcript (1647 for LDH-A, 1258 for LDH-B, and 3039 for gp130).

♣ Nonsense sequences have identical base composition to their antisense counterparts but in scrambled order.

be those with the highest affinity. Only Good1 was tested among these, as they are relatively close in target position, and it was desirable to test oligonucleotides predicted to have high affinity targeting different positions along the mRNA. The sequences NS-G1 and NS-G2 were randomly scrambled nonsense controls to Good1 and Good2 and had the same base composition as the antisense sequences. For human LDH-A and B, a single oligonucleotide was in each case chosen that was predicted to have the highest affinity (AS-A, out of 1647 and AS-B out of 1258 possible oligonucleotides, respectively; see Table 4-1).

Purification of antisense oligonucleotides: Phosphodiester oligonucleotides (15 bases) antisense to the human LDH-A and B mRNA were synthesized and HPLC purified at the 200 nmol scale by Life Technologies. Phosphorothioate oligonucleotides (15 bases) antisense to the rat gp130 mRNA were synthesized at the 1 μmol scale at the Oligonucleotide Synthesis Core facility of Massachusetts General Hospital (Boston, MA). The gp130 phosphorothioate oligonucleotides were dissociated from the solid bead supports by resuspending in 1 mL of 100% ammonium hydroxide and incubating overnight at 54°C. Full-length oligonucleotide with the 5' DMT group was separated on a 10 x 250 mm C-18 reverse phase column as previously described [60]. The terminal 5'-O-DMT group was detritylated by the addition of 1 mL of 40% aqueous acetic acid, incubated 20 min on ice, followed by the addition of 1 mL of 50% ethanol, and evaporated on a rotary vacuum. The oligonucleotide was desalted on a Sephadex G-10 column (Pharmacia, Piscataway, NJ), evaporated on a rotary vacuum, and resuspended in 1 mL HPLC grade water. The purity of the final material was assessed by analytical RP-HPLC on a 10 x 250 mm C-18 column. The concentration of the purified oligonucleotide was estimated from the absorbance at 260 nm using the following expression for the extinction coefficient:

$$\varepsilon_{260} = (15.34[A] + 12.16[G] + 8.70[T] + 7.60[C]) \times 0.9 \times 10^3\ M^{-1}\ cm^{-1}$$ [222].

Antisense assays with H35 cells: Antisense inhibition experiments against rat gp130 were performed with H35 rat hepatoma cells in 24 well plates under serum-free conditions. Lipofectin® (Life Technologies, Long Island, NY) was added to DMEM with 1 μM dexamethasone (Sigma, St. Louis, MO) at an equal charge ratio to the oligonucleotides (assuming 1 positive charge per molecule of Lipofectin® and 14 negative charges per 15 nucleotide oligonucleotides), and the medium was incubated for 45 min at room temperature.

Phosphorothioate oligonucleotides (600 nM) were added to the Lipofectin®-containing medium and incubated for another 15 min at room temperature. The cells were washed twice with phosphate buffered saline (pH 7.20), and the oligonucleotide-containing medium was added to two sets of plates. After 8 hours, the cells were scraped from one set of plates, washed with phosphate buffered saline (pH 7.20), and stored at –20°C until further use. The second set of plates was incubated for another 16 hours (24 hours of antisense treatment) with fresh medium containing 1 μM dexamethasone and 10 ng/mL recombinant human interleukin-6 (R&D Systems, Minneapolis, MN). The supernatants were then collected and stored at –20°C until further use. For timing experiments, antisense treatment was performed as described above. Replicate wells of a 24-well plate were sacrificed at various times after treatment, at which the cells were scraped, washed with phosphate buffered saline (pH 7.20), and stored at –20°C until further use.

Antisense experiments with human primary fibroblasts: Antisense inhibition experiments against LDH-A and LDH-B were performed using human foreskin fibroblasts in 6-well plates under serum-free conditions. The protocol was similar to that used with H35 cells, except that, prior to the experiment, the cells were switched to serum-free growth medium for 24 hours. After 4 hours of exposure to antisense oligonucleotides, 20 ng/mL of epidermal growth factor (Sigma, St. Louis, MO) in a change of fresh medium was added to the cells for another 20 hours. These cells were then washed with phosphate buffered saline (pH 7.20) and lysed in the plate. The lysate was centrifuged for 5 min at 10,000 x g at 4°C and stored at –20°C until further use.

Isolation of total RNA: Total RNA was isolated from approximately 2 x 10^6 hepatocytes or 0.2 x 10^5 fibroblasts using the Nucleospin II RNA isolation kit from Clontech (Palo Alto, CA), as per the manufacturer's instructions. The RNA was quantified using the absorbance at 260 nm and the purity assessed from the ratio of absorbance at 260 and 280 nm. The RNA used for all assays had a ratio of A_{260}/A_{280} greater than 1.90.

Reverse transcription and PCR of acute phase response gene transcripts: The mRNA sequences for rat gp130, rat GAPDH, rat and human LDH (isoforms A & B), and the rat and human 18S rRNA sequence were derived from their respective cDNA sequences, which were retrieved from the GenBank database. Gene-specific PCR primers were designed using the Oligo 4.0 software (Molecular Biology Insights Inc., Cascade, CO). Primer pairs that predicted

minimal primer-dimer (non-specific, template independent product) formation and those that yield a PCR product of 200-300 bp were selected (Table 4-1).

For reverse transcription, gene-specific downstream primers (Table 4-1) were used to generate each cDNA individually using the Access RTPCR system (Promega Corporation, Madison, WI) according to the manufacturer's instructions. Downstream primers were selected based on the predicted inability to cross-hybridize with the other transcripts of interest using the Oligo 4.0 program. The reverse transcribed template was stored at –20°C until further use.

PCR was performed using the Light Cycler v1.3 (Idaho Technology, Salt Lake City, UT) according to the manufacturer's instructions. A 1:40,000 dilution of SYBR Gold (Molecular Probes, Eugene, OR) dye was added directly to the PCR reaction mixture for fluorescent detection after each amplification cycle. The reaction conditions (magnesium chloride concentration, annealing temperature, and primer concentration) for each transcript were optimized so that primer-dimer formation was minimized. The specificity of the PCR products was verified using the melt curve generated by the Light Cycler (i.e., the presence of a single transition) as well as by electrophoresis on 2% agarose gels (i.e., the presence of a single band of the appropriate length).

A standard curve of concentration vs. cycle number was generated for each transcript to determine the copy number of the mRNA in hepatocytes. First, the transcript to be quantified was amplified and the amount of pure cDNA product estimated using the absorbance at 260 nm. Serial dilutions of the quantified PCR product were then used as the template for PCR to generate a standard curve of concentration vs. threshold cycle number and to determine the concentration of the specific cDNA in any unknown sample that is amplified along with the standards. This method allows calculation of the total number of cDNA molecules after reverse transcription. Assuming that the efficiency of reverse transcription is close to 100%, the number of specific mRNA transcripts/cell was then calculated.

Data analysis: Fluorescence data acquired after each cycle of amplification was extracted from the Light Cycler software and imported into a Microsoft Excel spreadsheet for further manipulations. The number of molecules, N, of an amplified transcript after n cycles of PCR can be related to the initial number of molecules N_o by:

$$N = N_o(1+\varepsilon)^n \tag{13}$$

where ε is the efficiency of each cycle; if ε=1, then the amount of product doubles in each cycle. During the early cycles of amplification, the efficiency is constant and close to unity, and the cycle number, n, at which the fluorescence intensity increases above a predetermined threshold value (which is somewhat variable, depending on the concentration and yield of the fluorescent dye, but generally between 0.2 and 0.3), allows computation of the initial number of copies N_o by

$$\frac{(N_o)_{\text{gene}}}{(N_o)_{\text{reference}}} = \frac{(1+\varepsilon_{\text{reference}})^{n_{\text{reference}}}}{(1+\varepsilon_{\text{gene}})^{n_{\text{gene}}}} \tag{14}$$

To calculate changes in antisense-treated mRNA, the amount of specific mRNA is first normalized to that of 18S rRNA in the same sample using equation (3). The fold-change after antisense treatment is calculated as the ratio of normalized mRNA between the treated sample and the untreated control. In all our calculations, the efficiency has been assumed to be 1.0. All PCR amplifications were performed in triplicate, and the average threshold cycle number was used for calculating fold-changes in mRNA.

LDH assay: The enzymatic activity of LDH (due to a combination of A & B isoforms) was measured using the lactate dehydrogenase kit (500-C, Sigma , St. Louis, MO) as per the manufacturer's instructions.

Western blots: Antisense oligonucleotide-treated H35 cell culture supernatants were collected, electrophoresed on 4-20% Tris-HCl gels (Bio-Rad, Hercules, CA), and transferred onto a nitrocellulose membrane (Bio-Rad) according to the manufacturer's protocol. The blots were blocked with 5% low-fat milk for 1 hour at room temperature, and incubated overnight at 4°C with a 1:2500 dilution of anti-human haptoglobin, goat IgG (ICN Biomedical, Costa Mesa, CA). Each blot was then washed three times for 5 min each, incubated for 1 hour at 37°C with an anti-goat IgG, horseradish peroxidase-conjugated secondary mouse antibody (ICN Biomedical) at a 1:5000 dilution, washed three times, developed using an enhanced chemiluminescence system (Pierce, Rockford, IL), and imaged on a GS525 Molecular Imager System (Bio-Rad).

Statistics: Data are reported as the mean and standard deviation of two independent experiments. Statistical comparisons among groups were performed using ANOVA followed by Tukeys' honest significant difference test with differences deemed significant at the level

($p<0.05$). Inferences on correlation of ΔG° values with mRNA levels were made using the one-tailed t test for the slope, i.e., on the hypothesis that the slope is positive.

4.D. Results

4.D.1. Description of kinetic RT-PCR technique and results

Kinetic PCR amplification following reverse transcription (kRT-PCR) is a relatively new development that takes advantage of the sensitivity of PCR while minimizing the confounding effects of primer-dimer formation and competitive cross-priming of unintended products. This technique is well-suited for the evaluation of antisense oligonucleotides, where sensitivity and precision are important requirements, as the targeted mRNAs are often of low abundance and only partial inhibition of basal expression levels is typically observed.

First, we calibrated the assay by creating standard curves for each transcript of interest from its corresponding cDNA, which was generated by primer-specific reverse transcription of total RNA isolated from primary rat hepatocytes, as described in Material and Methods. In kRT-PCR, the number of copies of starting material is determined from the early rounds of amplification, when the efficiency (number of copies of product per copy of template) for each round is close to unity. An example of kinetic PCR data for the 18S ribosomal RNA (which is used as a housekeeping standard) is shown in Figures 4-1a – 4-1c. The raw fluorescence is indistinguishable from background at early cycles, grows exponentially, then plateaus at higher cycle numbers, where the coupled effects of dNTP depletion, primer-dimer formation and amplification, and fluorescence quenching result in a plateau fluorescence level that is relatively insensitive to starting concentration (Figure 4-1a). By correcting for background and choosing a low threshold level during which the fluorescence is increasing exponentially, a concentration dependence consistent with theory (i.e., equation 2) is observed (Figure 4-1b). Note that some product is created at high cycle numbers in the absence of cDNA, which shows that amplification of primers does indeed occur and constrains the lower limit of detection. For samples of two different concentrations (N vs. N_o) amplified at the same average efficiency (ε), equation 2 predicts that the threshold cycle number (n) should be linear in the logarithm of starting concentration:

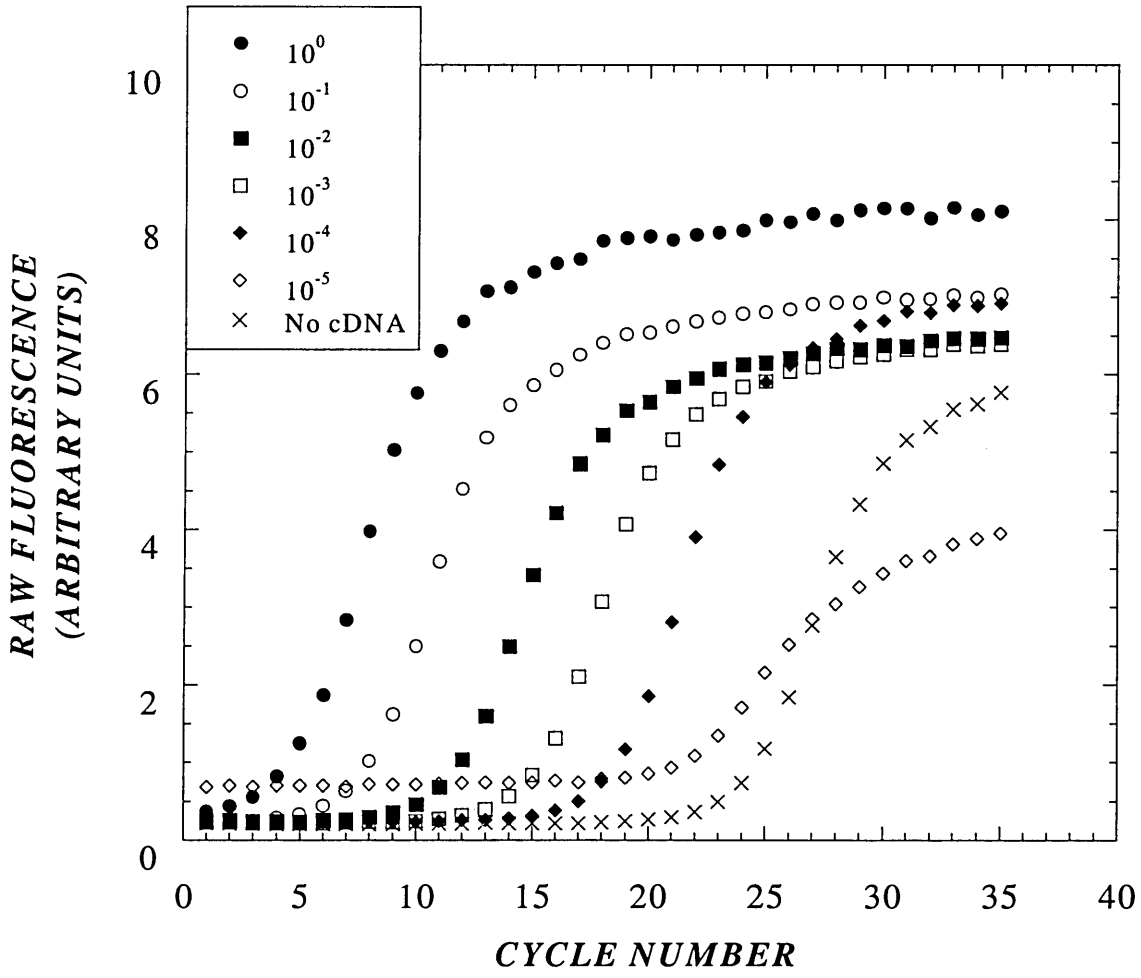

Figure 4-1a: Kinetic PCR dilution series using 18S cDNA

A) Raw fluorescence data for dilutions of a stock solution of 18S cDNA, ranging in relative concentration from 1 to $1x10^{-5}$, as well as primers only (no cDNA).

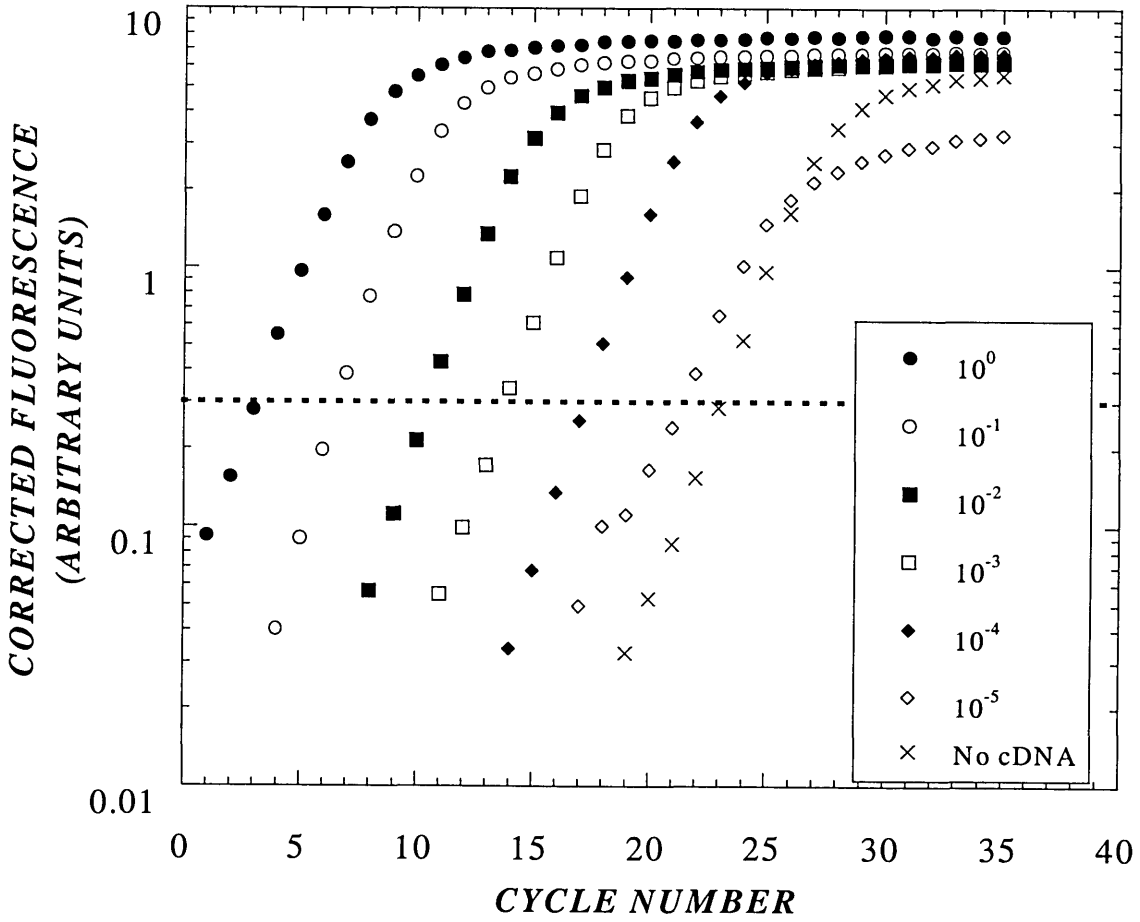

Figure 4-1b: Kinetic PCR dilution series using 18S cDNA

B) Background corrected fluorescence showing parallel curves passing a threshold (arbitrarily set within the regime of exponential growth of fluorescence with respect to cycle number) at equally spaced intervals of roughly 3.3 cycles/10-fold change in concentration.

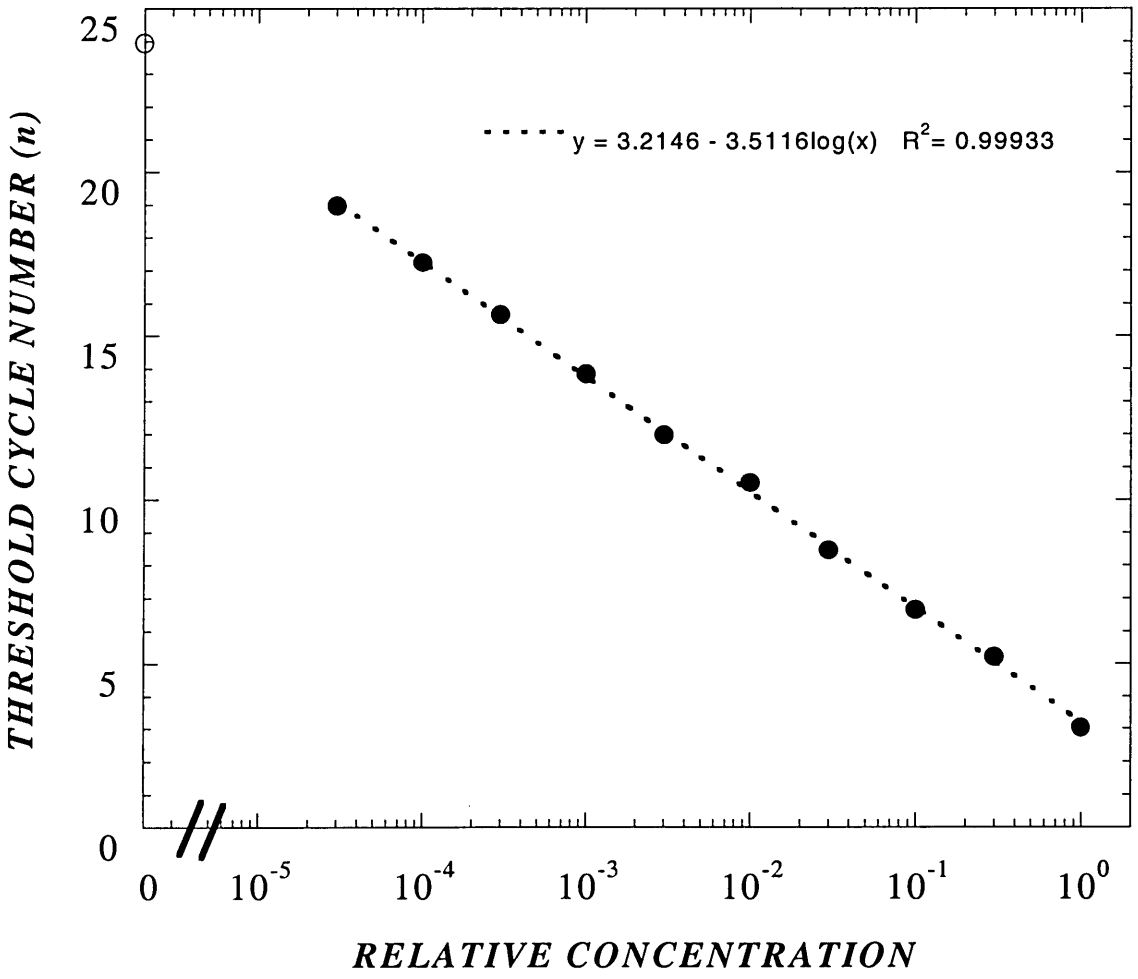

Figure 4-1c:Kinetic PCR dilution series using 18S cDNA

C) Standard curve of threshold cycle number (n) vs. log(c). Dotted line represents a best logarithmic fit ($n = 3.21 - 3.51 \log(c)$; $r^2 = 0.999$) to the data.

$$n - n_0 = -\frac{1}{\log(1+\varepsilon)} \log\left(\frac{N}{N_0}\right) \tag{15}$$

Indeed, this was observed, establishing a standard curve valid for nearly five orders of magnitude (Figure 4-1c). Standard curves were also generated for the albumin, LDH-A, LDH-B, and gp130 transcripts; these were used in the measurements described below. Assuming that all these transcripts were reverse-transcribed with similar efficiencies, one can compute an approximate lower bound for the detection limit of kinetic PCR as 10–100 copies of specific mRNA/cell (using our protocols).

4.D.2. Dynamics of inhibition of gp130 by antisense oligonucleotides

First, we studied the dynamics of mRNA inhibition using two antisense sequences (Table 4-1) directed against the mRNA encoding rat gp130 mRNA. Gp130 is a receptor subunit involved in signaling of IL-6 family cytokines and, as such, plays a critical role in a diverse array of biological processes including hematopoiesis, neuronal differentiation, activation of anti-apoptotic pathways in cardiac myocytes, and the hepatic acute phase response [223, 224]. Serum-free medium containing phosphorothioate antisense oligonucleotides at 600 nM, pre-incubated with an equal charge ratio of Lipofectin, was added to confluent plates of H35 cells. At various time points, the mRNA was harvested from replicate wells, reverse transcribed, and subjected to kinetic PCR analysis. Significant decreases in gp130 mRNA were observed after 4 hours of treatment with Good2, predicted by our molecular thermodynamic analysis to be a good inhibitor of gp130 mRNA, with the maximal inhibition of expression occurring around 8 hours and a return to basal expression by 24 hours (Figure 4-2). The oligonucleotide Bad1 (predicted to be an ineffective inhibitor despite being of the same length as Good2 and fully complementary to the rat gp130 mRNA) appeared to induce slight decreases in gp130 expression at parallel time points; however, none of these changes was statistically significant.

4.D.3. gp130 mRNA reduced with oligonucleotides predicted to be active

Using the 8 hour time point found to be most effective for Good2, we tested a small panel of oligonucleotides, including sequences predicted to have high affinity for the gp130 mRNA (Good1, Good2, Good3), as well as two that were predicted to have weak affinity (Bad1, Bad2) despite being fully complementary to the gp130 mRNA and of the same length as the "Good"

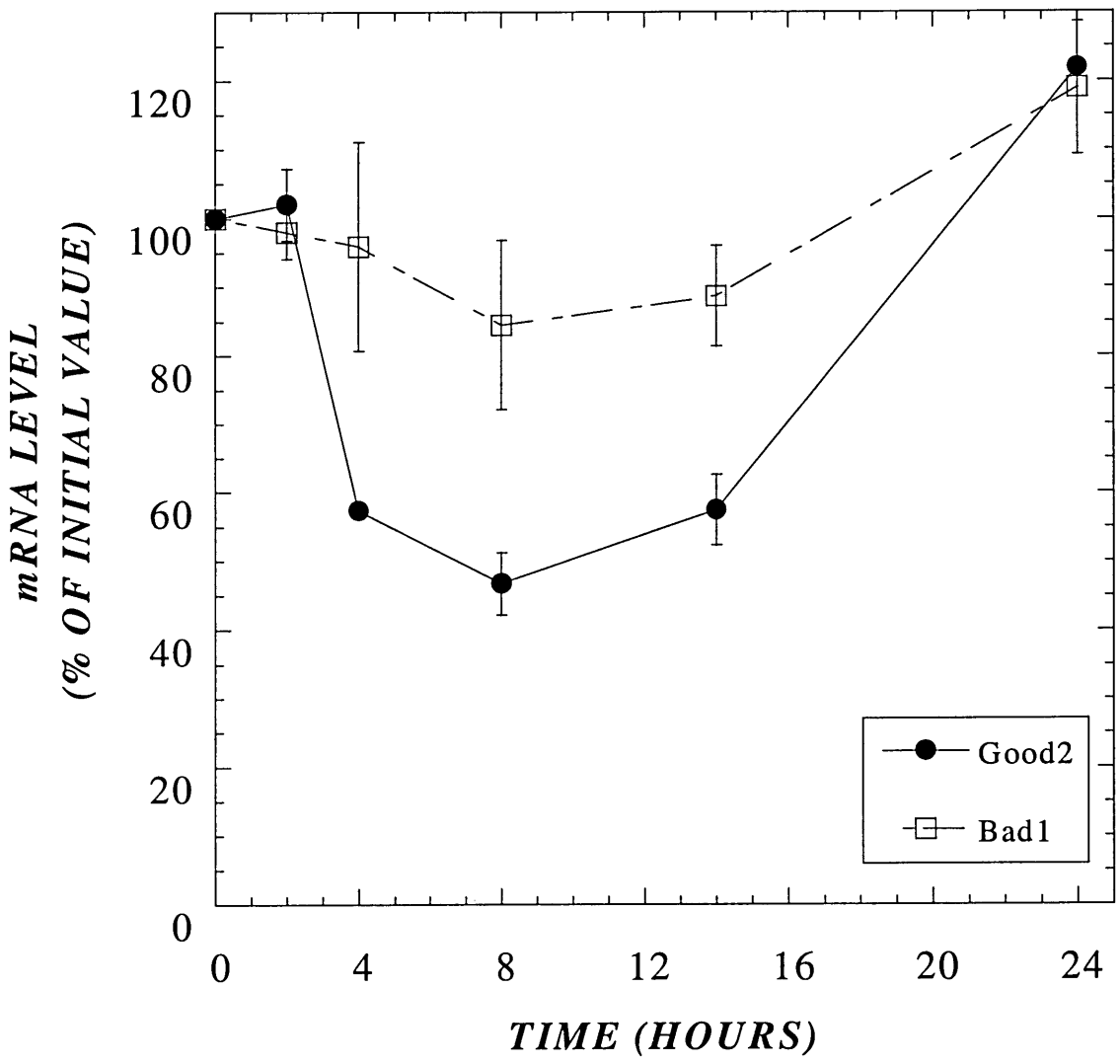

Figure 4-2: Time course of inhibition of gp130 mRNA in H35 cells
H35 cells were treated with phosphorothioate antisense oligonucleotides Good2 (filled circles) and Bad1 (open squares), at 600 nM concentration, under serum-free conditions. The cells were lysed at the indicated time intervals, after which the total mRNA was extracted and the level of gp130 mRNA quantified by reverse transcription and kinetic PCR. The mRNA levels are normalized to that of 18S rRNA and the changes in expression are determined relative to the untreated control. Good2, an oligonucleotide predicted to have high affinity for the gp130 mRNA show significant inhibition ($p<0.05$, as compared to untreated control) between 4-14 hours of exposure with maximal inhibition occurring after 8 hours. In contrast, Bad1, predicted to have low affinity, showed no significant reduction at any time. Recovery to at least basal levels could represent feedback in cellular processing in concert with oligonucleotide degradation.

sequences. Two (Good1 and Good2) of the three selected sequences were able to decrease gp130 mRNA by 50% after 8 hours; the third sequence was able to cause a 25% decrease in gp130 mRNA (Figure 4-3). Neither of the sequences predicted as poor antisense oligonucleotides (Bad1 and Bad2) significantly decreased the levels of gp130 mRNA. The sequence-specificity of the two most effective oligonucleotides was also evident, since their nonsense controls (NS-G1 and NS-G2) did not demonstrate any significant antisense inhibition (Figure 4-3).

4.D.4. Reduction in protein activity follows reduction of mRNA levels

The effectiveness of the antisense oligonucleotides at inhibiting the biological function of gp130 was further assessed by Western blot analysis of acute phase proteins using H35 cells. gp130 is the major signaling receptor for the IL-6 family of cytokine. In H35 cells as well as normal hepatocytes, gp130 signaling results in the up-regulation of haptoglobin and other positive acute phase proteins. In this experiment, H35 cells were exposed to oligonucleotide under serum-free conditions for 8 h (the sum of the earliest significant down-regulation of mRNA, 4 h, plus the estimated half-life of gp130 protein, 4 h [225]). Cells were subsequently exposed to IL-6 in a change to serum-containing medium for an additional 16 h, after which the proteins were extracted and probed for haptoglobin expression by Western blot analysis (Figure 4-4). In the absence of oligonucleotide, IL-6 resulted in an increase in secretion of haptoglobin, as expected. Good1, Good2, and Good3 all essentially abrogated haptoglobin secretion, whereas a significant amount of haptoglobin was secreted by cells exposed to Bad1, Bad2, NS-G1, or NS-G2.

4.D.5. Dose-dependent inhibition of LDH A and B mRNA and protein

Lactate dehydrogenase (LDH) is an abundant and well-characterized metabolic enzyme expressed by many cell types. There is evidence to suggest that the LDH protein is transcriptionally regulated, particularly in response to stimulation with epidermal growth factor (EGF) *in vitro* [226]. We tested the ability of rationally selected antisense oligonucleotides to modulate mRNA levels of two of its isoforms, LDH-A and B. Human foreskin fibroblasts were treated with phosphodiester oligonucleotides (Table 4-1) against LDH-A and B mRNA under serum-free conditions at varying concentrations, with the concentrations of Lipofectin adjusted

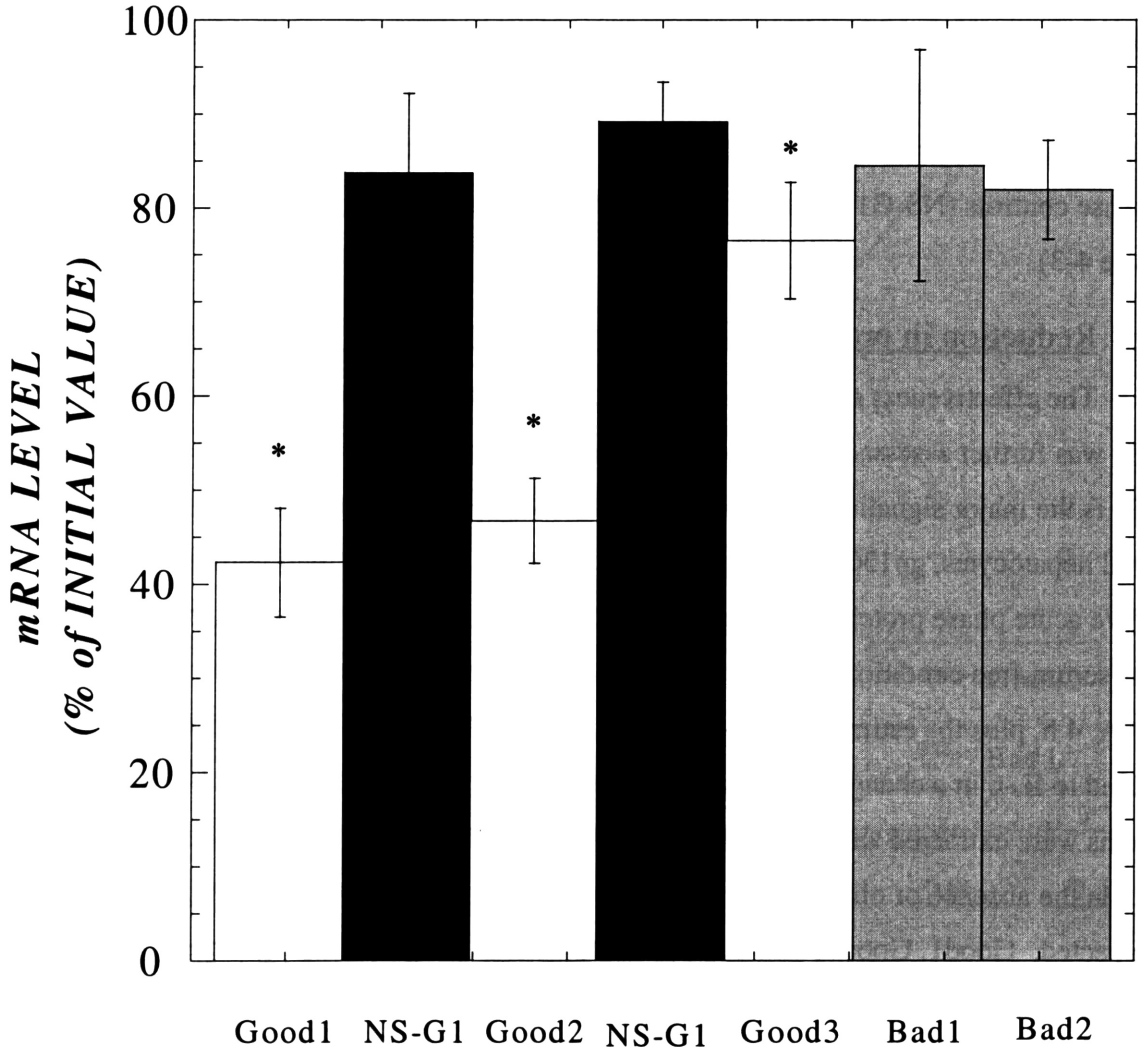

Figure 4-3: Inhibition of rat gp130 mRNA by predicted antisense oligonucleotides
H35 cells were treated with phosphorothioate antisense oligonucleotides at 600 nM concentration under serum-free conditions for 8 hours, after which gp130 mRNA levels were determined as in Figure 4-2. Statistical significance relative to untreated control is indicated by *($p < 0.05$). Of the 3 complementary oligonucleotides tested against the gp130 mRNA predicted to have high affinity, all resulted in significant inhibition, though Good3 was decidedly less effective. Concomitantly, neither Bad1 nor Bad2 (both predicted to have low affinity) resulted in significant inhibition. Nonsense sequences (non-complementary oligonucleotides), NS-G1 and NS-G2 showed no significant effect. These results confirm that predicted binding affinity is a useful tool in locating oligonucleotides that generate an antisense effect. The nonsense controls provide confirmation of the sequence-specificity of the activity.

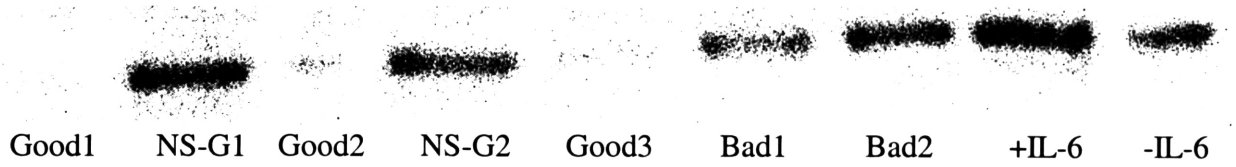

Figure 4-4: Modulation of haptoglobin production by gp130 antisense oligonucleotides
Supernatants were collected from antisense- or control-treated H35 cells 16 hours after addition of 10 ng/mL IL-6 (24 hours after antisense treatment). Western blot for haptoglobin was performed as described in Materials and Methods. Data shown represents one of two similar experiments. In response to IL-6 binding and signaling complex formation, gp130 transduces a signal resulting in the upregulation of haptoglobin secretion by hepatic cell lines (compare +IL-6 and –IL-6, above). However, the elimination of gp130 protein interrupts signal transduction and eliminates haptoglobin upregulation. Nonsense oligonucleotides and oligonucleotides of low affinity show little if any reduction of haptoglobin upregulation.

proportionately to maintain a constant charge ratio of 1:1. The degree of antisense inhibition of LDH-A and B mRNA in fibroblasts was dose-dependent, with significant effects observed at concentrations of 200 nM and higher for AS-A and 60 nM and higher for AS-B; in all cases, the inhibition of LDH-B by AS-B was greater than the corresponding inhibition of LDH-A by AS-A (Figure 4-5).

Because of the intracellular instability of phosphodiester oligonucleotides, it is often difficult to achieve sustained down-regulation of target mRNA and corresponding phenotypic modulation, without multiple administration of the oligonucleotide. Nonetheless, we observed changes in LDH enzyme activity of antisense-treated cells that were consistent with the changes in mRNA expression. To be able to detect changes in LDH activity, fibroblast cultures were serum-starved for 24 hours prior to the addition of antisense oligonucleotides to deplete intracellular pools of LDH protein; cells were then treated with antisense oligonucleotides for 4 hours, then challenged with medium containing serum and EGF for an additional 20 hours, upon which the cells were lysed in their plate and the lysate assayed for LDH activity. As with the isoform mRNA levels, the LDH enzymatic activity was inhibited in a dose-dependent manner (Figure 4-6); the greater inhibition using AS-B is also consistent with the mRNA inhibition results. The lesser extent of inhibition at the enzymatic level is likely due to a combination of transient mRNA inhibition over the 20 h duration of EGF stimulation before assaying for LDH activity, and also the fact that multiple isoforms contribute to the total LDH activity, only one of which was presumably inhibited by a particular oligonucleotide.

4.E. Discussion

The effectiveness of antisense oligonucleotides is limited by several factors, including: the delivery of oligonucleotides to cells, intracellular trafficking, affinity and specificity of hybridization to the target mRNA, and the susceptibility of oligonucleotides to degradation by both serum and intracellular nucleases [16]. The effectiveness of only a low fraction, perhaps ~10% [190, 216], of tested antisense oligonucleotides *in vitro* points out a sequence dependence, which suggests that affinity is very important in determining efficacy. We have previously developed a molecular thermodynamic model that predicts which antisense oligonucleotides will have the greatest affinity for a target mRNA, based on thermodynamics of unfolding existing secondary structure, duplex base pair stability, and structural rearrangements in the DNA:RNA

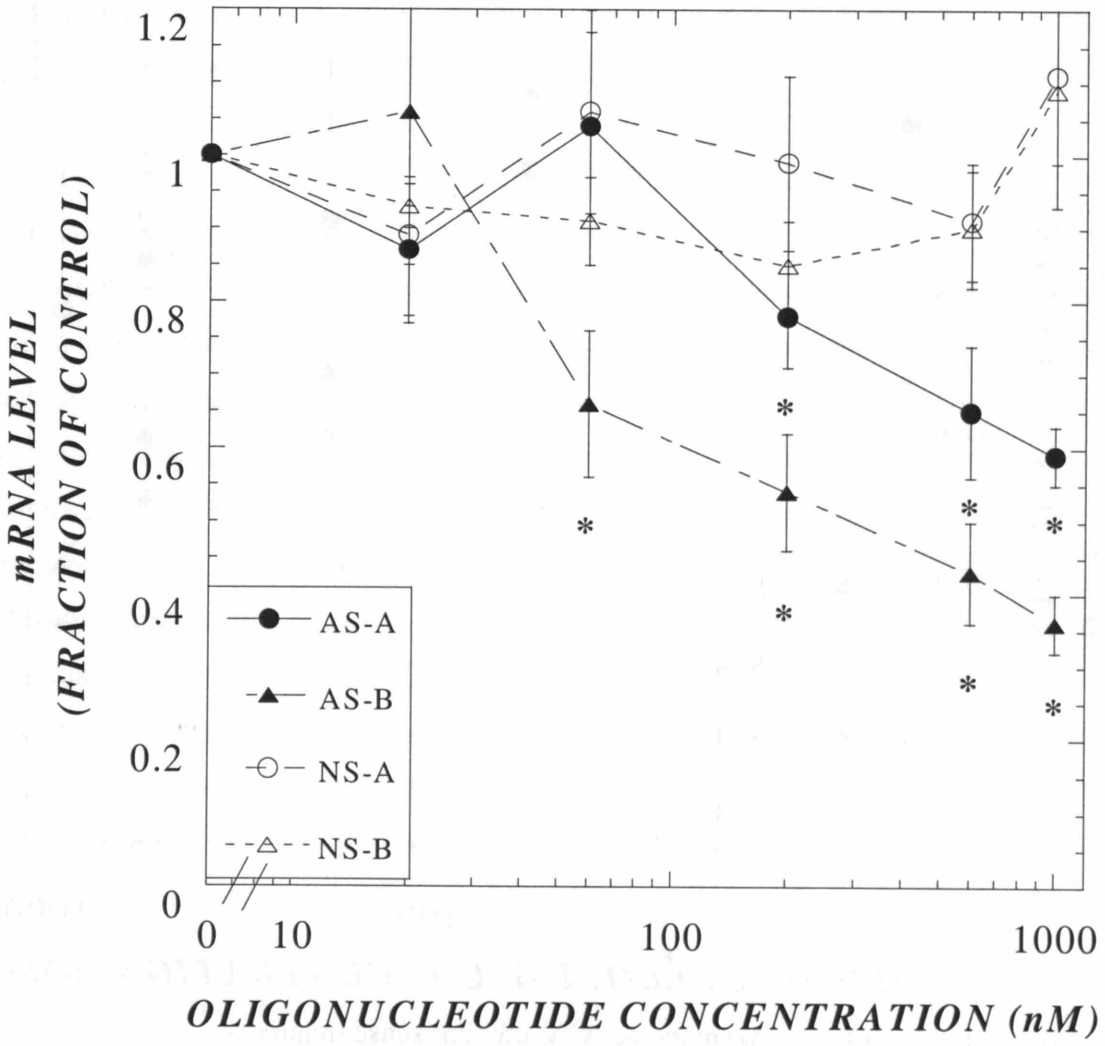

Figure 4-5: Inhibition of mRNA in human fibroblasts by antisense oligonucleotides
Oligonucleotides tested were LDH-A antisense (filled circles), LDH-B antisense (filled triangles), LDH-A nonsense (open circles), and LDH-B nonsense (open triangles). Fibroblasts were treated with each oligonucleotide for four hours. The mRNA levels are normalized to those of 18S rRNA, and the changes in expression are reported relative to the untreated control. Statistical significance relative to untreated control is indicated by * ($p<0.05$). In both cases, oligonucleotides predicted to have the highest affinity for their target mRNA showed significant inhibition of their target mRNA at sub-micromolar concentrations.

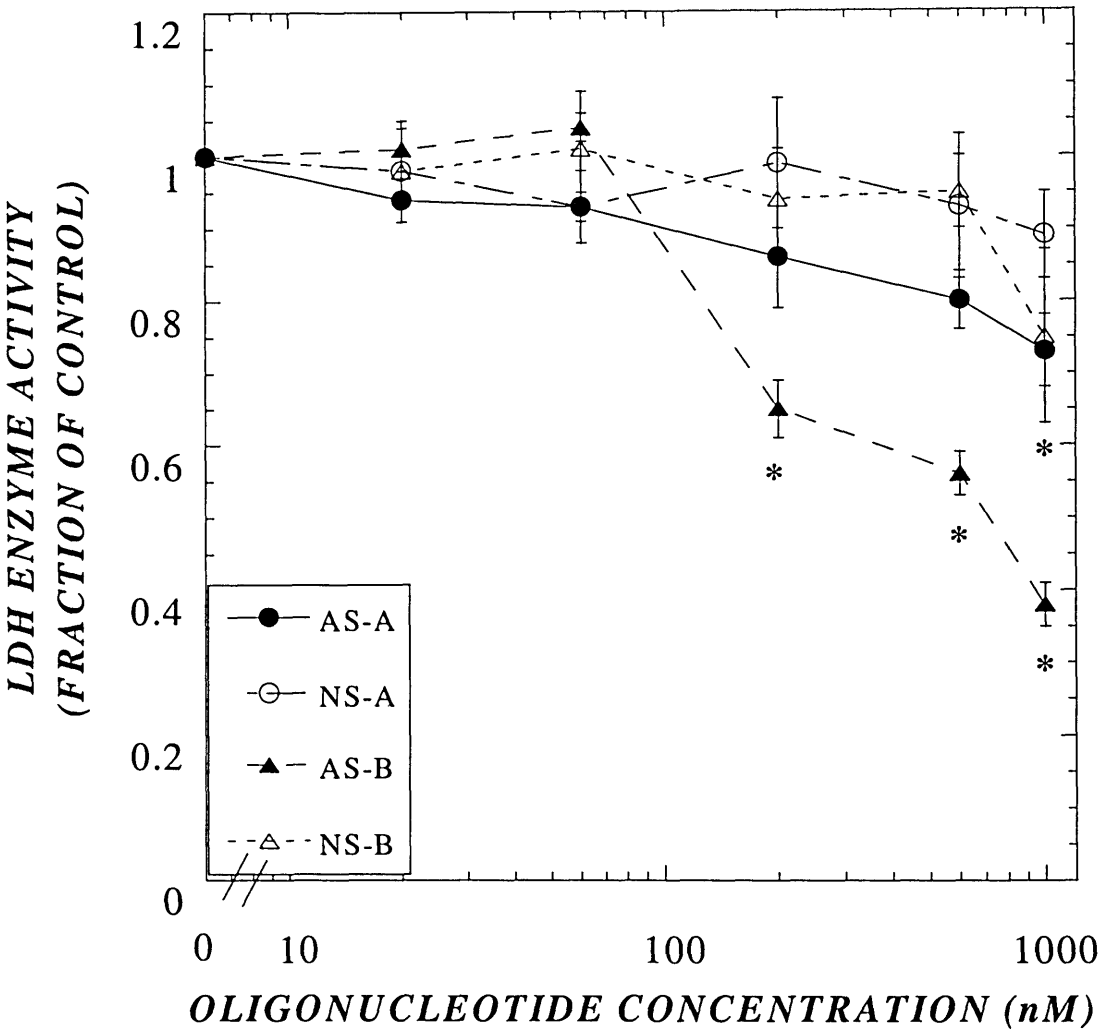

Figure 4-6: Inhibition of LDH enzymatic activity after antisense treatment
Fibroblasts were treated with each oligonucleotide for four hours. Intracellular LDH activity was measured 20 hours after the addition of 20 ng/mL EGF (24 hours after antisense treatment). Symbols represent the same quantities as in Figure 4-5. The activity levels are normalized to the untreated (no oligonucleotide) control, and statistical significance relative to untreated control is indicated by * ($p<0.05$). Changes in protein levels reflect changes in mRNA levels, even in the greater reduction due to AS-B versus AS-A.

duplex [201]. This approach has proven successful in correlating predicted free energy with observed binding affinity in solution [227] as well as with RNase-accessible sites on target mRNAs [169]. Here, we have demonstrated the ability of the model to predict (rationally design) antisense oligonucleotides that are effective inhibitors of target gene expression in living cells.

We have previously used the quantitative kinetic PCR method to follow the dynamics of abundant as well as rare mRNA transcripts in rat hepatocytes [228]. In this paper, we have applied kinetic PCR to evaluating antisense oligonucleotide efficacy. One of the key concerns regarding quantitative PCR is the potential for variability in the amplification efficiency (and amount of specific product) due to the characteristics (GC content, secondary structure) of the region being amplified [219]. With the kinetic PCR technique, we find a high level of consistency in replicate samples (run on different days), and we have obtained essentially identical results to those presented here using alternate primer pairs for several transcripts (data not shown). Furthermore, we have observed very minimal variability in reverse-transcription process (as inferred from the similar threshold cycle numbers obtained in kinetic PCR using cDNA generated in different reverse-transcription reactions from a single pool of mRNA). It is possible that the careful choice of amplification target (40-50% GC content) as well as the use of specific downstream primers for reverse transcription instead of random primers or oligo-dT offset any potential variations in amplification efficiency [219]. Therefore, the changes in mRNA levels of specific transcripts determined with kinetic PCR do not appear to have reverse-transcription or PCR artifacts. Another issue in quantitative PCR is the choice of appropriate reference gene for relative quantification of transcripts. The most commonly employed housekeeping genes are β-actin, GAPDH, and ribosomal (18S or 28S) RNA. Comparison of expression levels in response to cellular stress indicates that the levels of ribosomal RNAs are the most stable with respect to environmental perturbations [219]. As a result, for all antisense experiments, we used 18S rRNA as the reference gene.

Kinetic PCR allows us to compute the number of mRNA copies in a cell or the number of cDNA molecules in a PCR reaction. Using this approach, we estimated the number of mRNA molecules per rat hepatocyte for the transcripts of interest in this study (18S rRNA, LDH-A, LDH-B, and gp130; also GAPDH, albumin, and β-actin) to range from ~10^7 for 18S rRNA to

$\sim 10^2$ for gp130. In general, the levels are in the range that we would expect, with high expression of 18S rRNA and albumin and the least for gp130. In general, few absolute measurements of mRNA levels have been reported, but our measurement for albumin mRNA/hepatocyte of 56,000 is in excellent agreement with Peters [229], who reported 58,000 copies of albumin mRNA/hepatocyte. Dilution series with gp130 or LDH cDNA (data not shown) indicate that we can dilute the starting cDNA material only 10-fold without getting *any* interference from primer-dimer. Since the extent of antisense inhibition was generally 60% or less, this does not pose a major limitation on the applicability of the technique for antisense evaluation, though it is possible that for gp130 we could be slightly underestimating the effectiveness of antisense inhibition due to this effect.

The two main mechanisms of antisense inhibition are from steric interference with the translation process and enzymatic cleavage by RNase H [131]. Steric hindrance would result in a decrease in protein levels without altering the level of mRNA, whereas, in the enzymatic mechanism, RNase H recognizes an mRNA-oligonucleotide duplex, cleaves the mRNA, and thereby reduces the level of mRNA. The use of mRNA expression monitoring, whether by Northern blot or the kinetic PCR assay utilized here, assumes that the antisense is activating RNase H. Our data clearly shows a decrease in mRNA levels after antisense treatment for all targets tested, which suggests a strong role for RNase H cleavage in antisense inhibition for these systems.

Our rational prediction method has been successfully applied with two different oligonucleotide chemistries and three target mRNA – two isoforms of an abundant metabolic enzyme, LDH (using phosphodiester oligonucleotides), as well as a relatively scarce receptor molecule, gp130 (using phosphorothioate oligonucleotides). The free energy parameters used in predicting oligonucleotides were developed based on phosphodiester oligonucleotides, and it is known that phosphorothioate oligonucleotides exhibit significantly weaker binding for their targets than corresponding phosphodiester oligonucleotides [230]. However, the sequence dependence of the difference in phosphodiester and phosphorothioate oligonucleotides has yet to be quantified. Moreover, the cost incurred due to the restructuring of the RNA is a significant factor in determining the overall hybridization affinity, and this is completely unrelated to the choice of oligonucleotide chemistry. Regardless, the *relative* binding affinities among the

phosphorothioate oligonucleotides are not expected to be significantly affected by the alternative backbone chemistry.

The success rate of our model – four of five rationally selected antisense oligonucleotides proved to be potent inhibitors in cell culture – is striking. Based on ~70% correlation of thermodynamic prediction with affinity [201] and a 60-70% correlation of affinity and activity [193], we might have expected less than 50% effectiveness of our predictions. Furthermore, the accuracy of our predictions was not restricted to effective oligonucleotides, as the oligonucleotides that were predicted to be poor antisense inhibitors were not effective against rat gp130 mRNA. In fact, the predicted ΔG^{o}_{total} values (Table 4-1) correlate significantly with the gp130 mRNA levels after 8 hours of antisense treatment (Figure 4-3) ($p = 0.019$). As in our previous studies [201], the ΔG^{o} values of the individual steps correlated less strongly with experimental values, e.g., $p = 0.117$ for ΔG^{o}_{hyb}. Nonetheless, thermodynamic prediction of antisense oligonucleotide effectiveness is an imperfect science. Understanding of the thermodynamics of RNA folding is still emerging, a situation that is difficult to overcome in the absence of extensive structural information. It is possible that a single, lowest-energy folded structure does not exist and that mRNA molecules are continually sampling an ensemble of folding states. Furthermore, tertiary interactions, which are not captured in secondary structure-based RNA folding algorithms, may be important [165].

In summary, we have demonstrated the ability to improve selection of antisense oligonucleotides with potent activity *in vitro*. Our results suggest that, by using rationally selected antisense oligonucleotides, one can reduce the number of oligonucleotides to be screened from the dozens typically employed to a few per target mRNA. The quantitative evaluation of antisense efficiency confirms a dominant role for enzymatic cleavage in the observed inhibition. Combining this prediction scheme for oligonucleotides with improved delivery and targeting schemes will further enhance the efficiency and specificity for their myriad potential application in functional genomics, biotechnology, and therapeutics.

5. ***Appendices***

5.A. *2-1: Executing the thermodynamic predictions*

The computational method utilizes the program *mfold* 2.3 as produced by Michael Zuker and colleagues, as well as Perl scripts, Word and Excel, and Mathematica. A similar method has been produced by Turner's group at the University of Rochester and is available as a self-contained application, RNAstructure, from their web site. RNAstructure uses an updated folding algorithm as well as updated thermodynamic parameters. However, in comparison, both methods perform similarly, with perhaps a slight improvement in overall agreement with experimental data from RNAstructure. Below, the specific manipulations required to perform the folding calculations using our method will be described.

Beginning with the primary sequence of the mRNA/cDNA, the input file for the *mfold* application is created. The formatting of this file is very specific, requiring a semi-colon in the first line and the number one after the final base of the sequence (Figure 2-A1). Also required is the name of the sequence being folded on the second line of the file, by itself. As described in the manual for *mfold*, T bases are treated as U's, and additional characters can be substituted into the mRNA sequence to indicate particular base pairing features. As the sequences being folded were linear RNAs, the "lrna" program from within *mfold* was used (as opposed to "crna" for circular RNAs).From the UNIX prompt, the required command is:

Prompt: lrna

The credits for the program will appear, and the user will be asked to press return to continue. The following choices are selected in sequence when generating the "dot plot" for segment analysis. The program is run in regular mode, followed by selecting suboptimal plot mode. The minimum vector size is 1 with a window size of 0. The sequence file name is then entered and sequence number 1 chosen. The starting and ending nucleotides are then selected, with base 1 and the last base appearing as defaults. The seven default energy files are then selected. Printer output is desired, with the output going to the terminal with the default 80 columns. No ct file or region table is required. The "Begin folding" option is then selected. The folding counter will

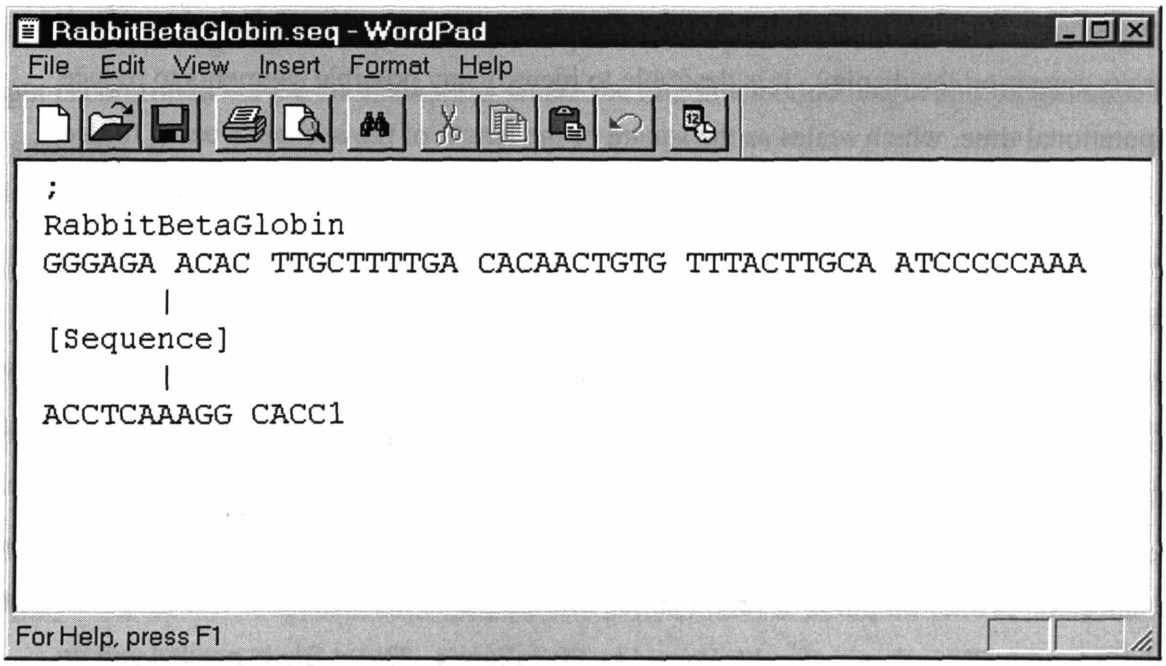

Figure 2-A1: Screen shot of sample input file

Specific formatting is required for the input file to *mfold*. The above screen shot shows the file format. The leading semi-colon is required, followed by the name of the sequence on a line by itself, followed by the mRNA/cDNA sequence to be folded. A one must follow the last base of the sequence and be the last character in the file.

count to a value ~2X the length of the sequence whereupon the "dot plot" will appear on the monitor. By using the right mouse button, a menu will appear that allows the user to change the energy interval over which the suboptimality will be displayed as well as changing the number of colors used in the display. Each color then represents a fractional energy window within the selected total increment from the minimum, which is also displayed in the lower left-hand corner of the "dot plot" that appears, initially. Any regions of self-contained folding are located using the cross-hairs. The bases at which the segment junctions occur can be selected, and their base numbers appear on the display. It is desirable to identify any possible segments to reduce computational time, which scales as the square of the length of the sequence being folded.

Once the lengths of any segments are determined, ΔG°_{UN} values are calculated for each of the segments. This can be done using the "dot plot" protocol above and selecting the optimal folding energy. The program is then used in N-Best mode to generate the output files from which ΔG°_{RE} values are obtained for each target region. Again, the selections are made in the following order. The regular run is chosen followed by N-best mode. The desired percentage is 10 with 1 traceback and a window size of 0. The sequence filename is then entered followed by selecting sequence 1. The start and end bases of the segment are entered and the default energy files selected. Printer output is desired but not with output to the terminal. The output file name for the structure file is then entered followed by 80 columns. The ct file is needed and its filename entered. No region table is required. To specify the target region for the oligonucleotide as being single-stranded, the "Single-Prohibit" (6) function is selected. The user is then asked to enter the first base that will be single stranded and the length of the region that will follow. Hence, the 5' base of the target region and the oligonucleotide length are entered separated by either a space or return. The "Begin Folding" option is then selected. The counter will begin and proceed until 2X of the length of the segment being folded. However, upon completion of the count-up, the output files will be written into the home directory of the program. This process is repeated for each target region along the mRNA. The output files are collected in a single directory and the energy values extracted using the "grep" command in UNIX.

Prompt:> more *.ct | grep EN > outputenergiesfile.txt

This command writes the filename and line of the file containing the energy value into the outputfile, which is then transferred to Excel for analysis. Two of the 4 energy parameters are completed. As this process is quite repetitive, FORTRAN scripts were written to automatically generate input files for the lrna program (Appendices 2-4 through 2-6).

To obtain the ΔG°_{OH} value for each oligonucleotide:target combination, a Perl script (Appendix 2-2) and Mathematica file (Appendix 2-3) are used. First the Perl script is run on an input file containing only the mRNA/cDNA sequence (no spaces or extraneous characters). The output is controlled via the command line where the oligonucleotide length and progression step are specified

Prompt:> process_seqs 17 1 inputfilename.txt > outputfilename.txt

where 17 is the length of the oligonucleotides and 1 is the step length. This command will generate all possible 17-mer target sequences in the mRNA in 5' to 3' order as one single line. This output file is the input to the Mathematica calculation file that calculates ΔG°_{OH}. To run the Mathematica file, it is only necessary to update the input filename to address the appropriate file and directory as well as to update the length of oligonucleotide (both bolded for emphasis in Appendix 2-3). From there, selecting compile entire notebook will generate all of the ΔG°_{OH} values. The input parameters in the Mathematica file have been structured to take into account the backwards nature of the input (i.e., that the first base is the 5' base of the mRNA not of the oligonucleotide) to ensure the calculation of the proper ΔG°_{OH} value. As a check that the processing using the Perl script was performed properly, the total number of calculated ΔG°_{OH} values is listed at the bottom of the output. The notebook file is then saved as text and opened in Word where the extraneous characters are replaced to generate a single column listing only the ΔG°_{OH} values (Figure 2-A2). These are transferred to Excel for analysis. The only remaining value to be calculated is ΔG°_{OS} which will require a number of similar techniques to those already described for each of the first three components.

A.)

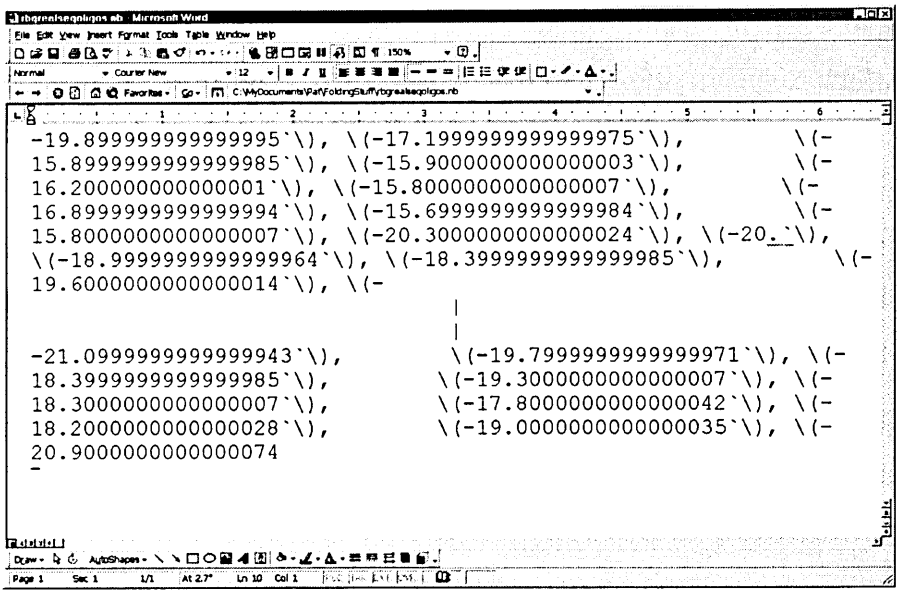

B.)

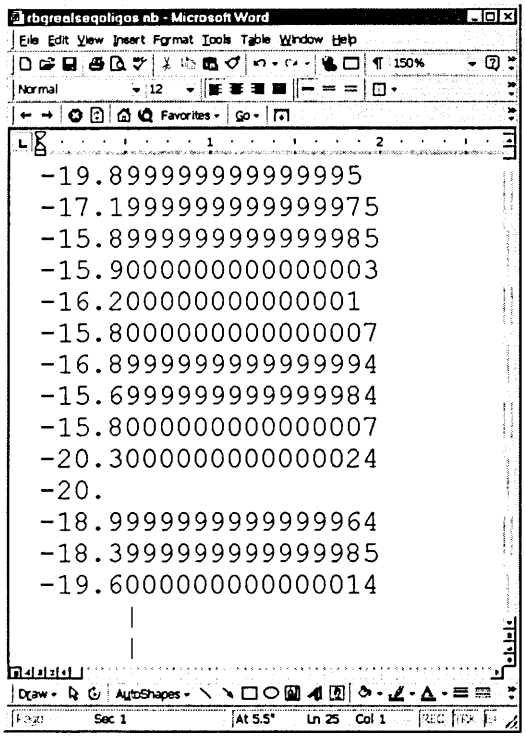

Figure 2-A2: Replacement of unnecessary characters

Mathematica output is converted to list of free energy values by using the "find and replace" feature to eliminate all extraneous characters from within the list of values. A.) The list of values as produced by Mathematica. The commas are replaced by carriage returns. All other characters are deleted (replaced with nothing) to result in B.) the final list of ΔG°_{OH} values, which are then imported into Excel for analysis.

To calculate ΔG°_{OS} values, the mRNA sequence is first converted to its exact complement in 5' – 3' order. This is accomplished using the "find and replace" feature of Word to replace bases by their complementary bases (taking advantage of capitalization to distinguish those bases that had been converted and those that were not). Subsequently, the order of the bases is inverted using Excel to generate the 5' – 3' complement. The oligonucleotides must be in 5' – 3' conformation to ensure use of the proper nearest neighbor pairs in calculating the folding energies. The Perl script is then applied to generate a list of the oligonucleotide sequences, again stepping by 1 base at a time. This file can then be used as an input for the lrna program run with DNA parameters. The window of folding is moved in steps the length of the oligonucleotides such that each of the ΔG°_{OS} is generated. By grepping for the energy values from the resulting files, a list of energies can be generated. However, because of the requirement to have the oligonucleotide sequences in 5' to 3' order, the ΔG°_{OS} values are in reverse order and are inverted using Excel. A sample of the Excel table containing all four energy components is shown in Figure 2-A3. Only the negative ΔG°_{OS} values are taken into account by applying the summation formula shown on the formula line (Figure 2-A3).

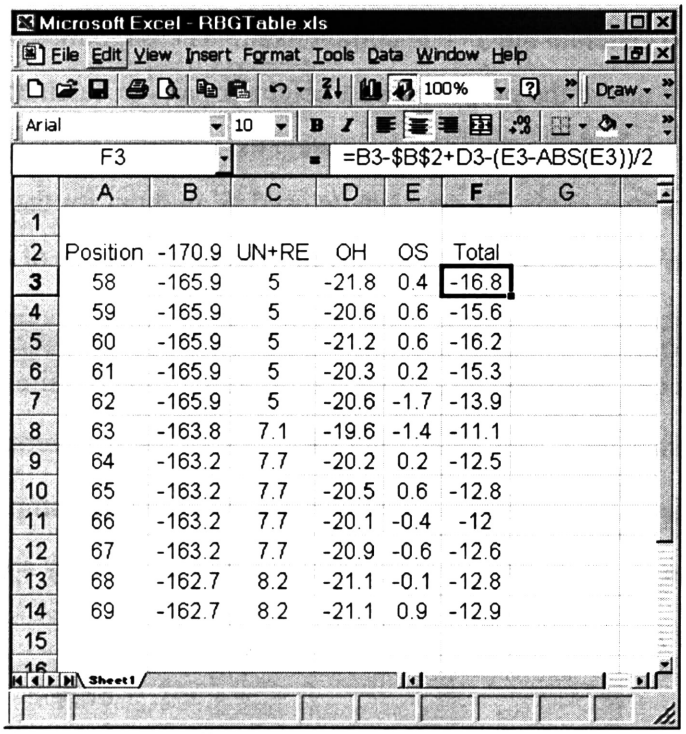

	A	B	C	D	E	F	G
1							
2	Position	-170.9	UN+RE	OH	OS	Total	
3	58	-165.9	5	-21.8	0.4	-16.8	
4	59	-165.9	5	-20.6	0.6	-15.6	
5	60	-165.9	5	-21.2	0.6	-16.2	
6	61	-165.9	5	-20.3	0.2	-15.3	
7	62	-165.9	5	-20.6	-1.7	-13.9	
8	63	-163.8	7.1	-19.6	-1.4	-11.1	
9	64	-163.2	7.7	-20.2	0.2	-12.5	
10	65	-163.2	7.7	-20.5	0.6	-12.8	
11	66	-163.2	7.7	-20.1	-0.4	-12	
12	67	-163.2	7.7	-20.9	-0.6	-12.6	
13	68	-162.7	8.2	-21.1	-0.1	-12.8	
14	69	-162.7	8.2	-21.1	0.9	-12.9	
15							

Figure 2-A3: Excel table containing all energy components

Position refers to the 5' base on the mRNA to which the 3' base of the oligonucleotide is complementary. The second column contains the total folding free energy for the mRNA or segment (-170.9 kcal/mole) followed by the constrained folding energy for each target region. The third column has the net folding cost, i.e., the constrained energy minus the native energy of folding. The values from the Mathematica worksheet are listed in the fourth column. The energies of folding the oligonucleotides are listed in column five. The formula in the sixth column accounts for all of the proper signs by subtracting the folding gains of the native mRNA and oligonucleotide to convert them to "unfolding" costs. Also, the formula ensures that only negative values of oligonucleotide folding are taken into account, eliminating possible but unfavorable oligonucleotide conformations.

5.B. *2-2: Process_seqs Perl script*

Perl script for generating oligonucleotide files for calculating ΔG°_{OS}. This Perl script was first written by Thomas Y. Lee and modified by SPW. The file creates a single-line list consisting of base segments of a user-defined length that are offset by a user-defined amount (Figure 2-A4). The appropriate command line for generating the a list of 17mers offset each by 1 base (Figure 2-A4) is:

Prompt:> process_seqs 17 1 inputfilename.txt > outputfilename.txt

```
::::::::::::::
process_seqs
::::::::::::::
#!/usr/athena/bin/perl

# ASSUMES:
# every line of input ends with a "\n"

# INPUTS
#$set_length = 10;
#$offset = 2;
#$input_file = "test_in.txt";
#$output_file = "test_out.txt";

# GET INPUTS
$set_length = @ARGV[0];
$offset = @ARGV[1];
$input_file = @ARGV[2];
$output_file = @ARGV[3];

# DEFAULTS

if ($set_length eq ""){
    $set_length = 10;
}

if ($offset eq ""){
    $offset = 1;
}

if ($input_file eq ""){
    $input_file == "&STDIN";
```

```
}

if ($output_file eq ""){
    $output_file = "&STDOUT";
}

#print "$set_length \t $offset \t $input_file \n";  #debug

# CONSTANTS
$end_of_line_marker = "\n";
$i = 0;
@input_array = ();
@sequence_array = ();
$num_input_lines = 0;
$sequence = "";
$temp = "";
$sequence_counter = 1;

open(FILE, "$input_file");

# careful!  We assume that every line ends with a \n and so
# we use "chop" to get rid of it. ... otherwise, you
# must use the s/end_of_line_marker//;

while($line = <FILE>){
#    $line =~s/$end_of_line_marker//;
    chop($line);
    push(@input_array,$line);
}
close (FILE);

open(OUTPUT_FILE, ">$output_file");

$num_input_lines = @input_array;

# OUTPUT_FILE HEADER
# print OUTPUT_FILE  ">no. of input lines: $num_input_lines\n";
# print OUTPUT_FILE  ">sequence length: $set_length \t offset:
$offset \t input
filename: $input_file \n";  #debug

# no error checking here.  We assume that there is at least one
line
# of input in the file.
# we also assume that the $offset is < $set_length
```

```
# main loop:  as long as there is input to read.
while(@input_array){

# initalize:
    $temp = join('',@sequence_array);
    $sequence = join('',$temp,shift(@input_array));
    @sequence_array = split('',$sequence);

    $sequence_length = @sequence_array;

    # while there are still enough bases in the $sequence
    while($sequence_length > $set_length){

#       print OUTPUT_FILE ">Sequence $sequence_counter\n";

        # print the number of bases that are of interest.
        for ($i = 0; $i < $set_length; $i++) {
            print OUTPUT_FILE  "$sequence_array[$i]";
        }
#       print OUTPUT_FILE  "\n";
        # remove $offset number of bases
        for ($j = 0; $j < $offset; $j++) {
            shift(@sequence_array);
        }
        $sequence_length = @sequence_array;
        $sequence_counter++;
    }
# if you get to this point, then the $sequence is now too short
and
# it is time to get the next line of input.
}   # end main loop.

# if you get to this point, you are out of input, and you are at
# the last sequence.
$temp = join('',@sequence_array);
# print OUTPUT_FILE ">Sequence $sequence_counter\n";
print OUTPUT_FILE "$temp\n";
close (OUTPUT_FILE);
```

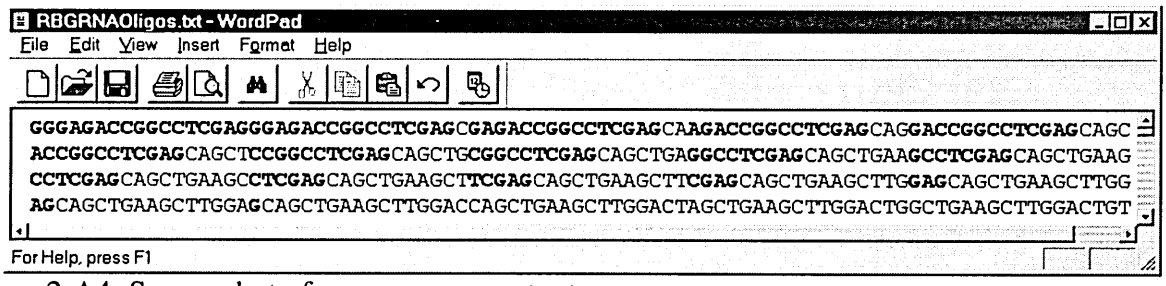

Figure 2-A4: Screen shot of process_seqs output

Each possible oligonucleotide from the mRNA sequence is written to an output file. Note that these "oligonucleotides" are actually the target sequences on the mRNA in 5' to 3' order, so the oligonucleotides would actually be those sequences complementary to the above (e.g., 5'-AAAGCAAGTGTTCTCCC-3' for the first position on the mRNA). Bold text has been added to emphasize the overlap that results from movement of the oligonucleotide sequences one base at a time. The process_seqs program can be run with any length oligonucleotides with any step size (though it will result in an infinite loop for a step size of 0). No spaces or other characters (other than return characters) can be included in the input to the process_seqs algorithm as these characters would be written into the output.

5.C. *2-3: Mathematica input file*

Mathematica input file for calculating ΔG°_{OH}. This was first written by Abbey Perumpanani and modified as needed by SPW.

```
(*****************************************************************
Mathematica-Compatible Notebook  This notebook can be used on any computer
system with Mathematica 3.0, MathReader 3.0, or any compatible application.
The data for the notebook  starts with the line of stars above.  To get the
notebook into a Mathematica-compatible application, do one of  the following:
* Save the data starting with the line of stars above into a file   with a
name ending in .nb, then open the file inside the application;  * Copy the
data starting with the line of stars above to the   clipboard, then use the
Paste menu command inside the application.  Data for notebooks contains only
printable 7-bit ASCII and can be sent directly in email or through ftp in
text mode.  Newlines can be CR, LF or CRLF (Unix, Macintosh or MS-DOS style).
NOTE: If you modify the data for this notebook not in a Mathematica-
compatible application, you must delete the line below containing the  word
CacheID, otherwise Mathematica-compatible applications may try to  use
invalid cache data.  For more information on notebooks and Mathematica-
compatible  applications, contact Wolfram Research:   web:
http://www.wolfram.com   email: info@wolfram.com   phone: +1-217-398-0700
(U.S.)  Notebook reader applications are available free of charge from
Wolfram Research.
*****************************************************************)
(*CacheID: 232*)   (*NotebookFileLineBreakTest NotebookFileLineBreakTest*)
(*NotebookOptionsPosition[     12898,        263]*)
(*NotebookOutlinePosition[     13550,        286]*) (*
CellTagsIndexPosition[     13506,        282]*) (*WindowFrame->Normal*)
Notebook[{ Cell["(* INPUT PARAMETERS *)", "Input"],  Cell["(* Input the
number of elements in each sublist *)", "Input"],  Cell[CellGroupData[{
Cell["n = 17", "Input"],  Cell[BoxData[     \(17\)], "Output"] }, Open  ]],
Cell["\<\ (* Input the replacement values here for each pair *)  (* Values
below are for 5' -> 3' RNA pairs NOT for \ complementary/oligonucleotide
sequences. *)\ \>", "Input"],  Cell["\<\ vals={{\"a\",\"a\"}->-
1,{\"a\",\"g\"}->-1.8,{\"a\",\"c\"}->-2.1,{\"a\",\"t\"}-\ >-
0.9,{\"g\",\"a\"}->-1.3,{\"g\",\"g\"}->-2.9,{\"g\",\"c\"}->-2.7,{\"g\",\"t\"\
}->-1.1,{\"c\",\"a\"}->-0.9,{\"c\",\"g\"}->-1.7,{\"c\",\"c\"}->-
2.1,{\"c\",\"\ t\"}->-0.9,{\"t\",\"a\"}->-0.6,{\"t\",\"g\"}->-
1.6,{\"t\",\"c\"}->-1.5,{\"t\",\ \"t\"}->-0.2,{\"A\",\"A\"}->-
1,{\"A\",\"G\"}->-1.8,{\"A\",\"C\"}->-2.1,{\"A\",\ \"T\"}->-
0.9,{\"G\",\"A\"}->-1.3,{\"G\",\"G\"}->-2.9,{\"G\",\"C\"}->-2.7,{\"G\
\",\"T\"}->-1.1,{\"C\",\"A\"}->-0.9,{\"C\",\"G\"}->-1.7,{\"C\",\"C\"}->-
2.1,{\ \"C\",\"T\"}->-0.9,{\"T\",\"A\"}->-0.6,{\"T\",\"G\"}->-
1.6,{\"T\",\"C\"}->-1.\ 5,{\"T\",\"T\"}->-0.2};\ \>", "Input"],  Cell["(* ---
----------END OF INPUT-----------------------*)", "Input"],  Cell["seq =
ReadList[\"RabbitBetaRealOligos.seqs\",Character];", "Input"],  Cell["t1 =
Partition[seq,n];", "Input"],  Cell["\<\ summ[j_]:=3.1 + \
Apply[Plus,Table[{t1[[j,i]],t1[[j,i+1]]},{i,1,Length[t1[[194]]]-1}]/.vals]\
\>", "Input"],  Cell["(* -------------------OUTPUT-------------------------
*)", "Input"],  Cell[CellGroupData[{
Cell["Table[summ[54],{i,1,Length[t1]}]", "Input"],  Cell[BoxData[     \({\(-
19.899999999999995`\), \(-17.199999999999975`\),        \(-
```

```
15.8999999999999985`\), \(-15.9000000000000003`\),        \(-
16.2000000000000001`\), \(-15.8000000000000007`\),       \(-
16.8999999999999994`\), \(-15.6999999999999984`\),        \(-
15.8000000000000007`\), \(-20.3000000000000024`\), \(-20.`\),       \(-
18.9999999999999964`\), \(-18.3999999999999985`\),        \(-
19.6000000000000014`\), \(-
                                  |
                [One value produced for each oligonucleotide]
                                  |
-21.0999999999999943`\),        \(-19.7999999999999971`\), \(-
18.3999999999999985`\),        \(-19.3000000000000007`\), \(-
18.3000000000000007`\),        \(-17.8000000000000042`\), \(-
18.2000000000000028`\),        \(-19.0000000000000035`\), \(-
20.9000000000000074`\)}\)], "Output"] }, Open  ]],  Cell[CellGroupData[{
Cell["Length[t1]", "Input"],  Cell[BoxData[     \(317\)], "Output"] }, Open
]] }, FrontEndVersion->"Microsoft Windows 3.0", ScreenRectangle->{{0, 1024},
{0, 702}}, WindowSize->{500, 504}, WindowMargins->{{Automatic, 184},
{Automatic, 11}} ]
(*******************************************************************
Cached data follows.  If you edit this Notebook file directly, not using
Mathematica, you must remove the line containing CacheID at the top of  the
file.  The cache data will then be recreated when you save this file  from
within Mathematica.
*******************************************************************)
(*CellTagsOutline CellTagsIndex->{} *)  (*CellTagsIndex CellTagsIndex->{} *)
(*NotebookFileOutline Notebook[{ Cell[1709, 49, 39, 0, 30, "Input"],
Cell[1751, 51, 67, 0, 30, "Input"],  Cell[CellGroupData[{ Cell[1843, 55, 23,
0, 30, "Input"], Cell[1869, 57, 36, 1, 29, "Output"] }, Open  ]], Cell[1920,
61, 176, 5, 84, "Input"], Cell[2099, 68, 684, 10, 174, "Input"], Cell[2786,
80, 72, 0, 30, "Input"], Cell[2861, 82, 73, 0, 30, "Input"], Cell[2937, 84,
39, 0, 30, "Input"], Cell[2979, 86, 115, 3, 66, "Input"], Cell[3097, 91, 72,
0, 30, "Input"],  Cell[CellGroupData[{ Cell[3194, 95, 48, 0, 30, "Input"],
Cell[3245, 97, 9533, 155, 713, "Output"] }, Open  ]],  Cell[CellGroupData[{
Cell[12815, 257, 27, 0, 30, "Input"], Cell[12845, 259, 37, 1, 29, "Output"]
}, Open  ]] } ] *)
(******************************************************************* End
of Mathematica Notebook file.
*******************************************************************)
```

5.D. 2-4: Batchlrna

```
      program repeat
      integer i, j, k, l, m, counter
      character*30 filename
      counter = 1
      DO 10 i=1,26
      DO 15 j=1,26
      DO 18 k=1,26
C     print *, i
C     print *, char(i)
      filename='RBGMYT70930Seq/'//char(i+64)//char(j+64)//char(k+64)
C     print *, filename
      open(unit=30, file=filename)
      write (30,20) '0'
      write (30,20) '0'
      write (30,20) '1'
      write (30,20) '10'
      write (30,20) '1'
      write (30,20) '0'
      write (30,20) 'NewT7Seq093000.txt'
      write (30,20) '1'
      write (30,20) '1'
      write (30,20) '510'
      write (30,20) 'dangle.dat'
      write (30,20) 'loop.dat'
      write (30,20) 'stack.dat'
      write (30,20) 'tstackh.dat'
      write (30,20) 'tstacki.dat'
      write (30,20) 'tloop.dat'
      write (30,20) 'miscloop.dat'
      write (30,20) 'y'
      write (30,20) 'n'
      if (counter.ge.10.and.counter.le.99) then
            write (30,70) counter,'rbgmyT7seqfull.out'
      endif
      if (counter.ge.100.and.counter.le.999) then
            write (30,60) counter,'rbgmyT7seqfull.out'
      endif
      if (counter.ge.1000.and.counter.le.9999) then
            write (30,30) counter,'rbgmyT7seqfull.out'
      endif
      if (counter.ge.1.and.counter.le.9) then
            write (30,80) counter,'rbgmyT7seqfull.out'
      endif
      write (30,20) '80'
      write (30,20) 'y'
      if (counter.ge.10.and.counter.le.99) then
            write (30,70) counter,'rbgmyT7seqfull.ct'
      endif
      if (counter.ge.100.and.counter.le.999) then
            write (30,60) counter,'rbgmyT7seqfull.ct'
      endif
      if (counter.ge.1000.and.counter.le.9999) then
```

```
            write (30,30) counter,'rbgmyT7seqfull.ct'
      endif
      if (counter.ge.1.and.counter.le.9) then
            write (30,80) counter,'rbgmyT7seqfull.ct'
      endif
      write (30,20) 'n'
      write (30,20) '10'
      write (30,20) '6'
      write (30,40) counter
      write (30,20) '17'
      write (30,20) '8'
      close (unit=30)
      counter = counter + 1
 18   continue
 15   continue
 10   continue
 20   format (A)
 30   format (I4,A)
 40   format (I4)
 60   format (I3,A)
 70   format (I2,A)
 80   format (I1,A)
      stop
      end
```

This program is used to generate input files for the lrna program. The variables that are adjusted for each run are:

the end values of the i, j, and k loops: The number of input files generated is controlled by these loops. The output filenames are written with the sequence AAA, AAB, etc. Each loop controls one of the letters (i.e., i controls the first character, j controls the second character, k controls the third character). The total number of generated files then is the product of the value of the 3 loops.

the directory name: This value follows the filename quantity (e.g., RBGMYT70930Seq). This quantity should be updated to avoid writing over previously generated input files. The directory must be created from the UNIX prompt prior to running the compiled, executable file.

the sequence file name: This filename is the appropriately structured sequence file as generated for lrna. (e.g., NewT7Seq093000.txt)

the first base and last base to be folded: These values are found 2 and 3 lines below the sequence file name (e.g., 1 and 510).

the output sequence file names: These will be the structure file (e.g., rbgmyt7seqful.out) and ct file (e.g., rbgmyt7seqful.ct). The leading values of these output files will be modified by the nested loops so as not to overwrite each other.

the oligonucleotide length: This line follows the counter line near the end of the file (e.g., 17).

5.E. 2-5: Batchcreate

```
      program repeat
      integer i, j, k, l, m
      character*30 filename
      l = 1
      i = 1
      k = 1
      j = 1
      DO 10 i=1,1
      DO 15 j=1,20
      DO 18 k=1,26
C     print *, i
C     print *, char(i)
      filename='EColi5SOligos/'//char(i+64)//char(j+64)//char(k+64)
C     print *, filename
      open(unit=30, file='EColi5SOligosbatch')
      write (30,20) './lrna < '//filename
      close (unit=i+10)
C     print *, l
      l = l + 1
 18   continue
 15   continue
 10   continue
 20   format (A)
 30   format (I4,A)
 40   format (I4)
      stop
      end
```

This program is used to generate the batch file that will run the multiple lrna jobs in succession. The variables that are adjusted for each run are:

the end values of the i, j, and k loops: This will insure that the batch file uses the same input files that were generated by batchlrna.

the directory name: This value follows the filename quantity (e.g., EColi5SOligos) and should match the directory used in the batchlrna file. This quantity should be updated to ensure the proper input files are selected.

the batch file name: This file will be created and written with the instructions to run the lrna jobs. This file will need to be made executable from the UNIX prompt prior to running.

5.F. 2-6: Batchlfp

```
      program repeat
      integer i, j, k, l, m, counter, counternew
      character*30 filename
      counter = 15
      counternew = 1
      DO 10 i=1,1
      DO 15 j=1,5
      DO 18 k=1,26
C     print *, i
C     print *, char(i)
      filename='EColi5SOligos/'//char(i+64)//char(j+64)//char(k+64)
C     print *, filename
      open(unit=30, file=filename)
      write (30,20) '0'
      write (30,20) '0'
      write (30,20) '1'
      write (30,20) '10'
      write (30,20) '1'
      write (30,20) '0'
      write (30,20) 'Ecoli5S.seq'
      write (30,20) '1'
      write (30,40) counternew
      write (30,40) counter
      write (30,20) 'dangle.datd'
      write (30,20) 'loop.datd'
      write (30,20) 'stack.datd'
      write (30,20) 'tstackh.datd'
      write (30,20) 'tstacki.datd'
      write (30,20) 'tloop.datd'
      write (30,20) 'miscloop.datd'
      write (30,20) 'y'
      write (30,20) 'n'
      if (counternew.ge.10.and.counternew.le.99) then
            write (30,70) counternew,'Ecoli5SOligo.out'
      endif
      if (counternew.ge.100.and.counternew.le.999) then
            write (30,60) counternew,'Ecoli5SOligo.out'
      endif
      if (counternew.ge.1000.and.counternew.le.9999) then
            write (30,30) counternew,'Ecoli5SOligo.out'
      endif
      if (counternew.ge.1.and.counternew.le.9) then
            write (30,80) counternew,'Ecoli5SOligo.out'
      endif
      write (30,20) '80'
      write (30,20) 'y'
      if (counternew.ge.10.and.counternew.le.99) then
            write (30,70) counternew,'Ecoli5SOligo.ct'
      endif
      if (counternew.ge.100.and.counternew.le.999) then
            write (30,60) counternew,'Ecoli5SOligo.ct'
      endif
```

```
      if (counternew.ge.1000.and.counternew.le.9999) then
            write (30,30) counternew,'Ecoli5SOligo.ct'
      endif
      if (counternew.ge.1.and.counternew.le.9) then
            write (30,80) counternew,'Ecoli5SOligo.ct'
      endif
      write (30,20) 'n'
      write (30,20) '10'
      write (30,20) '8'
      close (unit=30)
      counter = counter + 1
      counternew = counternew + 1
 18   continue
 15   continue
 10   continue
 20   format (A)
 30   format (I4,A)
 40   format (I4)
 60   format (I3,A)
 70   format (I2,A)
 80   format (I1,A)
      stop
      end
```

This program is used to generate the input files that will be used to calculate the oligonucleotide folding energies. The variables that are adjusted for each run are:

the end values of the i, j, and k loops: These need to be adjusted to generate enough input files for each oligonucleotide within the mRNA.

the initial value of the "counter" variable: This value should be the oligonucleotide length.

the directory name: This value follows the filename quantity (e.g., EColi5SOligos). This quantity should be updated to avoid writing over previously generated input files. The directory must be created from the UNIX prompt prior to running the compiled, executable file.

the output sequence file names: These will be the structure file (e.g., Ecoli5SOligo.out) and ct file (e.g., Ecoli5SOligo.ct). The leading values of these output files will be modified by the nested loops so as not to overwrite each other.

5.G. 3-1: Mechanistic Description of RNase H Activity

We found experimentally that the rate of cleavage product formation in RNase H assays followed first-order (exponential) kinetics. This rate is dependent on an interplay between association and dissociation of oligonucleotide:RNA duplexes and the kinetics of recognition and cleavage of duplexes by the ribonuclease H enzyme. Here, we present an analysis of the functional dependence of cleavage product formation under two regimes: binding limited and RNase H limited. In each case, we seek to find how the apparent first-order rate constant depends on measurable parameters of the oligonucleotide:RNA interaction.

We consider, in general, the reaction scheme:

$$O + M \underset{k_d}{\overset{k_a}{\leftrightarrow}} D \underset{(K_M, k_{cat})}{\overset{E}{\rightarrow}} X + O \tag{12}$$

where O is the oligonucleotide, M is the mRNA, D is the duplex that they form with association rate constant k_a and dissociation rate constant k_d, and X is the RNA cleavage product, which is formed in the presence of RNase H enzyme, E, with Michaelis-Menten parameters K_m and k_{cat}. Under the experimental conditions used, the total concentrations of oligonucleotide and mRNA, O_T and M_T, are each 50 nM; as a result, no simplification based on molar excess can be made. We consider two cases:

Case 1: Binding limited (catalysis >> binding)

If the rate of association is slower than catalysis, so must be the rate of dissociation, so the reaction network is essentially:

$$O + M \xrightarrow{k_a} D \xrightarrow[(K_M, k_{cat})]{E} X + O\,. \tag{13}$$

In this sequence, RNA is removed only by association with oligonucleotide, which is regenerated during the catalysis step, resulting in a first order decay on mRNA:

$$M = M_T e^{-k_a O_T t}\,. \tag{14}$$

Since the duplex is rapidly recognized by ribonuclease H and converted into RNA cleavage product and regenerated DNA oligonucleotide, the quasi-steady-state approximation applies on D:

$$\frac{dD}{dt} = k_a OM - \frac{k_{cat} E_0 D}{K_M + D} = 0. \tag{15}$$

This equation is simplified since, under the experimental conditions, $D << K_M$. Solving for D and combining with Eq. 15 and the mass balance $M_T = M + D + X$ gives an approximate profile for X, valid subject to the aforementioned approximations at times after the quasi-steady-state is established

$$\frac{X}{M_T} = 1 - \left(1 + \frac{k_a O_T}{k_{cat} E_0 / K_M} \right) e^{-k_a O_T t}. \tag{16}$$

Thus, first order kinetics are expected, with an effective rate constant

$$k_{eff} = k_a O_T. \tag{17}$$

The total concentration of oligonucleotide was fixed at 50 nM for all of the RNase experiments performed here. Therefore, the line corresponding to Eq. 17 is shown in Figure 3-7.

Case 2: Reaction limited (binding >> catalysis)

We begin with the rate equation for the formation of cleavage product:

$$\frac{dX}{dt} = v = \frac{k_{cat} E_0 D}{K_M + D} \approx \frac{k_{cat} E_0 D}{K_M}. \tag{18}$$

If binding is rapid, the oligonucleotide, mRNA, and duplex forms will essentially be in equilibrium. The equilibrium relationship among O, M, and D, along with mass balances on O and M and the rate equation for X provides four equations in the four unknowns O, M, D, and X. The solution for X is:

$$\frac{X}{M_T} = 1 - e^{-\frac{k_{cat} E_0}{K_M (1 + K_D / O_T)} t}. \tag{19}$$

Again, first-order kinetics is expected, in this case with a rate constant

$$k_{eff} = \frac{k_{cat} E_0}{K_M \left(1 + K_D / O_T \right)}. \tag{20}$$

For all of the oligonucleotides on which RNase assays were performed, the dissociation constant was significantly less than the oligonucleotide concentration. Therefore,

$$k_{eff} \approx \frac{k_{cat} E_0}{K_M}. \tag{21}$$

Based on the specifications of the ribonuclease H supplier (Promega) and published value of the Michaelis constant (0.2 μM, [215]), the expected value of k_{eff} under conditions of high binding is about 0.1 s^{-1}, two orders of magnitude higher than observed (Figure 3-7). Since we observed the predicted behavior for low k_a value and observe the predicted plateau, the discrepancies in magnitude may be due to loss of activity of the RNase H enzyme through storage, exposure to buffer, or product inhibition/degradation.

Protocol for RNase H cleavage assay

As the concentrations of oligonucleotide and mRNA used in the RNase H cleavage experiments are higher that those for the binding affinity assays, these assays can be performed in microcentrifuge tubes without concerns of significant loss to binding of the tube walls.

The most critical aspect in the preparation of the RNase cleavage experiments is to have your RNase H concentration low enough to prevent non-specific degradation from enzymatic and buffer components while high enough to achieve a binding-limited condition for the slowest binding oligonucleotides. This balance also depends on the target being used. Of the two targets that I used, the longer transcript, LDH-A, was much more susceptible to

RNase H cleavage buffer (1X):

0.1 M KCl, 10 mM $MgCl_2$, 1 mM DTT, and 50 mM Tris-HCl (pH 8.0)

Protocol:

1. Dilute stock oligonucleotide to the 3X concentration with cleavage buffer and water. Stock oligonucleotides should be stored at greater than 10 μM concentration. A good choice for the final working concentration to be tested is 50 nM oligonucleotide (150 nM initial dilution). This can be adjusted, as needed. A total volume of the final reaction mixture will be required such that 3 μL can be extracted for each time point with greater than 15 μL of total volume remaining after the last sample is removed. The excess volume provides ballast to the system, such that the change in volume due to evaporation is small, precluding the need for mineral oil.

2. Remove mRNA from -80°C freezer and place at 4°C to thaw.

3. Dilute RNase H (Promega) to 3X working concentration in cleavage buffer. Typical working concentrations of RNase H were 0.1 to 0.2 units/μL in the final reaction.

4. Add 1 volume of RNase H dilution to 1 volume of oligonucleotide dilution.

5. Retrieve RNA from refrigerator and dilute to 3X working concentration in cleavage buffer.

6. Place all reagents in 37°C water bath for 10 minutes.

7. At time 0, add 1 volume of RNA to oligonucleotide:RNase H mixture. Mix well and extract 3 μL for the time 0 sample. Add the sample to 9 μL of denaturing gel-loading buffer (Ambion). Different denaturing gel-loading buffers are required depending on the type of gel being used (see step 9, below). Store the sample on dry ice.

8. Extract samples at approximately 1', 2', 5', 10', 15', and 30'. If the RNA is particularly stable or the binding particularly slow, longer time points may be required.

9. Just prior to loading, heat the samples to 50-70°C (again, will change with stability of transcript). Immediately load on appropriate gel (either formaldehyde/agarose (reagents available from Ambion) for transcripts > 600 nt or 5/10% TBE-Urea (Bio-Rad) for shorter transcripts).

10. Electrophorese for ~20-60 minutes (depends on gel type and transcripts/cleavage product lengths) at 100-150 volts (constant voltage).

11. Stain gel using SYBR Gold (Molecular Probes) (stock at 10,000X concentration). Staining can require 1 to 16 h (stains longer than 4 h should be performed at 4°C) and should be protected from light exposure.

12. Measure the fluorescence signal from the gel using the Fluor-S system (Bio-Rad). Use Multi-Analyst software to measure the intensities of the full-length transcript and the two cleavage products. These intensities are used to calculate fraction cleaved which is then fit by a pseudo first-order kinetic equation to calculate k_{eff}.

5.H. 3-2: mRNA and Oligonucleotide Purity

Oligonucleotide and mRNA purity are critical factors in ensuring the accuracy of the K_D values obtained from the centrifugal technique. In the case of the mRNA, it is essential to verify the mRNA purity from the *in vitro* transcription reaction prior to proceeding. In the experiments described here, the first *in vitro* transcript was produced using the SP6 transcription enzyme system. However, it was found that this enzyme did not process through the mRNA completely, instead resulting in a large fraction of incomplete transcription products (Figure 3-A1). When this was discovered, the insert was cloned into another vector behind the T7 RNA polymerase promoter, and transcription was performed using the T7 polymerase. In this case, the resulting transcript was of full-length with no specific contaminants (Figure 3-A1). Depending on the length of the contaminants, binding affinity results for oligonucleotides that interacted with the incomplete transcripts could have been biased higher or lower with no consistency. Working with a single pure transcript of known concentration is essential to accurately measure K_D.

The purity of the oligonucleotide was also essential. It is recommended that oligonucleotides be used within 6 months of being resuspended and stored at -20°C or within 1 year of synthesis and storage at -20°C. However, even within this time frame, a significant amount of smaller sequences can exist even in HPLC purified oligonucleotide preparations. The presence of labeled degradation products can significantly affect the measurement of K_D by the centrifugal method. The presence of significant degradation products is suggested when the measured binding of the oligonucleotide saturates at a level significantly lower than 100%, e.g. 75-85% (Figure 3-A2). The most reliable method found for ensuring complete purification of the oligonucleotide from any degraded products was NucAway Spin columns (Ambion; Austin, TX). In addition, PAGE purification was possible, but elution and precipitation of radiolabeled oligonucleotides proved particularly challenging.

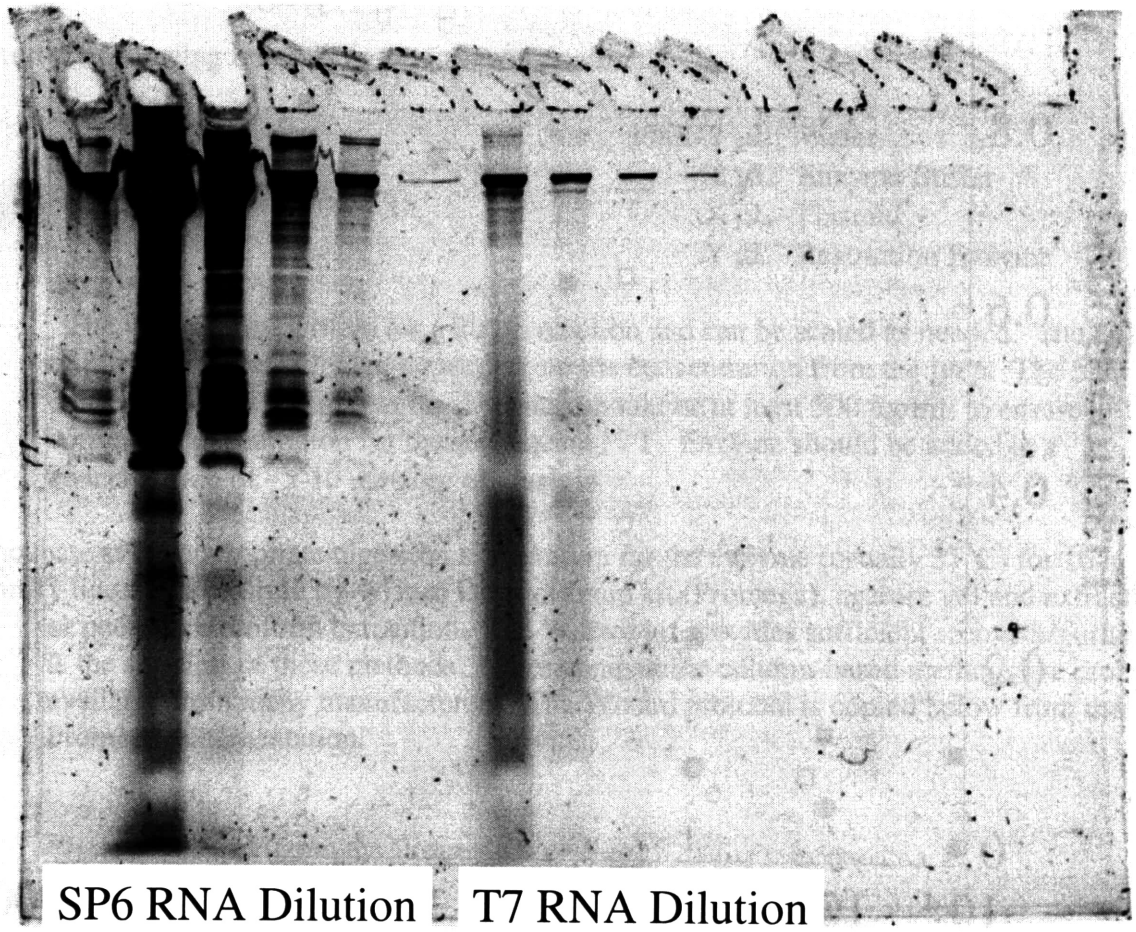

Figure 3-A1: Confirming RNA Purity from *in vitro* transcription
Transcription using the SP6 RNA polymerase and promoter results in a significant fraction (~10-20% by mass) of incomplete transcription products. Some RNA polymerases are sensitive to local structure and fall off the template prior to completion of the mRNA. However, use of the T7 polymerase and promoter eliminates this product, yielding the full length product almost exclusively. Signal intensity exaggerated to prove elimination of smaller cleavage product not due to lower concentration of T7 product (last dilution of SP6 RNA comparable to highest concentration of T7).

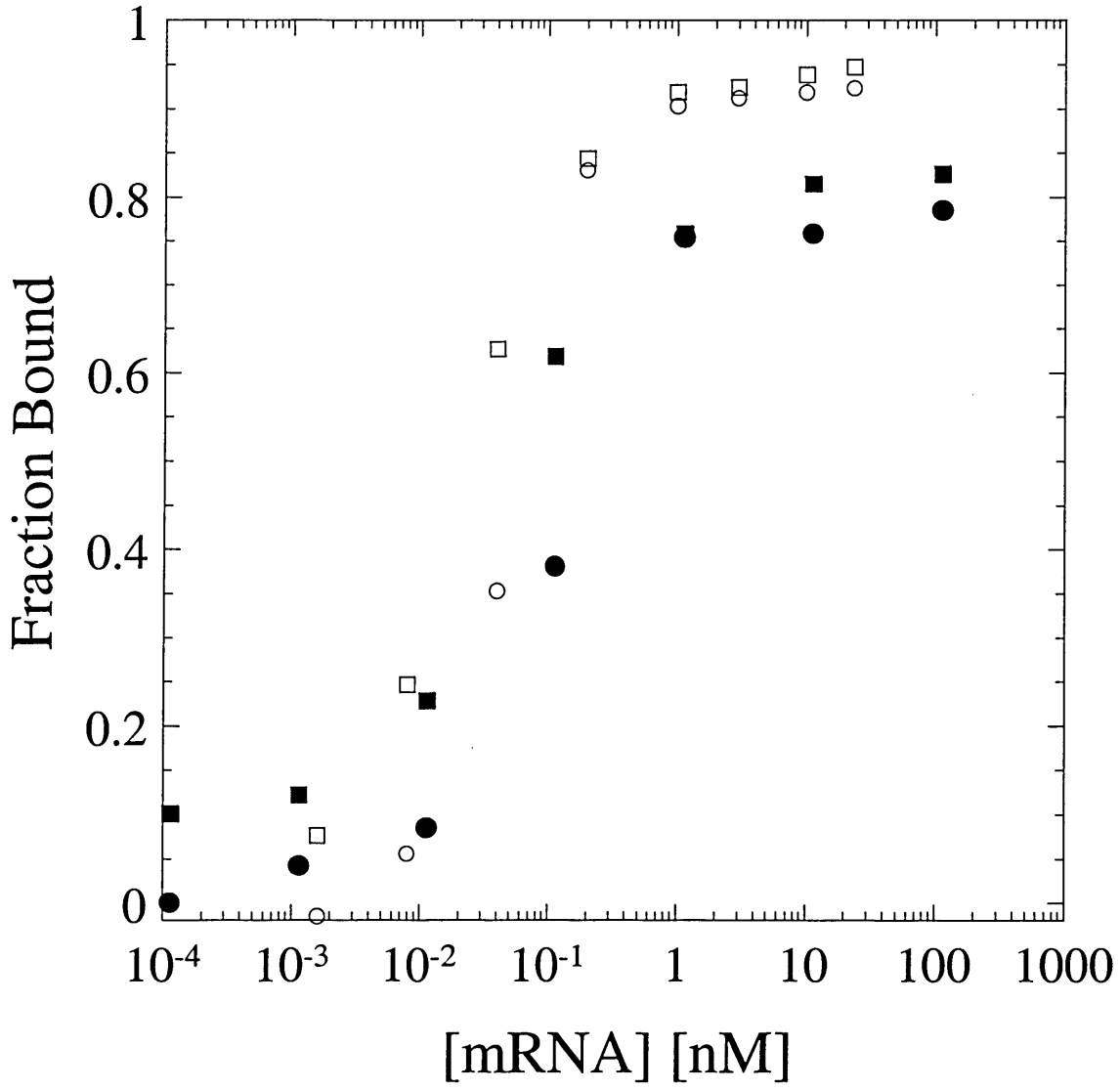

Figure 3-A2: Binding Saturation due to Degraded Oligonucleotide
Binding curves are shown for oligonucleotides 139 (circles) and 259 (squares) complementary to the RBG mRNA. Closed symbols show binding in the presence of degraded oligonucleotide products. Open symbols show binding following purification of the full-length oligonucleotide. Saturating fractional binding increased from 78% to 92% and 83% to 95% for oligonucleotides 139 and 259, respectively. In no case was complete binding seen in the presence of oligonucleotide degradation products, with saturation values varying between 75 and 85%, typically.

Linearization of plasmid template for* In Vitro *Transcription (IVT)

Plasmids prepared from Qiagen prep kits (Mini, Midi, Maxi) are sufficient for application in *in vitro* transcription.

1. Add the following reagents in the following order:

17-X-Y µL	Water
2 µL	Enzyme Buffer
X µL	Plasmid*
Y µL	Restriction Enzyme*

* The volumes are written for a 20 µL reaction and can be scaled as needed. The volume of plasmid added will vary depending on the concentration from the prep. The final concentration of plasmid in the digestion should be at least 500 µg/mL to ensure sufficient concentration for the subsequent IVT. Enzyme should be added at a concentration of ~5-10 units/µg of plasmid.

2. Incubate at the appropriate digestion temperature for the enzyme (usually 37°C) for 16 h.
3. Purify linearized plasmid by Wizard DNA cleanup kit (Promega), agarose gel and extraction, or phenol-chloroform extraction. The Wizard kit provides sufficient recovery/purity and is the simplest of these methods. Other comparable column-based methods are probably available from many manufacturers. The Wizard protocol is copied below from the Promega documentation.

Wizard Protocol (from the Promega Web Site):

Notes:

1. Thoroughly mix the Wizard ® DNA Clean-Up Resin before removing an aliquot. If crystals or aggregates are present, dissolve by warming the resin to 37°C for 10 minutes. The resin itself is insoluble. Cool to 25–30°C before use.

2. The binding capacity of 1ml of resin is approximately 20µg of DNA.

Materials to Be Supplied by the User:

80% isopropanol (2-propanol, reagent grade)
Prewarmed (65–70°C) deionized water or TE buffer
Disposable 3ml Luer-Lok ® syringes

Note: The sample volume must be between 50 and 500µl. If the sample volume is less than 50µl, bring the volume up to at least 50µl with sterile water.

1. Use one Wizard ® Minicolumn for each sample. Remove and set aside the plunger from a 3ml disposable syringe. Attach the Syringe Barrel to the Luer-Lok® extension of each Minicolumn.
2. Add 1ml of Wizard ® DNA Clean-Up Resin to a 1.5ml microcentrifuge tube. Add the sample (50–500μl) to the Clean-Up Resin and mix by gently inverting several times.
3. Pipet the Wizard ® DNA Clean-Up Resin containing the bound DNA into the Syringe Barrel. Insert the syringe plunger slowly and gently push the slurry into the Minicolumn with the syringe plunger.
4. Detach the syringe from the Minicolumn and remove the plunger from the syringe. Reattach the Syringe Barrel to the Minicolumn. To wash the column, pipet 2 mL of 80% isopropanol into the syringe. Insert the plunger into the syringe and gently push the solution through the Minicolumn.
5. Remove the Syringe Barrel and transfer the Minicolumn to a 1.5ml microcentrifuge tube. Centrifuge the Minicolumn for 2 minutes at maximum speed (10,000 x g) to dry the resin.
6. Transfer the Minicolumn to a new microcentrifuge tube. Apply 50μl (see Table 1) of prewarmed (65–70°C) water or TE buffer (10mM Tris-HCl [pH 7.6], 1mM EDTA) to the Minicolumn and wait 1 minute. (The DNA will remain intact on the Minicolumn for up to 30 minutes.) Centrifuge the Minicolumn for 20 seconds at maximum speed (10,000 x g) to elute the bound DNA fragment.
7. Remove and discard the Minicolumn. The purified DNA may be stored in the microcentrifuge tube at 4°C or –20°C.

Protocol for IVT (from Ambion MegaScript Kit)

Note: The choice of enzyme system used for the IVT does matter. SP6 is "old technology" and should be considered only as a last resort. T7 and T3 are both very common and reliable.

1. **Thaw the frozen reagents --** Place the RNA Polymerase Enzyme Mix on ice, it is stored in glycerol and will not be frozen at –20°C. Vortex the 10X Reaction Buffer and the 4 ribonucleotide solutions (ATP, CTP, GTP, and UTP) until they are completely in solution. Once they are thawed, store the ribonucleotides on ice, but ***keep the 10X Reaction Buffer at room temperature while assembling the reaction***. All reagents should be microfuged briefly before opening to prevent loss and/or contamination of material that may be present around the rim of the tube.
2. **Assemble transcription reaction at room temperature --** The spermidine in the 10X Reaction Buffer can coprecipitate the template DNA if the reaction is assembled on ice. Add the 10X Reaction Buffer after the water and the NTPs are already in the tube. The following amounts are for a single 20 μl reaction.
3. **Mix thoroughly –**

   12-X μl Nuclease-free Water
   2 μl ATP solution
   2 μl CTP solution
   2 μl GTP solution
   2 μl UTP solution
   2 μl 10X Reaction Buffer
   1 μg (in X μl H_2O) linear template DNA
   2 μl Enzyme Mix

   Gently flick the tube or pipette the mixture up and down gently, and then microfuge tube briefly to collect the reaction mixture at the bottom of the tube. For convenience, mix equal volumes of the four ribonucleotides solutions together and add 8 μl of the mixture to a standard 20 μl reaction instead of adding the ribonucleotides separately. Reactions can be scaled for desired recovery. Typically, 20-40 µg/20 µl reaction (specs for kit say ~100 µg, but I never got that sort of yield).

4. **Incubate at 37°C, 2–4 hours --** The first time a new template is transcribed, the recommended incubation time is 2–4 hours. The optimal incubation time for a given template will vary depending on the size and transcriptional efficiency of your template. For short transcripts (less than 500 nt), a longer incubation time (up to ~16 hours) may be advantageous, since more transcription initiation events are required to synthesize a given mass amount of RNA, compared to transcription of longer templates.

5. **Remove template DNA --** For many applications it may not be necessary to degrade the template DNA, since it will be present at a very low concentration relative to the RNA.

   a. Add 1 μl DNase 1, and mix well (the reaction may be viscous).

b. Incubate at 37°C for 15 minutes

6. Phenol:chloroform extraction and isopropanol precipitation -- This is the most rigorous method for purifying transcripts. It will remove all enzyme and most of the free nucleotides from MEGAscript reactions. Since the RNA is precipitated, it can also be used for buffer exchange.

a. Add 115 μl Nuclease-free Water and 15 μl Ammonium Acetate Stop Solution, and mix thoroughly.
b. Extract with an equal volume of phenol/chloroform (it can be water-saturated, buffer-saturated, or acidic), and then with an equal volume of chloroform. (Optional: back-extract the organic phase with 50 μl dH2 O.)
c. Precipitate the RNA by adding 1 volume of isopropanol and mixing well.
d. Chill the mixture for at least 15 minutes at -20°C. Centrifuge at 4°C for 15 minutes at maximum speed to pellet the RNA. Carefully remove the supernatant solution and resuspend the RNA in a solution or buffer appropriate for your application.
e. Store frozen at -70°C.

5.I. *3-3: Execution of centrifugal and gel-shift assays*

In all experiments involving mRNA, freshly autoclaved tips were used. This was found to be sufficient to eliminate most concerns of RNase degradation of the mRNA. The centrifugal assay is performed in plates available from Corning specifically designed to have a non-binding surface that limits absorption of biological molecules to low levels [Product #: 3600]. These plates were used to ensure that when working with very low oligonucleotide concentrations no oligonucleotide would be "lost". While the mRNA was generally maintained at a significantly higher concentration, for the highest affinity oligonucleotides, minimum RNA concentrations were in the picomolar range and adsorption was also a concern. The use of adhesive plate sealers limited evaporation over the 16+ hours required for some measurements with generally >95% of the hybridization volume retained. The only exception was the outermost wells, where evaporation was a significant problem. Hence, these wells were not used for long-term incubations in any cases.

For equilibrium K_D measurements, hybridization reactions were left for at least 16 hours but less than 20 hours with no changes in fractional binding having been observed over this time frame. For each condition, 53 μL of mRNA at the desired concentration and 53 μL of radiolabeled oligonucleotide at the minimum detectable concentration are added to each well of the plate. Each of the dilutions is performed to a final dilution of 1X hybridization buffer so that following mixing the buffer concentration is still 1X. The total volume could be increased to ~ 250 μL if additional sensitivity was required, but this was not done in this case to avoid splashing onto the plate cover or cross contamination of the wells. The concentration of oligonucleotide prior to addition to the mRNA was diluted to ~10-40 cpm/μL thereby yielding 1000-4000 cpm in the final scintillation count. The sealed plate was then placed at 37°C for 16+ hours after which it was returned to the bench. 100 μL of hybridization volume were removed from each well and added to each filter apparatus. The filter was centrifuged for ~50 seconds at 8,200 g (10,000 rpm on an Eppendorf microcentrifuge). The membrane is then inverted into a new centrifuge tube and centrifuged for 30 seconds at 8,200 g to collect the retentate. The samples are then measured immediately or placed on dry-ice for analysis at a later time. Since the fractions have been separated, already, complex separation or formation after separation will

not affect the final scintillation count. No difference was seen between the counts recovered from frozen or unfrozen samples.

The volumes of each of the fraction are measured using a 10-100μL pipet. After collecting the volume at the bottom of the tube (if necessary), the pipet is set to a volume ~5 μL below the expected volume of the fraction. The volume is then taken up by the pipet. If solution remains in the tube, the uptake volume of the pipet is increased by 1 μL and the process repeated until the end of the pipet fills with air. The pipet volume is then decreased by 1 μL, and the step increases in pipet volume are decreased to 0.2 μL. The volume on the pipet at which the pipet tip first begins to fill with air is used as the final volume measured. In tests where a random volume was placed in the tube and then measured using this method, errors were found to be no more than 1 μL, or in general <3-5% of the total measurement.

Once the volume is recovered completely from the tube, it is added directly to the scintillation fluid (Ultima Gold, Packard Biosciences). Many scintillation fluids were tested to ensure complete solubilization of the 1M NaCl containing buffer. 5 mL of scintillation fluid were found to be sufficient to completely solubilize the 30-60 μL of hybridization volume that would typically be added. However, following addition of the hybridization solution, the vial must be mixed vigorously, to eliminate precipitation of the oligonucleotide-containing hybridization volume. It was found most convenient to write the volume of the sample directly onto the lid of the scintillation vial and then record them all during/after counting, but this is certainly not essential. Scintillation counts were run for 10 minutes each to ensure collection of a sufficient sample size to accurately measure the counts within. This is particularly important at the highest mRNA concentration where the counts will be contained mostly in the retentate fraction, little free oligonucleotide being present. The background counts from vials containing only scintillation fluid were subtracted from all measured points. Background measurements were performed at least at the beginning of each set of counts, though usually at the beginning, end, and up to twice internally depending on the total number of samples being counted. No difference was seen between vials containing only scintillation fluid and those containing 1X hybridization buffer. As the only readout from the scintillation counter was paper printouts, the values were hand-transcribed into Excel for analysis. Original printouts were taped into a laboratory notebook for later reference.

Oligonucleotide:mRNA hybridization for centrifugal and gel-shift assays

For all manipulations involving RNA, only fresh, sterile tips (had not been opened subsequent to autoclaving) were used. If concerns of RNase contamination still exist, treat tips with DEPC-water prior to autoclaving. The work surface and pipets should be wiped with RNaseZap (Ambion) prior to use with RNA. This further limits RNase contamination. (Side note: I and others have found that products from Ambion are generally speaking the best among comparable groups of products, both by price and quality.)

All mRNA and oligonucleotide dilutions were performed in Non-Binding Surface plates (Corning), when possible. When dilution volumes exceeded 330 µl, Eppendorf tubes were used for the initial dilution and the volume subsequently transferred to an appropriate number of wells on the plate.

All radioactive materials should be handled and disposed of properly.

Hybridization buffer (from Turner's group information):

1M NaCl, 0.5 mM EDTA, and 20 mM sodium cacodylate, pH 7.0

Procedure:

1. Plan experimental dilutions – These will depend on the age of the radiolabel as well as the concentration of the stock RNA, but an example of a typical matrix for one of my experiments is shown below:

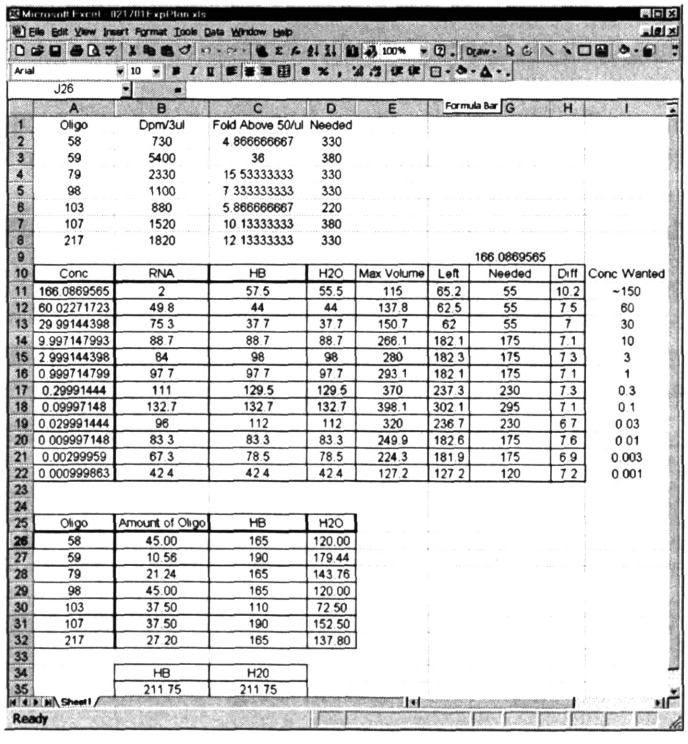

Oligo	Dpm/3ul	Fold Above 50/ul	Needed
58	730	4.866666667	330
59	5400	36	380
79	2330	15.53333333	330
98	1100	7.333333333	330
103	880	5.866666667	220
107	1520	10.13333333	380
217	1820	12.13333333	330

166.0869565

Conc	RNA	HB	H2O	Max Volume	Left	Needed	Diff	Conc Wanted
166.0869565	2	57.5	55.5	115	65.2	55	10.2	~150
60.02271723	49.8	44	44	137.8	62.5	55	7.5	60
29.99144398	75.3	37.7	37.7	150.7	62	55	7	30
9.997147993	88.7	88.7	88.7	266.1	182.1	175	7.1	10
2.999144398	84	98	98	280	182.3	175	7.3	3
0.999714799	97.7	97.7	97.7	293.1	182.1	175	7.1	1
0.29991444	111	129.5	129.5	370	237.3	230	7.3	0.3
0.09997148	132.7	132.7	132.7	398.1	302.1	295	7.1	0.1
0.029991444	96	112	112	320	236.7	230	6.7	0.03
0.009997148	83.3	83.3	83.3	249.9	182.6	175	7.6	0.01
0.00299959	67.3	78.5	78.5	224.3	181.9	175	6.9	0.003
0.000999863	42.4	42.4	42.4	127.2	127.2	120	7.2	0.001

Oligo	Amount of Oligo	HB	H2O
58	45.00	165	120.00
59	10.56	190	179.44
79	21.24	165	143.76
98	45.00	165	120.00
103	37.50	110	72.50
107	37.50	190	152.50
217	27.20	165	137.80

HB	H2O
211.75	211.75

The "Oligo" section at the top of the matrix lists the oligonucleotide name, the current label concentration (an indicator of the efficiency of the labeling reaction and measured for each oligonucleotide when labeled and calculated, thereafter), the ratio of the current label concentration to the minimum/working level, and the total volume required for the experiment.

The next section shows the dilutions that are necessary for the mRNA. The columns are as follows: Final concentration in the hybridization mixture, amount of RNA from the prior dilution that is required to reach the concentration (except for the first row where it indicates the amount of stock mRNA), the amount of 2X hybridization buffer that should be added to each dilution, the amount of water that should be added to each dilution, the maximum volume that the dilution achieves (to determine if the use of Eppendorf tubes is necessary), the volume remaining after extracting the amount required for the next serial dilution, the needed volume, and the final excess (should not be less than 5 µL in any case). The final two columns show the desired concentration points and the normalized difference between the actual and the desired. Shading indicates those dilutions that exceed 330 µL and will require Eppendorf tubes.

The third section shows the oligonucleotide dilutions required to reach the final working concentration and volume required for the experiment. The columns are as follows: the oligonucleotide name, the amount of the stock, labeled oligonucleotide required, the amount of 2X hybridization buffer required, and the amount of water required. Thus, both the mRNA and oligonucleotide are in 1X hybridization buffer at their final dilution.

The final box contains the dilution to obtain the required amount of 1X hybridization required to perform the controls. This dilution, as it contains no nucleic acids, can be performed in the plate or in an Eppendorf tube depending on the required volume.

2. Plan out the locations on the plate where these dilutions will be performed (example below). The outermost wells on the plate should not be used for hybridization reactions, as they tend to evaporate more than their internal counterparts.

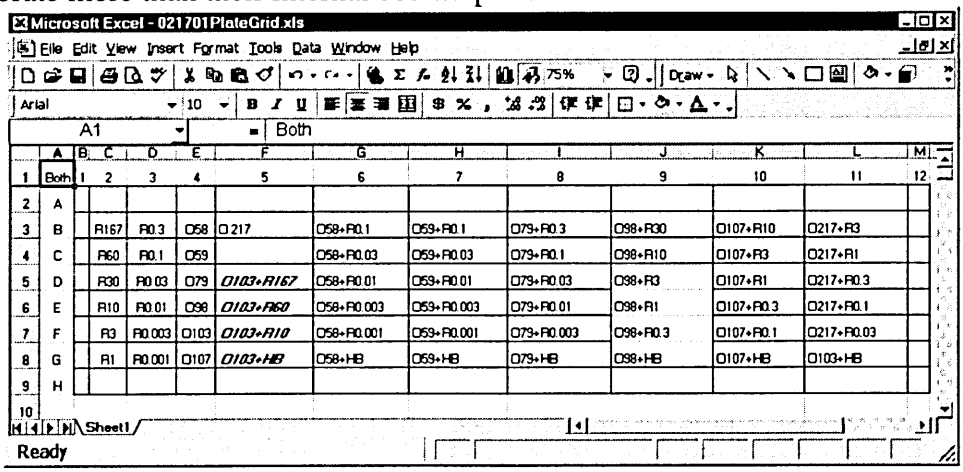

	A	B	C	D	E	F	G	H	I	J	K	L	M
1	Both	1	2	3	4	5	6	7	8	9	10	11	12
2	A												
3	B	R167	R0.3	O58	O217	O58+R0.1	O59+R0.1	O79+R0.3	O98+R30	O107+R10	O217+R3		
4	C	R60	R0.1	O59		O58+R0.03	O59+R0.03	O79+R0.1	O98+R10	O107+R3	O217+R1		
5	D	R30	R0.03	O79	*O103+R167*	O58+R0.01	O59+R0.01	O79+R0.03	O98+R3	O107+R1	O217+R0.3		
6	E	R10	R0.01	O98	*O103+R60*	O58+R0.003	O59+R0.003	O79+R0.01	O98+R1	O107+R0.3	O217+R0.1		
7	F	R3	R0.003	O103	*O103+R10*	O58+R0.001	O59+R0.001	O79+R0.003	O98+R0.3	O107+R0.1	O217+R0.03		
8	G	R1	R0.001	O107	*O103+HB*	O58+HB	O59+HB	O79+HB	O98+HB	O107+HB	O103+HB		
9	H												
10													

Not having planned the plate beforehand will surely result in a pipetting mistake. The labels indicate the locations of the mRNA dilutions (e.g., R167), oligonucleotide dilutions (O58), and the hybridization wells (O58 + R0.1). Controls were run with oligonucleotides mixed with 1X hybridization buffer (O58 + HB).

3. Add 2X hybridization buffer and water to dilution and hybridization wells as delineated by the experimental plan and plate grid.

4. Remove mRNA from -80°C freezer and place at 4°C to thaw.

5. Remove labeled oligonucleotides from 4°C and add correct volumes to appropriate wells. Return labeled, stock oligonucleotides to refrigerator.

6. Pipet 55 μL of diluted oligonucleotide to each appropriate well. To yield 100 μL for the centrifugal assay while providing excess for plate wetting, etc., 110 μL are used. When gel-shift assays are also being performed, an additional 10 μL per gel lane should be added.

7. Remove thawed mRNA from refrigerator, spin down, and add to appropriate well. Perform serial dilutions as described by experimental plan.

8. Pipet 55 μL of diluted mRNA to each appropriate well. To yield 100 μL for the centrifugal assay while providing excess for plate wetting, etc., 110 μL are used. When gel-shift assays are also being performed, an additional 10 μL per gel lane should be added.

9. Seal the plate tightly with an adhesive plate sealer. Incubate in the warm room (37°C) for desired time. Equilibrium measurements were made between 16 and 20 hours of incubation.

For centrifugal assay (for gel-shift, skip to next section):

10. Prepare and label Microcon tubes. Prepare bucket of dry ice. Add scintillation fluid to the required number of vials. Either 7mL or 20 mL vials are sufficient.

11. Remove plate from warm room and peel back adhesive sealer to uncover wells to be assayed.

12. Add 100 μL of hybridization mixture to each filter, pipetting all of the wells for a given oligonucleotide and the same time.

13. Transfer loaded filters to microcentrifuge and centrifuge at 10,000 rpm (~8,200 g) for 40-50 seconds. The resulting permeate should be about 50 μL.

14. Invert the filter into a new tube, placing the collected permeate on dry ice.

15. Collect the retentate by centrifuging the inverted filter for 20 seconds at 10,000 rpm.

16. Place the filter into a scintillation vial and label the cap. Place the retentate on dry ice. Retentate and permeate samples can be stored at -20°C for up to 2 days with no appreciable change in signal recovery.

17. Thaw retentate and permeate samples on ice. Spin down quickly, to collect contents at the bottom of the tube.

18. Set the pipet at less than the expected volume for the fraction being measured. Pipet up the volume in the tube, twice. If no air bubble exists in the pipet tip subsequent to the second uptake, increase the volume setting on the pipet by 1 µL. When an air bubbles appears, reduce the pipet uptake setting by 1 µL and increase in increments of 0.2 µL. The first reading at which the air bubble reappears is the volume of the collected fraction. Add this volume to the scintillation vial and label the cap. This technique was able to measure volumes within 1-2 µL, or 2-6% of typical values.

19. Count all vials. Calculate fraction bound for each retentate/permeate pair by:

$$f = \frac{R - V_R\left(P/V_P\right)K_{memb}}{R+P}; \quad K_{memb} = \frac{[\text{free oligo}]_{retentate}}{[\text{free oligo}]_{permeate}} = \frac{R_{free}/V_R}{P/V_P}$$

where: P, R = total CPM in permeate, retentate fractions
V_P, V_R = volume of permeate and retentate fractions
K_{memb} is determined experimentally on the oligonucleotide only sample.

20. Calculate K_D from:

$$f = \frac{M_T}{M_T + K_D}$$

where: M_T = the concentration of mRNA used for each sample (assumed constant).

For gel-shift assay:

10. Remove 10 µL of hybridization volume from the plate and add to 2 µL of 6X loading buffer (contains glycerol, xylene cyanole, and bromophenol blue; recipe from Maniatis; Thanks, Arul!)

11. Add 12 µL of mixture to each well of a 15-well, 4-20% TBE Ready Gel (Bio-Rad).

12. Electrophorese for ~45 minutes (until the dye front reaches 75% of the way down the gel) at 80-100 volts (constant voltage).

13. Remove gel from apparatus and separate plates, leaving the gel on the larger, plastic plate.

14. Adhere a piece of 2-ply (folded over onto itself) Whatman filter paper to the gel. Trim paper to size of gel with 1 inch margin.

15. Dry gel for 45 minutes at 80°C under vacuum.

16. Erase GS-525 beta-imaging cartridge.

17. Transfer dried gel to exposing "darkroom". Tape down gel securely and cover with securely taped cover foil (Bio-Rad).

18. Expose gel for 16-48 hours, depending on signal required.

19. Scan cartridge using GS-525 Molecular Imager (Bio-Rad).

20. Using Multi-Analyst software (Bio-Rad), measure intensity of bound and free radioactivity bands. Calculate fraction bound as intensity of bound band divided by the total of the bound and free bands. Calculate K_D as above for centrifugal assay.

5.J. 4-1: Antisense assay protocol

Materials:

Lipofectin reagent (Gibco/Invitrogen) – A newer product, OligofectAMINE seems to be less stressful for the cells and should be evaluated for future antisense applications, as that is it's designated purpose.

Oligonucleotides – Oligonucleotides should be HPLC purified and resuspended in TE (or other alkaline buffer) to at least 10 μM concentration. Resuspended oligonucleotides can be stored at -20°C for 6 months to 1 year. To simplify matters, resuspended oligonucleotides should be filtered by 4 mm syringe filter into sterile microcentrifuge tubes for storage.

Serum-Free Medium – DMEM has traditionally been used, but Gibco recommends trying their Opti-MEM product.

Note: Volumes and concentrations will vary, depending on the cells and plate well size. The procedure below is used for a 24-well plate and can be scaled as needed. Cells should be fed with fresh medium on the day prior to use in experiments.

Procedure:

1. Dilute lipofectin in serum-free medium and let stand for 30-45 minutes at room temperature – to a concentration with positive charges equal to the negative charges of the oligonucleotide. The stock lipofectin is 746 μM in positive charges. A total of 15 mL lipofectin media is sufficient for 1 24-well plate.

2. Aliquot lipofectin media into the appropriate number of tubes, 1 tube per oligonucleotide.

3. Add oligonucleotide directly to lipofectin media. Mix gently. Let stand for 15 minutes.

4. Aspirate medium from cells and wash with 0.5 mL of PBS or DMEM per well.

5. Add 0.5 mL of oligonucleotide:lipofectin:media to each well of the plate.

6. Incubate at 37°C for the required time. The level of CO2 used in culturing should be used for antisense assays.

For the assays described here, these specific conditions were used:

Fibroblast antisense (LDH-A and LDH-B):

6-well plates (2 mL media per well)
Prior to the experiment, the cells were switched to serum-free growth medium for 24 hours.

4 hours of exposure to oligonucleotides – Samples for RT-PCR collected.

20 ng/mL of epidermal growth factor (Sigma, St. Louis, MO) in a change of fresh DMEM for 20 hours (total of 24 hours from beginning of experiment).

Washed with PBS (pH 7.20) and lysed in the plate. The lysate was centrifuged for 5 minutes at 10,000g at 4°C and stored at –20°C until assayed for LDH activity.

H-35 rat hepatoma cells (gp130):

24-well plates

Lipofectin was added to DMEM with 1 μM dexamethasone

Phosphorothioate oligonucleotides

Cells washed twice with PBS (pH 7.20)

8 hours exposure to oligonucleotides (or other time for kinetic experiments) – RT-PCR samples collected by scraping, washing with PBS, and storing at –80°C.

16 hours (24 hours of antisense treatment) with fresh medium containing 1 μM dexamethasone and 10 ng/mL recombinant human interleukin-6 – Cell supernatants were then collected and stored at –20°C for Western blotting.

5.K. *4-2: kRT-PCR Quantification of Gene Expression*

The protocol for RT-PCR was developed by Arul Jayaraman and grows from the Access RT-PCR kit from Promega.

Materials:
Access RT-PCR kit (Promega)
LightCycler Optimizer Kit (Idaho Technologies)
AmpliTAQ DNA Polymerase (Roche)

Notes:
1. RNA was isolated using the ClonTech NucleoSpin RNA II kit as well as the Qiagen RNeasy kit with comparable results. For confidence in removing all of the genomic DNA contamination, the NucleoSpin kit has a step where genomic DNA is cleaved by DNase I. However, the vortex shearing step of the Qiagen method appears adequate for most RT-PCR applications.

2. It is important to use the proper amount of RNA template in the RT reaction. Ideally, the threshold cycle on the LightCycler for the 18S control gene should be around 7 and no fewer than 5. The gene of interest should have a threshold cycle number of less than 30. The cell number required to recover this quantity of RNA should be established prior to commencing with full-scale experiments.

3. RNase free solutions, tips, and tubes should be used for RT-PCR preparation.

4. Prior to RT, RNA templates should be in water and stored at -80°C. Templates should be used within 2 weeks of RNA isolation to avoid RNase degradation problems.

5. All reagents should be kept on ice during reaction preparations. RNA templates should be stored at -80°C and thawed on ice. They should be returned to -80°C as soon as reactions are prepared.

6. AmpliTaq polymerase should be diluted in Idaho Technology enzyme diluent prior to use in PCR reactions. 1 µL of enzyme is added to 11.5 µL of diluent.

Procedure:
Reverse Transcription (RT)
1. Set up the reaction adding the reagents in the following order (amounts for a 15 µL reaction and can be scaled as needed):

Nuclease-Free Water:	9.3-X µL
AMV/Tfl buffer:	3.0 µL
dNTPs, 10 µM concentration:	0.3 µL
Mg_2SO_4:	0.6 µL
Lower Primer, 10 µM concentration:	1.5 µL
Template:	X µL

RT Enzyme:	0.3 µL

Note: Where possible, a master mix should be made. Master mixes contain all of the reagents with the exception of the primer and/or template depending on whether one gene or multiple genes are being run.

2. Mix the tubes gently, spin down, and incubate for 45 minutes at 48°C.

3. To inactivate the RT, heat the reaction to 94°C for 2 minutes. Return the reactions to 4°C for immediate use or store at -20°C for PCR at a later time.

Polymerase Chain Reaction (PCR) (All reagents are specifically those provided by Idaho Tech.)

4. Thaw SYBR Gold stock solution and prepare a 1:6000 dilution.

5. Set up the reaction adding the reagents in the following order (amounts for a 10 µL reaction, maximum for the LightCycler cuvettes):

Nuclease-Free Water:	4-X µL
$MgCl_2$ Buffer:	1.0 µL
dNTPs, 2 µM concentration:	1.0 µL
Upper Primer, 10 µM concentration:	1.0 µL
Lower Primer, 10 µM concentration:	1.0 µL
Template:	X µL
Diluted AmpliTaq Polymerase (see Note):	1.0 µL
SYBR Gold (1:6000):	1.0 µL

Note: Where possible, a master mix should be made. Master mixes contain all of the reagents with the exception of the primers and/or template depending on whether one gene or multiple genes are being run.

6. Mix well, spin down, and pipet 5-10 µL of reaction mixture into a LightCycler cuvette.

7. Spin briefly at maximum to collect reaction in bottom of reaction cuvette. Adaptors are available from Idaho Technology to allow the cuvettes to fit into a standard tabletop microcentrifuge.

8. CAREFULLY seal reaction cuvettes with provided stoppers. Cuvette sealers should be angled directly into the cuvettes. Any sideways motion will likely snap the cuvettes. Sealing is important to ensure that the reaction mixture doesn't bubble up and boil away during PCR cycling.

9. Load cuvettes into LightCycler in a consecutive stretch of wells. Two wells to either side of the sample tubes should be blocked from light by tape or the blanks provided by Idaho Tech.

10. Start LightCycler control software, ensuring that the switch on the back of the LightCycler is in the on position.

11. In the software, choose user and click on LightCycler button.

12. Select appropriate programs, number of cycles (30-40), and the appropriate annealing temperature for the primer pair.

13. Click unlock at least twice. Move carousel until first sample tube is just to the right of the arrow.

14. Click load, select the appropriate storage directory and filename, and enter the number of samples being run.

15. In the software, label each of the samples. Click done.

16. After double-checking that all of the programs/parameters are set correctly, click run/stop.

Data Analysis

17. Exit the LightCycler program and click on Run Profile.

18. Ensure that the user is set properly and locate the filename for the desired run.

19. Using the shift key, select all of the sample profiles and, by visual inspection, make sure they look correct.

20. Click exit and enter melting curves.

21. Locate the file and select all correct (as determined from run profile) profiles. Ensure that the peaks are single, sharp, and at the right temperature. Adjust the number of averaged points to ~10 to verify that the peaks are correct.

22. Click exit and enter quantitation.

23. Locate the file and select all of the correct samples.

24. Click set noise band and adjust level as low as possible while maintaining log-linear behavior in the lower graph. The scale of the upper graph can be adjusted to improve inspection of noise level. Record the threshold fluorescence value. Set noise band back to 0.

25. Click save and provide the proper storage location/filename.

26. Open the saved QNT file using Microsoft Excel.

27. In columns D-H, enter the following (Capital letters B-H refer to column headings):

D: "=10^CX", where X is the row number
E: "=DX-DY", where X is the row number and Y is X-1
F: "=T-DY", where T is the threshold fluorescence as measured in step 24
G: "=FX/EX"
H: "=GX+BY", this is the desired quantity.

Note: The calculations in columns E-H serve to provide the "actual" threshold cycle number by linearly interpolating between the points that bridge the threshold value. For simplicity, these equations need only be done for the row corresponding to the row in column D that first exceeds the value of the threshold.

28. Enter the column H values for the 18S control and the gene of interest for a treated and control sample into the following formulae to get the normalized ratio of the quantity of RNA in the treated samples to the quantity of RNA in the control samples (all efficiencies, ε, are assumed to be 1):

$$\overline{R}_{\text{gene, treat}} = \frac{\left(1+\varepsilon_{18S}\right)^{n_{18S,\text{treat}}}}{\left(1+\varepsilon_{gene}\right)^{n_{\text{gene,treat}}}}$$

$$\overline{R}_{\text{gene, control}} = \frac{\left(1+\varepsilon_{18S}\right)^{n_{18S,\text{control}}}}{\left(1+\varepsilon_{gene}\right)^{n_{\text{gene,control}}}}$$

$$f = \frac{\overline{R}_{\text{gene, treat}}}{\overline{R}_{\text{gene, control}}}$$

where: $\overline{R}_{\text{gene}}$ is the normalized quantity of RNA in the treatment or control sample
n is the threshold cycle number as obtained from column H of the worksheet for the gene of interest and the control gene, 18S rRNA
f is the fold-change of the normalized quantity of the gene of interest in the treated sample relative to the normalized quantity in the control (untreated) sample.

A sample spreadsheet containing the calculations described above is shown below.

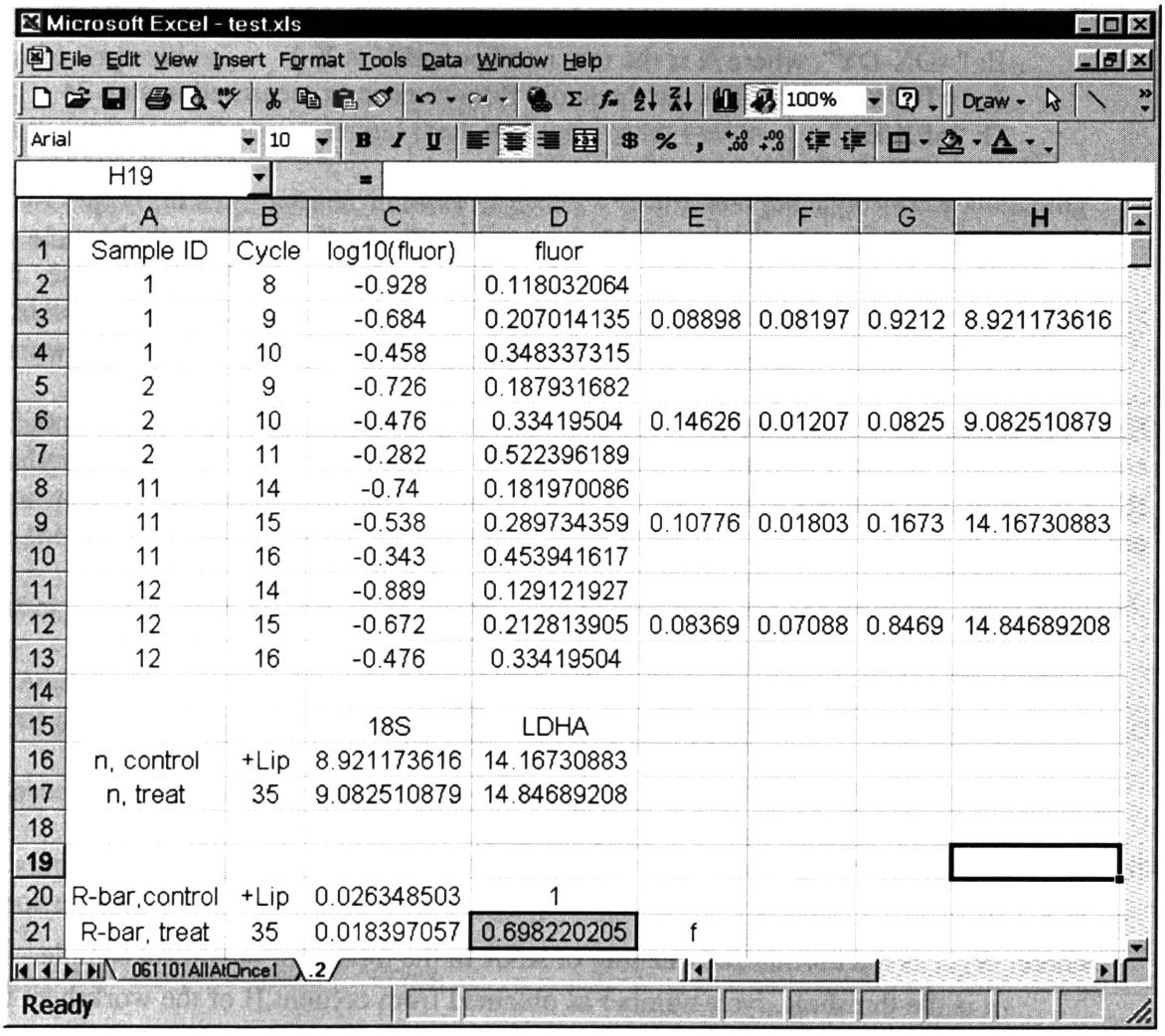

Microsoft Excel - test.xls

File Edit View Insert Format Tools Data Window Help

H19

	A	B	C	D	E	F	G	H
1	Sample ID	Cycle	log10(fluor)	fluor				
2	1	8	-0.928	0.118032064				
3	1	9	-0.684	0.207014135	0.08898	0.08197	0.9212	8.921173616
4	1	10	-0.458	0.348337315				
5	2	9	-0.726	0.187931682				
6	2	10	-0.476	0.33419504	0.14626	0.01207	0.0825	9.082510879
7	2	11	-0.282	0.522396189				
8	11	14	-0.74	0.181970086				
9	11	15	-0.538	0.289734359	0.10776	0.01803	0.1673	14.16730883
10	11	16	-0.343	0.453941617				
11	12	14	-0.889	0.129121927				
12	12	15	-0.672	0.212813905	0.08369	0.07088	0.8469	14.84689208
13	12	16	-0.476	0.33419504				
14								
15			18S	LDHA				
16	n, control	+Lip	8.921173616	14.16730883				
17	n, treat	35	9.082510879	14.84689208				
18								
19								
20	R-bar,control	+Lip	0.026348503	1				
21	R-bar, treat	35	0.018397057	0.698220205	f			

061101AllAtOnce1 .2

Ready

Many of the cycle numbers and fluorescence values have been deleted for clarity. The threshold fluorescence for these samples was found to be 0.2, a typical value.

5.L. *4-3: LDH assay protocol: cell lysis*

The protocol for lysing cells was developed in concert with Avi Robinson and is detailed below.

Materials needed:

- P1000 Pipet; ~50 Sterile Blue Tips; 5 or 10 ml serological pipet
- Timer
- Two Eppendorf tube racks; 72 1.5 ml Eppendorf Tubes
- A microcentrifuge at 4C with the head for 1.5-ml tubes inserted (try to change the head before you start, if possible)
- Lysis Buffer (0.5% NP40, 1mM $MgCl_2$, 1XPBS); PBS
- A container with ice to hold the plate (using the cover of a box of blue tips will allow you to keep the plate on ice as you work with it).

Protocol:

1) Label and organize the tubes. You will need 24 tubes for the collected media, 24 for the cell pellet, and 24 for the lysate. Spread out the 24 for the media in one rack (your working rack); store the other 48 in the second rack (your storage rack).
2) Place the PBS in the water bath.
3) Set up your hood with your working materials, including an aspirator flask.
4) Collect your ice and place it in the hood (you will want to do this as late as possible so that the ice will not melt).
5) [Bring plate to hood.] Collect media into the Eppendorf tubes using a P1000 pipet.
6) Wash cells with ~ 0.5 ml PBS per well. Aspirate.
7) Pipet ~13-14 ml of the lysis buffer into a 15 ml Falcon tube.
8) Place plate on ice.
9) Start timer.
10) At T=20 seconds, add 0.5 ml of lysis buffer to the first well using a P1000 pipet. Continue adding lysis buffer to the first 12 wells, at 20 second intervals. One should finish with the twelfth well at T= 4 minutes. Cover the plate and rest it flat on the ice for a few minutes.
11) At T= 8 minutes 20 seconds, begin adding lysis buffer to the second set of twelve wells, again at 20 second intervals, until T=12 minutes.
12) While you are waiting, spread out the 24 tubes for the cell pellets on the working rack. Also, make sure that the ice isn't melting too quickly. You may need to pour off some water into the sink so that the water will not seep into the plate.
13) At T=20 minutes 20 seconds, collect the lysis buffer + cells from the first 12 wells, using a P1000 pipet, at 20 second intervals. Cover the plate again and leave it on the ice.
14) Take the tubes to the cold room and centrifuge for 5 minutes at 1500 – 2000 rpm.
15) Return to the hood. The timer should read 26-27 minutes.
16) At T = 28 minutes 20 seconds collect the lysis buffer + cells from the second set of 12 wells, until T= 32 minutes.
17) Return to the cold room. Remove the first 12 tubes from the centrifuge and replace them with the second set; centrifuge for 5 minutes at 1500 – 2000 rpm.

18) Decant the lysates from the centrifuged cells into the Eppendorf tubes labeled "lysates" without disturbing the pellet. It is not necessary to get all of the supernatant, since we use only 10 µl per test; it is more important not to decant the pellet together with the supernatant.
19) Store samples for further testing.

5.M. 4-4: LDH assay protocol: assay execution

The protocol for performing the LDH activity assay in a 96-well format was developed in concert with Avi Robinson and is detailed below.

Materials needed:
1 Eppendorf Rack
30 1.5 ml Eppendorf Tubes
Foam "rack" for placing Eppendorf tubes into water bath
Pipets and pipet tips of all sizes
Timer
96 well plate
Sigma Pyruvate Substrate (Lot:068H6067; store at 4C)
Sigma Color Reagent (Lot:058H6094; store at 4C)
Sigma NADH-containing vial (Lot: 127H6049; store dark and desiccated at RT)
30-35 ml 0.4M NaOH

Protocol:

1) Label the 24 Eppendorf tubes and set them up in the foam rack.
2) Pipet ~ 1.0 ml of pyruvate substrate into each of 3 NADH-containing vials. Mix gently.
3) Pipet the 1.0 ml from two of the vials into the third (ensures uniform concentrations).
4) Pipet 100 µl from the vial into each of 24 Eppendorf tubes.
5) Incubate the tubes in a 37°C bath for a few minutes. Also incubate the remaining substrate that is in the vial, so that you can quickly make an extra sample if necessary.
   [5) If necessary, thaw the lysate samples.]
6) Retrieve the tubes from the water bath and return them to the workbench.
7) Start timer.
8) At T = 30 seconds, pipet 10 µl of sample into the first 1.5ml tube. Proceed to do this over 30 second intervals for all 24 samples, until T=12 minutes.
9) Return the tubes to the water bath.
10) Prepare standards at the following dilutions:

1. 100 µl pyruvate substrate,	10 µl H2O
2. 80	30
3. 60	50
4. 40	70
5. 20	90
6. 10	100

11) Return the lysate samples to the freezer and the pyruvate substrate to the refrigerator. Retrieve the coloring reagent from the refrigerator.
12) At T ~ 26.5-27 minutes, retrieve the sample tubes from water bath.
13) At T = 28 minutes 20 seconds, add 100 µl of coloring reagent to the first standard. Continue to add to the 6 standards, at 20 second intervals, until T = 30 minutes. Then add to the samples, at 30 second intervals, starting at 30 minutes 30 seconds, until T= 42 minutes. [One

thereby adds the coloring reagent exactly 30 minutes after mixing the sample and the substrate.]

14) At T = 48 minutes 20 seconds add 1 ml 0.4 M NaOH to the first standard, and subsequently to the rest of the standards at 20 second intervals and to the samples at 30 second intervals, until T = 1 hour 2 minutes. Mix well by inversion. [One thus adds the NaOH exactly 20 minutes after the addition of the color reagent.]
15) Transfer the samples to the plate for OD reading. Pipet 100ul / well of each sample into three wells (triplicate). One will use 90 of the 96 wells (6 std., 24 samples).
16) Set up the plate reader and read the plate.
    a) Make sure the plate reader machine is on.
    b) Open Softmax (Apple, Applications, Softmax Alias)
    c) Go to Setup, Instrument. The wavelength should be Endpoint L1, 450 nm.
    d) Go to Setup, Template, and set up the template. The standards have the following concentrations: 1. 0
        2. 280
        3. 640
        4. 1040
        5. 1530
        6. 2000
    e) Go to Control, Reader Status to make sure the computer and the plate reader are connected.
    f) Go to Control, Read Plate to read the plate.
17) Analyze the data.
    a) Fit the standard curve to a quadratic.
    b) Save the data to disk before exiting.[!!]

6. Bibliography

1. Holkeri, H. 2000, http://www.un.org/News/Press/docs/2000/20001129.gasm222.doc.html.
2. *American Cancer Society.* 1997, http://www.cancer.org/statistics/96cff/facts.html.
3. *Inflammatory Bowel Disease.* 2000, http://familydoctor.org/handouts/252.html.
4. Cerra, F.B., M. West, G. Keller, J. Mazuski, and R.L. Simmons, *Hypermetabolism/organ failure: the role of the activated macrophage as a metabolic regulator.* Prog Clin Biol Res, 1988. **264**: p. 27-42.
5. Beal, A.L. and F.B. Cerra, *Multiple organ failure syndrome in the 1990s. Systemic inflammatory response and organ dysfunction.* Jama, 1994. **271**(3): p. 226-33.
6. *Isis Pharmaceuticals, Inc., Form 10-K, December 31, 1998.* 2001, http://www.isip.com/10K_123198/10K.htm.
7. Lander, E.S., *et al.*, *Initial sequencing and analysis of the human genome. International Human Genome Sequencing Consortium.* Nature, 2001. **409**(6822): p. 860-921.
8. Roth, C.M. and M.L. Yarmush, *Nucleic Acid Biotechnology*, in *Annual Review of Biomedical Engineering*, M.L. Yarmush, K.R. Diller, and M. Toner, Editors. 1999, Annual Reviews: Palo Alto, CA. p. 265-297.
9. Zamecnik, P.C. and M.L. Stephenson, *Inhibition of Rous sarcoma virus replication and cell transformation by a specific oligodeoxynucleotide.* Proc Natl Acad Sci U S A, 1978. **75**(1): p. 280-4.
10. Roush, W., *Antisense aims for a renaissance.* Science, 1997. **276**(5316): p. 1192-3.
11. Rawls, R.L., *Optimistic about antisense.* Chemical and Engineering News, 1997. **75**(22): p. 35-39.
12. *Antisense '97: A roundtable on the state of the industry.* Nature Biotechnology, 1997. **15**: p. 519-524.
13. Tomizawa, J.I., T. Itoh, G. Selzer, and T. Som, *Inhibition of ColE1 RNA primer formation by a plasmid-specified small RNA.* Proc Natl Acad Sci USA, 1981. **78**(3): p. 1421-5.
14. Tomizawa, J.I. and T. Itoh, *Plasmid ColE1 incompatibility determined by interaction of RNA I with primer transcript.* Proc Natl Acad Sci USA, 1981. **78**(10): p. 6096-100.
15. Izant, J.G. and H. Weintraub, *Constitutive and conditional suppression of exogenous and endogenous genes by anti-sense RNA.* Science, 1985. **229**(4711): p. 345-52.
16. Walton, S.P., C.M. Roth, and M.L. Yarmush, *Antisense Technology*, in *The Biomedical Engineering Handbook.* 2000, CRC Press LLC: Boca Raton, FL. p. 103-1 - 103-19.
17. Akhtar, S., R. Kole, and R.L. Juliano, *Stability of antisense DNA oligodeoxynucleotide analogs in cellular extracts and sera.* Life Sci, 1991. **49**(24): p. 1793-801.
18. Geselowitz, D.A. and L.M. Neckers, *Bovine serum albumin is a major oligonucleotide-binding protein found on the surface of cultured cells.* Antisense Res Dev, 1995. **5**(3): p. 213-7.
19. Biessen, E.A., H. Vietsch, J. Kuiper, M.K. Bijsterbosch, and T.J. Berkel, *Liver uptake of phosphodiester oligodeoxynucleotides is mediated by scavenger receptors.* Mol Pharmacol, 1998. **53**(2): p. 262-9.

20. Chaudhuri, G., *Scavenger receptor-mediated delivery of antisense mini-exon phosphorothioate oligonucleotide to Leishmania-infected macrophages. Selective and efficient elimination of the parasite.* Biochem Pharmacol, 1997. **53**(3): p. 385-91.
21. Bijsterbosch, M.K., *et al.*, *In vivo fate of phosphorothioate antisense oligodeoxynucleotides: predominant uptake by scavenger receptors on endothelial liver cells.* Nucleic Acids Res, 1997. **25**(16): p. 3290-6.
22. Loke, S.L., *et al.*, *Characterization of oligonucleotide transport into living cells.* Proc Natl Acad Sci U S A, 1989. **86**(10): p. 3474-8.
23. Yakubov, L.A., *et al.*, *Mechanism of oligonucleotide uptake by cells: involvement of specific receptors?* Proc Natl Acad Sci U S A, 1989. **86**(17): p. 6454-8.
24. Shoji, Y., S. Akhtar, A. Periasamy, B. Herman, and R.L. Juliano, *Mechanism of cellular uptake of modified oligodeoxynucleotides containing methylphosphonate linkages.* Nucleic Acids Res, 1991. **19**(20): p. 5543-50.
25. Thierry, A.R. and A. Dritschilo, *Intracellular availability of unmodified, phosphorothioated and liposomally encapsulated oligodeoxynucleotides for antisense activity.* Nucleic Acids Res, 1992. **20**(21): p. 5691-8.
26. Tam, R.C., *et al.*, *Biological availability and nuclease resistance extend the in vitro activity of a phosphorothioate-3'hydroxypropylamine oligonucleotide.* Nucleic Acids Res, 1994. **22**(6): p. 977-86.
27. Marcusson, E.G., B. Bhat, M. Manoharan, C.F. Bennett, and N.M. Dean, *Phosphorothioate oligodeoxyribonucleotides dissociate from cationic lipids before entering the nucleus.* Nucleic Acids Res, 1998. **26**(8): p. 2016-23.
28. Stein, C.A., *Two problems in antisense biotechnology: in vitro delivery and the design of antisense experiments.* Biochim Biophys Acta, 1999. **1489**(1): p. 45-52.
29. Wagner, R.W., M.D. Matteucci, D. Grant, T. Huang, and B.C. Froehler, *Potent and selective inhibition of gene expression by an antisense heptanucleotide.* Nat Biotechnol, 1996. **14**(7): p. 840-4.
30. Crooke, S.T., *Molecular mechanisms of action of antisense drugs.* Biochim Biophys Acta, 1999. **1489**(1): p. 31-44.
31. Monia, B.P., *et al.*, *Evaluation of 2'-modified oligonucleotides containing 2'-deoxy gaps as antisense inhibitors of gene expression.* J Biol Chem, 1993. **268**(19): p. 14514-22.
32. de Diesbach, P., *et al.*, *Identification, purification and partial characterisation of an oligonucleotide receptor in membranes of HepG2 cells.* Nucleic Acids Res, 2000. **28**(4): p. 868-74.
33. Hawley, P. and I. Gibson, *Interaction of oligodeoxynucleotides with mammalian cells.* Antisense Nucleic Acid Drug Dev, 1996. **6**(3): p. 185-95.
34. Caselmann, W.H., S. Eisenhardt, and M. Alt, *Synthetic antisense oligodeoxynucleotides as potential drugs against hepatitis C.* Intervirology, 1997. **40**(5-6): p. 394-9.
35. Dokka, S. and Y. Rojanasakul, *Novel non-endocytic delivery of antisense oligonucleotides.* Adv Drug Deliv Rev, 2000. **44**(1): p. 35-49.
36. Bergan, R., Y. Connell, B. Fahmy, and L. Neckers, *Electroporation enhances c-myc antisense oligodeoxynucleotide efficacy.* Nucleic Acids Res, 1993. **21**(15): p. 3567-73.
37. Tonkinson, J.L. and C.A. Stein, *Patterns of intracellular compartmentalization, trafficking and acidification of 5'-fluorescein labeled phosphodiester and*

phosphorothioate oligodeoxynucleotides in HL60 cells. Nucleic Acids Res, 1994. **22**(20): p. 4268-75.
38. Geselowitz, D.A. and L.M. Neckers, *Analysis of oligonucleotide binding, internalization, and intracellular trafficking utilizing a novel radiolabeled crosslinker.* Antisense Res Dev, 1992. **2**(1): p. 17-25.
39. Li, B., J.A. Hughes, and M.I. Phillips, *Uptake and efflux of intact antisense phosphorothioate deoxyoligonucleotide directed against angiotensin receptors in bovine adrenal cells.* Neurochem Int, 1997. **31**(3): p. 393-403.
40. Matteucci, M., *Oligonucleotide analogues: an overview.* Ciba Found Symp, 1997. **209**(2): p. 5-14; discussion 14-8.
41. SantaLucia, J., *JSLHOME.*, http://jsl1.chem.wayne.edu/.
42. Walder, R.Y. and J.A. Walder, *Role of RNase H in hybrid-arrested translation by antisense oligonucleotides.* Proc Natl Acad Sci U S A, 1988. **85**(14): p. 5011-5.
43. Dagle, J.M., D.L. Weeks, and J.A. Walder, *Pathways of degradation and mechanism of action of antisense oligonucleotides in Xenopus laevis embryos.* Antisense Res Dev, 1991. **1**(1): p. 11-20.
44. Schiedlmeier, B., *et al.*, *Nuclear transformation of Volvox carteri.* Proc Natl Acad Sci USA, 1994. **91**(11): p. 5080-4.
45. Lesh, R.E., A.P. Somlyo, G.K. Owens, and A.V. Somlyo, *Reversible permeabilization. A novel technique for the intracellular introduction of antisense oligodeoxynucleotides into intact smooth muscle.* Circ Res, 1995. **77**(2): p. 220-30.
46. Spiller, D.G. and D.M. Tidd, *Nuclear delivery of antisense oligodeoxynucleotides through reversible permeabilization of human leukemia cells with streptolysin O.* Antisense Res Dev, 1995. **5**(1): p. 13-21.
47. Zhao, Q., *et al.*, *Comparison of cellular binding and uptake of antisense phosphodiester, phosphorothioate, and mixed phosphorothioate and methylphosphonate oligonucleotides.* Antisense Res Dev, 1993. **3**(1): p. 53-66.
48. Boutorine, A.S. and E.V. Kostina, *Reversible covalent attachment of cholesterol to oligodeoxyribonucleotides for studies of the mechanisms of their penetration into eucaryotic cells.* Biochimie, 1993. **75**(1-2): p. 35-41.
49. Alahari, S.K., *et al.*, *Inhibition of expression of the multidrug resistance-associated P-glycoprotein of by phosphorothioate and 5' cholesterol-conjugated phosphorothioate antisense oligonucleotides.* Mol Pharmacol, 1996. **50**(4): p. 808-19.
50. Krieg, A.M., *et al.*, *Modification of antisense phosphodiester oligodeoxynucleotides by a 5' cholesteryl moiety increases cellular association and improves efficacy.* Proc Natl Acad Sci U S A, 1993. **90**(3): p. 1048-52.
51. Degols, G., J.P. Leonetti, M. Benkirane, C. Devaux, and B. Lebleu, *Poly(L-lysine)-conjugated oligonucleotides promote sequence-specific inhibition of acute HIV-1 infection.* Antisense Res Dev, 1992. **2**(4): p. 293-301.
52. Leonetti, J.P., G. Degols, J.P. Clarenc, N. Mechti, and B. Lebleu, *Cell delivery and mechanisms of action of antisense oligonucleotides.* Prog Nucleic Acid Res Mol Biol, 1993. **44**: p. 143-66.
53. Lu, X.M., *et al.*, *Antisense DNA delivery in vivo: liver targeting by receptor-mediated uptake.* J Nucl Med, 1994. **35**(2): p. 269-75.

54. Citro, G., *et al.*, *Inhibition of leukemia cell proliferation by receptor-mediated uptake of c-myb antisense oligodeoxynucleotides.* Proc Natl Acad Sci U S A, 1992. **89**(15): p. 7031-5.
55. Deshpande, D., D. Toledo-Velasquez, D. Thakkar, W. Liang, and Y. Rojanasakul, *Enhanced cellular uptake of oligonucleotides by EGF receptor-mediated endocytosis in A549 cells.* Pharm Res, 1996. **13**(1): p. 57-61.
56. Bonfils, E., *et al.*, *Drug targeting: synthesis and endocytosis of oligonucleotide-neoglycoprotein conjugates.* Nucleic Acids Res, 1992. **20**(17): p. 4621-9.
57. Wu, G.Y. and C.H. Wu, *Specific inhibition of hepatitis B viral gene expression in vitro by targeted antisense oligonucleotides.* J Biol Chem, 1992. **267**(18): p. 12436-9.
58. Roth, C.M., *et al.*, *Targeted antisense modulation of inflammatory cytokine receptors.* Biotechnology and Bioengineering, 1997. **55**: p. 72-81.
59. Basu, S. and E. Wickstrom, *Synthesis and characterization of a peptide nucleic acid conjugated to a D-peptide analog of insulin-like growth factor 1 for increased cellular uptake.* Bioconjug Chem, 1997. **8**(4): p. 481-8.
60. Rajur, S.B., C.M. Roth, J.R. Morgan, and M.L. Yarmush, *Covalent protein-oligonucleotide conjugates for efficient delivery of antisense molecules.* Bioconjug Chem, 1997. **8**(6): p. 935-40.
61. Reinis, M., M. Damkova, and E. Korec, *Receptor-mediated transport of oligodeoxynucleotides into hepatic cells.* J Virol Methods, 1993. **42**(1): p. 99-105.
62. Probst, J.C., *Antisense oligodeoxynucleotide and ribozyme design.* Methods, 2000. **22**(3): p. 271-81.
63. Dokka, S., D. Toledo-Velasquez, X. Shi, L. Wang, and Y. Rojanasakul, *Cellular delivery of oligonucleotides by synthetic import peptide carrier.* Pharm Res, 1997. **14**(12): p. 1759-64.
64. Subramanian, A., P. Ranganathan, and S.L. Diamond, *Nuclear targeting peptide scaffolds for lipofection of nondividing mammalian cells.* Nat Biotechnol, 1999. **17**(9): p. 873-7.
65. Zelphati, O. and F.C. Szoka, Jr., *Mechanism of oligonucleotide release from cationic liposomes.* Proc Natl Acad Sci USA, 1996. **93**(21): p. 11493-8.
66. Ryser, J.-P. and W.-C. Shen, *Drug-poly(lysine) conjugates: their potential for chemotherapy and for the study of endocytosis*, in *Targeting of drugs with synthetic systems*, G. Gregoriadis, J. Senior, and G. Poste, Editors. 1986, Plenum Press Corporation: New York. p. 103-121.
67. Wu-Pong, S., *The role of multivalent cations in oligonucleotide cellular uptake.* Biochem Mol Biol Int, 1996. **39**(3): p. 511-9.
68. Benimetskaya, L., *et al.*, *Mac-1 (CD11b/CD18) is an oligodeoxynucleotide-binding protein.* Nat Med, 1997. **3**(4): p. 414-20.
69. Vlassov, V.V., L.A. Balakireva, and L.A. Yakubov, *Transport of oligonucleotides across natural and model membranes.* Biochim Biophys Acta, 1994. **1197**(2): p. 95-108.
70. Bennett, C.F., T.P. Condon, S. Grimm, H. Chan, and M.Y. Chiang, *Inhibition of endothelial cell adhesion molecule expression with antisense oligonucleotides.* J Immunol, 1994. **152**(7): p. 3530-40.
71. Lavigne, C. and A.R. Thierry, *Enhanced antisense inhibition of human immunodeficiency virus type 1 in cell cultures by DLS delivery system.* Biochem Biophys Res Commun, 1997. **237**(3): p. 566-71.

72. Leonetti, J.P., P. Machy, G. Degols, B. Lebleu, and L. Leserman, *Antibody-targeted liposomes containing oligodeoxyribonucleotides complementary to viral RNA selectively inhibit viral replication.* Proc Natl Acad Sci U S A, 1990. **87**(7): p. 2448-51.
73. Lodish, H., *et al.*, *Molecular Cell Biology.* 3rd ed. 1995, New York: Scientific American Books, Inc.
74. Zohlnhofer, D., *et al.*, *The hepatic interleukin-6 receptor. Down-regulation of the interleukin- 6 binding subunit (gp80) by its ligand.* FEBS Lett, 1992. **306**(2-3): p. 219-22.
75. Huang, G.M., J. Farkas, and L. Hood, *High-throughput cDNA screening utilizing a low order neural network filter.* Biotechniques, 1996. **21**(6): p. 1110-4.
76. Volz, B., G. Orberger, S. Porwoll, H.P. Hauri, and R. Tauber, *Selective reentry of recycling cell surface glycoproteins to the biosynthetic pathway in human hepatocarcinoma HepG2 cells.* J Cell Biol, 1995. **130**(3): p. 537-51.
77. Ghosh, M.K., K. Ghosh, O. Dahl, and J.S. Cohen, *Evaluation of some properties of a phosphorodithioate oligodeoxyribonucleotide for antisense application.* Nucleic Acids Res, 1993. **21**(24): p. 5761-6.
78. Manoharan, M., *2'-carbohydrate modifications in antisense oligonucleotide therapy: importance of conformation, configuration and conjugation.* Biochim Biophys Acta, 1999. **1489**(1): p. 117-30.
79. Lesnik, E.A., *et al.*, *Oligodeoxynucleotides containing 2'-O-modified adenosine: synthesis and effects on stability of DNA:RNA duplexes.* Biochemistry, 1993. **32**(30): p. 7832-8.
80. Monia, B.P., J.F. Johnston, H. Sasmor, and L.L. Cummins, *Nuclease resistance and antisense activity of modified oligonucleotides targeted to Ha-ras.* J Biol Chem, 1996. **271**(24): p. 14533-40.
81. McKay, R.A., *et al.*, *Enhanced activity of an antisense oligonucleotide targeting murine protein kinase C-alpha by the incorporation of 2'-O-propyl modifications.* Nucleic Acids Res, 1996. **24**(3): p. 411-7.
82. Nagel, K.M., S.G. Holstad, and K.E. Isenberg, *Oligonucleotide pharmacotherapy: an antigene strategy.* Pharmacotherapy, 1993. **13**(3): p. 177-88.
83. Iribarren, A.M., D.O. Cicero, and P.J. Neuner, *Resistance to degradation by nucleases of (2'S)-2'-deoxy-2'-C- methyloligonucleotides, novel potential antisense probes.* Antisense Res Dev, 1994. **4**(2): p. 95-8.
84. Agrawal, S., J. Temsamani, W. Galbraith, and J. Tang, *Pharmacokinetics of antisense oligonucleotides.* Clin Pharmacokinet, 1995. **28**(1): p. 7-16.
85. Milligan, J.F., M.D. Matteucci, and J.C. Martin, *Current concepts in antisense drug design.* J Med Chem, 1993. **36**(14): p. 1923-37.
86. Crooke, S.T., *et al.*, *Pharmacokinetic properties of several novel oligonucleotide analogs in mice.* J Pharmacol Exp Ther, 1996. **277**(2): p. 923-37.
87. Geary, R.S., *et al.*, *Pharmacokinetic Properties of 2'-O-(2-Methoxyethyl)-Modified Oligonucleotide Analogs in Rats.* J Pharmacol Exp Ther, 2001. **296**(3): p. 890-897.
88. Galbraith, W.M., W.C. Hobson, P.C. Giclas, P.J. Schechter, and S. Agrawal, *Complement activation and hemodynamic changes following intravenous administration of phosphorothioate oligonucleotides in the monkey.* Antisense Res Dev, 1994. **4**(3): p. 201-6.

89. Peyrottes, S., J.J. Vasseur, J.L. Imbach, and B. Rayner, *Oligodeoxynucleoside phosphoramidates (P-NH2): synthesis and thermal stability of duplexes with DNA and RNA targets.* Nucleic Acids Res, 1996. **24**(10): p. 1841-8.
90. Heidenreich, O., S. Gryaznov, and M. Nerenberg, *RNase H-independent antisense activity of oligonucleotide N3 '--> P5 ' phosphoramidates.* Nucleic Acids Res, 1997. **25**(4): p. 776-80.
91. Skorski, T., D. Perrotti, M. Nieborowska-Skorska, S. Gryaznov, and B. Calabretta, *Antileukemia effect of c-myc N3'-->P5' phosphoramidate antisense oligonucleotides in vivo.* Proc Natl Acad Sci U S A, 1997. **94**(8): p. 3966-71.
92. Hawley, P., J.S. Nelson, K.L. Fearon, G. Zon, and I. Gibson, *Comparison of binding of N3'-->P5' phosphoramidate and phosphorothioate oligonucleotides to cell surface proteins of cultured cells.* Antisense Nucleic Acid Drug Dev, 1999. **9**(1): p. 61-9.
93. Gryaznov, S.M., *Oligonucleotide N3'-->P5' phosphoramidates as potential therapeutic agents.* Biochim Biophys Acta, 1999. **1489**(1): p. 131-40.
94. Gryaznov, S., *et al.*, *Oligonucleotide N3'-->P5' phosphoramidates as antisense agents.* Nucleic Acids Res, 1996. **24**(8): p. 1508-14.
95. Boulme, F., *et al.*, *Modified (PNA, 2'-O-methyl and phosphoramidate) anti-TAR antisense oligonucleotides as strong and specific inhibitors of in vitro HIV-1 reverse transcription.* Nucleic Acids Res, 1998. **26**(23): p. 5492-500.
96. Leydier, C., *et al.*, *4'-Thio-RNA: synthesis of mixed base 4'-thio-oligoribonucleotides, nuclease resistance, and base pairing properties with complementary single and double strand.* Antisense Res Dev, 1995. **5**(3): p. 167-74.
97. Kawasaki, A.M., *et al.*, *Uniformly modified 2'-deoxy-2'-fluoro phosphorothioate oligonucleotides as nuclease-resistant antisense compounds with high affinity and specificity for RNA targets.* J Med Chem, 1993. **36**(7): p. 831-41.
98. Boiziau, C., B. Larrouy, B.S. Sproat, and J.J. Toulme, *Antisense 2'-O-alkyl oligoribonucleotides are efficient inhibitors of reverse transcription.* Nucleic Acids Res, 1995. **23**(1): p. 64-71.
99. Johansson, H.E., G.J. Belsham, B.S. Sproat, and M.W. Hentze, *Target-specific arrest of mRNA translation by antisense 2'-O- alkyloligoribonucleotides.* Nucleic Acids Res, 1994. **22**(22): p. 4591-8.
100. Brown-Driver, V., T. Eto, E. Lesnik, K.P. Anderson, and R.C. Hanecak, *Inhibition of translation of hepatitis C virus RNA by 2-modified antisense oligonucleotides.* Antisense Nucleic Acid Drug Dev, 1999. **9**(2): p. 145-54.
101. Prakash, T.P., *et al.*, *2'-O-[2-[N,N-(dialkyl)aminooxy]ethyl]-modified antisense oligonucleotides.* Org Lett, 2000. **2**(25): p. 3995-8.
102. Vickers, T.A., J.R. Wyatt, T. Burckin, C.F. Bennett, and S.M. Freier, *Fully modified 2' MOE oligonucleotides redirect polyadenylation.* Nucleic Acids Res, 2001. **29**(6): p. 1293-1299.
103. Wahlestedt, C., *et al.*, *Potent and nontoxic antisense oligonucleotides containing locked nucleic acids.* Proc Natl Acad Sci U S A, 2000. **97**(10): p. 5633-8.
104. Petersen, M., *et al.*, *The conformations of locked nucleic acids (LNA).* J Mol Recognit, 2000. **13**(1): p. 44-53.

105. Sanghvi, Y.S., *et al.*, *Antisense oligodeoxynucleotides: synthesis, biophysical and biological evaluation of oligodeoxynucleotides containing modified pyrimidines.* Nucleic Acids Res, 1993. **21**(14): p. 3197-203.
106. Pickering, J.G., *et al.*, *Processing of chimeric antisense oligonucleotides by human vascular smooth muscle cells and human atherosclerotic plaque. Implications for antisense therapy of restenosis after angioplasty.* Circulation, 1996. **93**(4): p. 772-80.
107. Maier, M., K. Bleicher, H. Kalthoff, and E. Bayer, *Enzymatic degradation of various antisense oligonucleotides: monitoring and fragment identification by MECC and ES-MS.* Biomed Pept Proteins Nucleic Acids, 1995. **1**(4): p. 235-42.
108. Agrawal, S., *et al.*, *Mixed-backbone oligonucleotides as second generation antisense oligonucleotides: in vitro and in vivo studies.* Proc Natl Acad Sci U S A, 1997. **94**(6): p. 2620-5.
109. Hebb, M.O. and H.A. Robertson, *End-capped antisense oligodeoxynucleotides effectively inhibit gene expression in vivo and offer a low-toxicity alternative to fully modified phosphorothioate oligodeoxynucleotides.* Brain Res Mol Brain Res, 1997. **47**(1-2): p. 223-8.
110. Park, W.S., *et al.*, *Inhibition of HIV-1 replication by a new type of circular dumbbell RNA/DNA chimeric oligonucleotides.* Biochem Biophys Res Commun, 2000. **270**(3): p. 953-60.
111. Summerton, J., *Morpholino antisense oligomers: the case for an RNase H-independent structural type.* Biochim Biophys Acta, 1999. **1489**(1): p. 141-58.
112. Ekker, S.C., *Morphants: a new systematic vertebrate functional genomics approach.* Yeast, 2000. **17**(4): p. 302-306.
113. Arora, V., *et al.*, *c-Myc antisense limits rat liver regeneration and indicates role for c-Myc in regulating cytochrome P-450 3A activity.* J Pharmacol Exp Ther, 2000. **292**(3): p. 921-8.
114. Qin, G., M. Taylor, Y.Y. Ning, P. Iversen, and L. Kobzik, *In vivo evaluation of a morpholino antisense oligomer directed against tumor necrosis factor-alpha.* Antisense Nucleic Acid Drug Dev, 2000. **10**(1): p. 11-6.
115. Jubin, R., *et al.*, *Hepatitis C virus internal ribosome entry site (IRES) stem loop IIId contains a phylogenetically conserved GGG triplet essential for translation and IRES folding.* J Virol, 2000. **74**(22): p. 10430-7.
116. Lacerra, G., *et al.*, *Restoration of hemoglobin A synthesis in erythroid cells from peripheral blood of thalassemic patients.* Proc Natl Acad Sci U S A, 2000. **97**(17): p. 9591-6.
117. Ghosh, C. and P.L. Iversen, *Intracellular delivery strategies for antisense phosphorodiamidate morpholino oligomers.* Antisense Nucleic Acid Drug Dev, 2000. **10**(4): p. 263-74.
118. Schmajuk, G., H. Sierakowska, and R. Kole, *Antisense oligonucleotides with different backbones. Modification of splicing pathways and efficacy of uptake.* J Biol Chem, 1999. **274**(31): p. 21783-9.
119. Nasevicius, A., J. Larson, and S.C. Ekker, *Distinct requirements for zebrafish angiogenesis revealed by a VEGF-A morphant.* Yeast, 2000. **17**(4): p. 294-301.
120. Nasevicius, A. and S.C. Ekker, *Effective targeted gene 'knockdown' in zebrafish.* Nat Genet, 2000. **26**(2): p. 216-20.

121. Shepherd, I.T., C.E. Beattie, and D.W. Raible, *Functional Analysis of Zebrafish GDNF.* Dev Biol, 2001. **231**(2): p. 420-435.
122. Bauer, H., Z. Lele, G.J. Rauch, R. Geisler, and M. Hammerschmidt, *The type I serine/threonine kinase receptor Alk8/Lost-a-fin is required for Bmp2b/7 signal transduction during dorsoventral patterning of the zebrafish embryo.* Development, 2001. **128**(6): p. 849-858.
123. Yang, Z., N. Liu, and S. Lin, *A Zebrafish Forebrain-Specific Zinc Finger Gene Can Induce Ectopic dlx2 and dlx6 Expression.* Dev Biol, 2001. **231**(1): p. 138-148.
124. Howard, E.W., L.A. Newman, D.W. Oleksyn, R.C. Angerer, and L.M. Angerer, *SpKrl: a direct target of (&bgr;)-catenin regulation required for endoderm differentiation in sea urchin embryos.* Development, 2001. **128**(3): p. 365-375.
125. Maran, A., *et al.*, *Blockage of NF-kappa B signaling by selective ablation of an mRNA target by 2-5A antisense chimeras.* Science, 1994. **265**(5173): p. 789-92.
126. Mukai, S., *et al.*, *2-5A antisense telomerase RNA therapy for intracranial malignant gliomas.* Cancer Res, 2000. **60**(16): p. 4461-7.
127. Maran, A., *et al.*, *2',5'-Oligoadenylate-antisense chimeras cause RNase L to selectively degrade bcr/abl mRNA in chronic myelogenous leukemia cells.* Blood, 1998. **92**(11): p. 4336-43.
128. Kushner, D.M., *et al.*, *2-5A antisense directed against telomerase RNA produces apoptosis in ovarian cancer cells.* Gynecol Oncol, 2000. **76**(2): p. 183-92.
129. Verheijen, J.C., *et al.*, *Synthesis and RNAse L binding and activation of a 2-5A-(5')-DNA-(3')-PNA chimera, a novel potential antisense molecule.* Nucleosides Nucleotides Nucleic Acids, 2000. **19**(10-12): p. 1821-30.
130. Verheijen, J.C., *et al.*, *2,5-oligoadenylate-peptide nucleic acids (2-5A-PNAs) activate RNase L.* Bioorg Med Chem, 1999. **7**(3): p. 449-55.
131. Baker, B.F. and B.P. Monia, *Novel mechanisms for antisense-mediated regulation of gene expression.* Biochim Biophys Acta, 1999. **1489**(1): p. 3-18.
132. Ma, M., *et al.*, *Intracellular mRNA cleavage induced through activation of RNase P by nuclease-resistant external guide sequences.* Nat Biotechnol, 2000. **18**(1): p. 58-61.
133. Stein, C.A., *Is irrelevant cleavage the price of antisense efficacy?* Pharmacol Ther, 2000. **85**(3): p. 231-6.
134. Helene, C. and J.J. Toulme, *Specific regulation of gene expression by antisense, sense and antigene nucleic acids.* Biochim. Biophys. Acta, 1990. **1049**: p. 99-125.
135. Cook, P.D., *Medicinal chemistry of antisense oligonucleotides--future opportunities.* Anticancer Drug Des, 1991. **6**(6): p. 585-607.
136. Uhlmann, E. and A. Peyman, *Antisense oligonucleotides: A new therapeutic principle.* Chem. Rev, 1990. **90**: p. 544-584.
137. Verma, S. and F. Eckstein, *Modified oligonucleotides: synthesis and strategy for users.* Annu Rev Biochem, 1998. **67**: p. 99-134.
138. Svinarchuk, F.P., D.A. Konevetz, O.A. Pliasunova, A.G. Pokrovsky, and V.V. Vlassov, *Inhibition of HIV proliferation in MT-4 cells by antisense oligonucleotide conjugated to lipophilic groups.* Biochimie, 1993. **75**(1-2): p. 49-54.
139. Letsinger, R.L., G.R. Zhang, D.K. Sun, T. Ikeuchi, and P.S. Sarin, *Cholesteryl-conjugated oligonucleotides: synthesis, properties, and activity as inhibitors of*

replication of human immunodeficiency virus in cell culture. Proc Natl Acad Sci U S A, 1989. **86**(17): p. 6553-6.
140. de Smidt, P.C., T. Le Doan, S. de Falco, and T.J. van Berkel, *Association of antisense oligonucleotides with lipoproteins prolongs the plasma half-life and modifies the tissue distribution.* Nucleic Acids Res, 1991. **19**(17): p. 4695-700.
141. Reed, M.W., D. Fraga, D.E. Schwartz, J. Scholler, and R.D. Hinrichsen, *Synthesis and evaluation of nuclear targeting peptide-antisense oligodeoxynucleotide conjugates.* Bioconjug Chem, 1995. **6**(1): p. 101-8.
142. Woolf, T.M., D.A. Melton, and C.G. Jennings, *Specificity of antisense oligonucleotides in vivo.* Proc Natl Acad Sci U S A, 1992. **89**(16): p. 7305-9.
143. Altschul, S.F., *et al.*, *Gapped BLAST and PSI-BLAST: a new generation of protein database search programs.* Nucleic Acids Res, 1997. **25**(17): p. 3389-402.
144. Smith, L., K.B. Andersen, L. Hovgaard, and J.W. Jaroszewski, *Rational selection of antisense oligonucleotide sequences.* Eur J Pharm Sci, 2000. **11**(3): p. 191-8.
145. Andreyev, H.J., P.J. Ross, D. Cunningham, and P.A. Clarke, *Antisense treatment directed against mutated Ki-ras in human colorectal adenocarcinoma.* Gut, 2001. **48**(2): p. 230-7.
146. Monia, B.P., *et al.*, *Sequence-specific antitumor activity of a phosphorothioate oligodeoxyribonucleotide targeted to human C-raf kinase supports an antisense mechanism of action in vivo.* Proc Natl Acad Sci U S A, 1996. **93**(26): p. 15481-4.
147. Jayaraman, A., S.P. Walton, M.L. Yarmush, and C.M. Roth, *Rational selection and quantitative evaluation of antisense oligonucleotides.* Biochim Biophys Acta, 2001. **1520**(2): p. 105-14.
148. Clever, J., C. Sassetti, and T.G. Parslow, *RNA secondary structure and binding sites for gag gene products in the 5' packaging signal of human immunodeficiency virus type 1.* J Virol, 1995. **69**(4): p. 2101-9.
149. Koeller, D.M., *et al.*, *A cytosolic protein binds to structural elements within the iron regulatory region of the transferrin receptor mRNA.* Proc Natl Acad Sci U S A, 1989. **86**(10): p. 3574-8.
150. Stull, R.A., G. Zon, and F.C. Szoka, *An in vitro messenger RNA binding assay as a tool for identifying hybridization-competent antisense oligonucleotides.* Antisense Nucleic Acid Drug Dev, 1996. **6**(3): p. 221-8.
151. Zhu, T., S. Pooyan, Z. Wei, M.J. Leibowitz, and S. Stein, *Gel shift assay: demonstration of enhanced binding of oligo(delta)-L-ornithine-oligodeoxynucleotide conjugates to complementary DNA and RNA.* Antisense Nucleic Acid Drug Dev, 1996. **6**(1): p. 69-74.
152. Bruice, T.W. and W.F. Lima, *Control of complexity constraints on combinatorial screening for preferred oligonucleotide hybridization sites on structured RNA.* Biochemistry, 1997. **36**(16): p. 5004-19.
153. Ho, S.P., *et al.*, *Potent antisense oligonucleotides to the human multidrug resistance-1 mRNA are rationally selected by mapping RNA-accessible sites with oligonucleotide libraries.* Nucleic Acids Res, 1996. **24**(10): p. 1901-7.
154. Ho, S.P., D.H. Britton, Y. Bao, and M.S. Scully, *RNA mapping: selection of potent oligonucleotide sequences for antisense experiments.* Methods Enzymol, 2000. **314**(6): p. 168-83.
155. Southern, E.M., *et al.*, *Arrays of complementary oligonucleotides for analysing the hybridisation behaviour of nucleic acids.* Nucleic Acids Res, 1994. **22**(8): p. 1368-73.

156. Milner, N., K.U. Mir, and E.M. Southern, *Selecting effective antisense reagents on combinatorial oligonucleotide arrays.* Nat Biotechnol, 1997. **15**(6): p. 537-41.
157. Sohail, M., *et al., Antisense oligonucleotides selected by hybridisation to scanning arrays are effective reagents in vivo.* Nucleic Acids Res, 2001. **29**(10): p. 2041-51.
158. Tu, G.C., Q.N. Cao, F. Zhou, and Y. Israel, *Tetranucleotide GGGA motif in primary RNA transcripts. Novel target site for antisense design.* J Biol Chem, 1998. **273**(39): p. 25125-31.
159. Matveeva, O.V., *et al., Identification of sequence motifs in oligonucleotides whose presence is correlated with antisense activity.* Nucleic Acids Res, 2000. **28**(15): p. 2862-5.
160. Wakita, T. and J.R. Wands, *Specific inhibition of hepatitis C virus expression by antisense oligodeoxynucleotides. In vitro model for selection of target sequence.* J Biol Chem, 1994. **269**(19): p. 14205-10.
161. Tsiang, M., C.S. Gibbs, L.C. Griffin, K.E. Dunn, and L.L. Leung, *Selection of a suppressor mutation that restores affinity of an oligonucleotide inhibitor for thrombin using in vitro genetics.* J Biol Chem, 1995. **270**(33): p. 19370-6.
162. Castier, Y., *et al., The activity of c-myb antisense oligonucleotide to prevent intimal hyperplasia is nonspecific.* J Cardiovasc Surg (Torino), 1998. **39**(1): p. 1-7.
163. Wyatt, J.R., *et al., Combinatorially selected guanosine-quartet structure is a potent inhibitor of human immunodeficiency virus envelope-mediated cell fusion.* Proc Natl Acad Sci U S A, 1994. **91**(4): p. 1356-60.
164. Zarrinkar, P.P. and J.R. Williamson, *The kinetic folding pathway of the Tetrahymena ribozyme reveals possible similarities between RNA and protein folding.* Nat Struct Biol, 1996. **3**(5): p. 432-8.
165. Wu, M. and I. Tinoco, *RNA folding causes secondary structure rearrangement.* Proc Natl Acad Sci U S A, 1998. **95**(20): p. 11555-60.
166. Silverman, S.K., M. Zheng, M. Wu, I. Tinoco, Jr., and T.R. Cech, *Quantifying the energetic interplay of RNA tertiary and secondary structure interactions.* Rna, 1999. **5**(12): p. 1665-74.
167. Walter, A.E., *et al., Coaxial stacking of helixes enhances binding of oligoribonucleotides and improves predictions of RNA folding.* Proc Natl Acad Sci U S A, 1994. **91**(20): p. 9218-22.
168. Zuker, M., *On finding all suboptimal foldings of an RNA molecule.* Science, 1989. **244**(4900): p. 48-52.
169. Mathews, D.H., M.E. Burkard, S.M. Freier, J.R. Wyatt, and D.H. Turner, *Predicting oligonucleotide affinity to nucleic acid targets.* Rna, 1999. **5**(11): p. 1458-69.
170. Zuker, M. and P. Stiegler, *Optimal computer folding of large RNA sequences using thermodynamics and auxiliary information.* Nucleic Acids Res, 1981. **9**(1): p. 133-48.
171. Jaeger, J.A., D.H. Turner, and M. Zuker, *Improved predictions of secondary structures for RNA.* Proc Natl Acad Sci U S A, 1989. **86**(20): p. 7706-10.
172. Jaeger, J.A., D.H. Turner, and M. Zuker, *Predicting optimal and suboptimal secondary structure for RNA.* Methods Enzymol, 1990. **183**: p. 281-306.
173. Turner, D.H., *et al., Improved parameters for prediction of RNA structure.* Cold Spring Harb Symp Quant Biol, 1987. **52**(2): p. 123-33.

174. Patzel, V., U. Steidl, R. Kronenwett, R. Haas, and G. Sczakiel, *A theoretical approach to select effective antisense oligodeoxyribonucleotides at high statistical probability.* Nucleic Acids Res, 1999. **27**(22): p. 4328-34.
175. Jaroszewski, J.W., J.L. Syi, M. Ghosh, K. Ghosh, and J.S. Cohen, *Targeting of antisense DNA: comparison of activity of anti-rabbit beta-globin oligodeoxyribonucleoside phosphorothioates with computer predictions of mRNA folding.* Antisense Res Dev, 1993. **3**(4): p. 339-48.
176. Laptev, A.V., Z. Lu, A. Colige, and D.J. Prockop, *Specific inhibition of expression of a human collagen gene (COL1A1) with modified antisense oligonucleotides. The most effective target sites are clustered in double-stranded regions of the predicted secondary structure for the mRNA.* Biochemistry, 1994. **33**(36): p. 11033-9.
177. Ho, S.P., *et al.*, *Mapping of RNA accessible sites for antisense experiments with oligonucleotide libraries.* Nat Biotechnol, 1998. **16**(1): p. 59-63.
178. Sczakiel, G., M. Homann, and K. Rittner, *Computer-aided search for effective antisense RNA target sequences of the human immunodeficiency virus type 1.* Antisense Res Dev, 1993. **3**(1): p. 45-52.
179. Stein, C.A., *How to design an antisense oligodeoxynucleotide experiment: a consensus approach.* Antisense Nucleic Acid Drug Dev, 1998. **8**(2): p. 129-32.
180. Prati, E.G., P. Scheidegger, A.R. Sburlati, and J.E. Bailey, *Antisense strategies for glycosylation engineering of Chinese hamster ovary (CHO) cells.* Biotechnol Bioeng, 1998. **59**(4): p. 445-50.
181. Peyman, A., *et al.*, *Inhibition of viral growth by antisense oligonucleotides directed against the IE110 and the UL30 mRNA of herpes simplex virus type-1.* Biol Chem Hoppe Seyler, 1995. **376**(3): p. 195-8.
182. Lefebvre d'Hellencourt, C., L. Diaw, P. Cornillet, and M. Guenounou, *Inhibition of human TNF alpha and LT in cell-free extracts and in cell culture by antisense oligonucleotides.* Biochim Biophys Acta, 1996. **1317**(3): p. 168-74.
183. Lima, W.F., V. Brown-Driver, M. Fox, R. Hanecak, and T.W. Bruice, *Combinatorial screening and rational optimization for hybridization to folded hepatitis C virus RNA of oligonucleotides with biological antisense activity.* J Biol Chem, 1997. **272**(1): p. 626-38.
184. Ramsay, G., *DNA chips: state-of-the art.* Nat Biotechnol, 1998. **16**(1): p. 40-4.
185. Sugimoto, N., *et al.*, *Thermodynamic parameters to predict stability of RNA/DNA hybrid duplexes.* Biochemistry, 1995. **34**(35): p. 11211-6.
186. SantaLucia, J., H.T. Allawi, and P.A. Seneviratne, *Improved nearest-neighbor parameters for predicting DNA duplex stability.* Biochemistry, 1996. **35**(11): p. 3555-62.
187. Zuker, M. and A.B. Jacobson, *"Well-determined" regions in RNA secondary structure prediction: analysis of small subunit ribosomal RNA.* Nucleic Acids Res, 1995. **23**(14): p. 2791-8.
188. Hines, W.W. and D.C. Montgomery, *Probability and statistics in engineering and management science.* 3 ed. 1990, New York: John Wiley & Sons, Inc. 732.
189. Goodchild, J., *et al.*, *Inhibition of human immunodeficiency virus replication by antisense oligodeoxynucleotides.* Proc Natl Acad Sci U S A, 1988. **85**(15): p. 5507-11.
190. Gewirtz, A.M., D.L. Sokol, and M.Z. Ratajczak, *Nucleic acid therapeutics: state of the art and future prospects.* Blood, 1998. **92**(3): p. 712-36.

191. Mologni, L., P. leCoutre, P.E. Nielsen, and C. Gambacorti-Passerini, *Additive antisense effects of different PNAs on the in vitro translation of the PML/RAR-α gene.* Nucleic Acids Res, 1998. **26**(8): p. 1934-8.
192. Sclavi, B., M. Sullivan, M.R. Chance, M. Brenowitz, and S.A. Woodson, *RNA folding at millisecond intervals by synchrotron hydroxyl radical footprinting.* Science, 1998. **279**(5358): p. 1940-3.
193. Matveeva, O., *et al.*, *Prediction of antisense oligonucleotide efficacy by in vitro methods.* Nat Biotechnol, 1998. **16**(13): p. 1374-5.
194. Montarras, D., *et al.*, *Autonomous differentiation in the mouse myogenic cell line, C2, involves a mutual positive control between insulin-like growth factor II and MyoD, operating as early as at the myoblast stage.* J Cell Sci, 1996. **109**(Pt 3)(4): p. 551-60.
195. Walton, S., C. Roth, and M. Yarmush, *Antisense Technology*, in *The Biomedical Engineering Handbook.* 2000, CRC Press LLC: Boca Raton, FL. p. 103-1 - 103-19.
196. Andreyev, H.J., P.J. Ross, D. Cunningham, and P.A. Clarke, *Antisense treatment directed against mutated Ki-ras in human colorectal adenocarcinoma.* Gut, 2001. **48**(2): p. 230-237.
197. Eckardt, S., P. Romby, and G. Sczakiel, *Implications of RNA structure on the annealing of a potent antisense RNA directed against the human immunodeficiency virus type 1.* Biochemistry, 1997. **36**(42): p. 12711-21.
198. Lima, W.F., B.P. Monia, D.J. Ecker, and S.M. Freier, *Implication of RNA structure on antisense oligonucleotide hybridization kinetics.* Biochemistry, 1992. **31**(48): p. 12055-61.
199. Zuker, M., J.A. Jaeger, and D.H. Turner, *A comparison of optimal and suboptimal RNA secondary structures predicted by free energy minimization with structures determined by phylogenetic comparison.* Nucleic Acids Res, 1991. **19**(10): p. 2707-14.
200. Mathews, D.H., J. Sabina, M. Zuker, and D.H. Turner, *Expanded sequence dependence of thermodynamic parameters improves prediction of RNA secondary structure.* J Mol Biol, 1999. **288**(5): p. 911-40.
201. Walton, S.P., G.N. Stephanopoulos, M.L. Yarmush, and C.M. Roth, *Prediction of antisense oligonucleotide binding affinity to a structured RNA target.* Biotechnol Bioeng, 1999. **65**(1): p. 1-9.
202. Cazenave, C., N. Loreau, N.T. Thuong, J.J. Toulme, and C. Helene, *Enzymatic amplification of translation inhibition of rabbit beta-globin mRNA mediated by anti-messenger oligodeoxynucleotides covalently linked to intercalating agents.* Nucleic Acids Res, 1987. **15**(12): p. 4717-36.
203. Goodchild, J., E.d. Carroll, and J.R. Greenberg, *Inhibition of rabbit beta-globin synthesis by complementary oligonucleotides: identification of mRNA sites sensitive to inhibition.* Arch Biochem Biophys, 1988. **263**(2): p. 401-9.
204. Schwille, P., F. Oehlenschlager, and N.G. Walter, *Quantitative hybridization kinetics of DNA probes to RNA in solution followed by diffusional fluorescence correlation analysis.* Biochemistry, 1996. **35**(31): p. 10182-93.
205. Patzel, V., J. zu Putlitz, S. Wieland, H.E. Blum, and G. Sczakiel, *Theoretical and experimental selection parameters for HBV-directed antisense RNA are related to increased RNA-RNA annealing.* Biol Chem, 1997. **378**(6): p. 539-43.

206. Helene, C. and J.J. Toulme, *Specific regulation of gene expression by antisense, sense and antigene nucleic acids.* Biochim Biophys Acta, 1990. **1049**(2): p. 99-125.
207. Bommarito, S., N. Peyret, and J. SantaLucia, *Thermodynamic parameters for DNA sequences with dangling ends.* Nucleic Acids Res, 2000. **28**(9): p. 1929-34.
208. Tabaska, J.E., R.B. Cary, H.N. Gabow, and G.D. Stormo, *An RNA folding method capable of identifying pseudoknots and base triples.* Bioinformatics, 1998. **14**(8): p. 691-9.
209. Rivas, E. and S.R. Eddy, *A dynamic programming algorithm for RNA structure prediction including pseudoknots.* J Mol Biol, 1999. **285**(5): p. 2053-68.
210. Juan, V. and C. Wilson, *RNA secondary structure prediction based on free energy and phylogenetic analysis.* J Mol Biol, 1999. **289**(4): p. 935-47.
211. Ding, Y. and C.E. Lawrence, *Statistical prediction of single-stranded regions in RNA secondary structure and application to predicting effective antisense target sites and beyond.* Nucleic Acids Res, 2001. **29**(5): p. 1034-1046.
212. Vickers, T.A., J.R. Wyatt, and S.M. Freier, *Effects of RNA secondary structure on cellular antisense activity.* Nucleic Acids Res, 2000. **28**(6): p. 1340-7.
213. Scherr, M., J.J. Rossi, G. Sczakiel, and V. Patzel, *RNA accessibility prediction: a theoretical approach is consistent with experimental studies in cell extracts.* Nucleic Acids Res, 2000. **28**(13): p. 2455-61.
214. Matveeva, O., B. Felden, S. Audlin, R.F. Gesteland, and J.F. Atkins, *A rapid in vitro method for obtaining RNA accessibility patterns for complementary DNA probes: correlation with an intracellular pattern and known RNA structures.* Nucleic Acids Res, 1997. **25**(24): p. 5010-6.
215. Haruki, M., Y. Tsunaka, M. Morikawa, S. Iwai, and S. Kanaya, *Catalysis by Escherichia coli ribonuclease HI is facilitated by a phosphate group of the substrate.* Biochemistry, 2000. **39**(45): p. 13939-44.
216. Myers, K.J. and N.M. Dean, *Sensible use of antisense: how to use oligonucleotides as research tools.* Trends Pharmacol Sci, 2000. **21**(1): p. 19-23.
217. Kang, J.J., G.A. Kaysen, H. Jones, Jr., and M.J. Holland, *Rat liver transcript profiling in normal and disease states using a kinetic polymerase chain reaction assay.* Methods, 1997. **13**(4): p. 437-43.
218. Fink, L., *et al.*, *Real-time quantitative RT-PCR after laser-assisted cell picking.* Nat Med, 1998. **4**(11): p. 1329-33.
219. Freeman, W.M., S.J. Walker, and K.E. Vrana, *Quantitative RT-PCR: pitfalls and potential.* Biotechniques, 1999. **26**(1): p. 112-22, 124-5.
220. Baumann, H., K.R. Prowse, S. Marinkovic, K.A. Won, and G.P. Jahreis, *Stimulation of hepatic acute phase response by cytokines and glucocorticoids.* Ann N Y Acad Sci, 1989. **557**: p. 280-95.
221. Ronnov-Jessen, L., B. van Deurs, J.E. Celis, and O.W. Petersen, *Smooth muscle differentiation in cultured human breast gland stromal cells.* Lab Invest, 1990. **63**(4): p. 532-43.
222. Schweitzer, M. and J.W. Engels, *Analysis of antisense oligonucleotides*, in *Antisense -- From Technology to Therapy*, R. Schlingensiepen, W. Brysch, and K.H. Schlingensiepen, Editors. 1997, Blackwell Wissenschaft: Berlin. p. 79-103.

223. Hunter, J.J. and K.R. Chien, *Signaling pathways for cardiac hypertrophy and failure.* N Engl J Med, 1999. **341**(17): p. 1276-83.
224. Kishimoto, T., S. Akira, M. Narazaki, and T. Taga, *Interleukin-6 family of cytokines and gp130.* Blood, 1995. **86**(4): p. 1243-54.
225. Gerhartz, C., *et al.*, *Biosynthesis and half-life of the interleukin-6 receptor and its signal transducer gp130.* Eur J Biochem, 1994. **223**(1): p. 265-74.
226. Matrisian, L.M., G. Rautmann, B.E. Magun, and R. Breathnach, *Epidermal growth factor or serum stimulation of rat fibroblasts induces an elevation in mRNA levels for lactate dehydrogenase and other glycolytic enzymes.* Nucleic Acids Res, 1985. **13**(3): p. 711-26.
227. Walton, S.P., G.N. Stephanopoulos, M.L. Yarmush, and C.M. Roth, *Thermodynamic and Kinetic Characterization of Antisense Oligodeoxynucleotide Binding to a Structured mRNA.* Biophys J (in press), 2001.
228. Jayaraman, A., M.L. Yarmush, and C.M. Roth, *Dynamics of gene expression in rat hepatocytes under stress.* Metab Eng, 2000. **2**(3): p. 239-51.
229. Peters, T., Jr., *Serum albumin.* Adv Protein Chem, 1985. **37**: p. 161-245.
230. Stein, C.A., C. Subasinghe, K. Shinozuka, and J.S. Cohen, *Physicochemical properties of phosphorothioate oligodeoxynucleotides.* Nucleic Acids Res, 1988. **16**(8): p. 3209-21.